Selective Analysis of Petroleum Fractions by Mass Spectrometry

by

Haoxuan Zhu
B.Sc., Tianjin Medical University, 2014

A Thesis Submitted in Partial Fulfillment
of the Requirements for the Degree of

MASTER OF SCIENCE

in the Department of Chemistry

Supervisory Committee

Selective Analysis of Petroleum Fractions by Mass Spectrometry

by

Haoxuan Zhu
B.Sc., Tianjin Medical University, 2014

Supervisory Committee

Dr. J. Scott McIndoe, Department of Chemistry
Supervisor

Dr. Robin G. Hicks, Department of Chemistry
Departmental Member

Abstract

Supervisory Committee
Dr. J. Scott McIndoe, Department of Chemistry
Supervisor
Dr. Robin G. Hicks, Department of Chemistry
Departmental Member

Electrospray ionization mass spectrometry (ESI-MS) is a fast and sensitive technique that is ideal for detecting low concentration species of interest within complex mixtures. Because ESI-MS simply transfers charged species to the gas phase, only ions pre-formed in solution are visible. Accordingly, the charged tag, 3-(4-(bromomethyl)benzyl)-1-methylimidazolium hexafluorophosphate, was designed and synthesized to allow selective detection of phenols in petroleum fractions. Pressurized sample infusion (PSI) was optimized and used for time dependent analyses. PSI ESI-MS was applied to measure O-alkylation of the phenol species leading to rate information about the overall reaction along with dynamic information about reaction progress. The relative intensity of the charged tag was used to determine semi-quantitatively the presence of phenols in different petroleum fractions.

Other derivatization methods in petroleomics were also explored. 1-[3-(Dimethylamino)propyl]-3-ethylcarbodiimide methiodide (EDT) derivatization followed by PSI ESI-MS analysis was applied for the selective measurement and identification of naphthenic acids in petroleum fractions. The reactions of standard naphthenic acids and EDT were studied by PSI ESI-MS to assess the efficiency of EDT and the rate of reactions.

The same petroleum fractions were analysed by cold Electron ionization (Cold EI) gas chromatography-mass spectrometry (GC/MS) and classical EI GC/MS. The combination spectra from the subtraction from cold EI spectra to classical EI spectra provide us a new dimension to cold EI analysis of complex matrices. Meanwhile, a Python program was written to rapidly screen cold EI GC/MS data for routine tasks, such as retention time comparison on different instrument parameters for single petroleum sample and spectrum comparison on the same retention time for different petroleum samples.

Table of Contents

List of Schemes

List of Tables

List of Figures

List of numbered structures

Chapter 3:

R= alkyl group

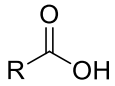

1.

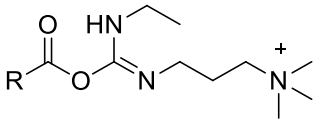

2.

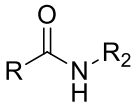

3.

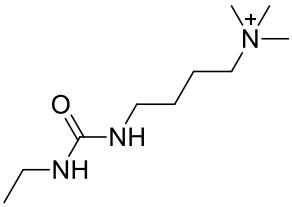

4.

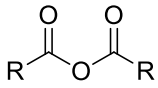

5.

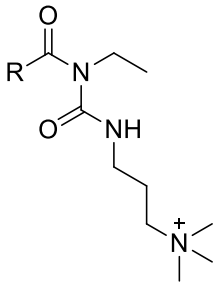

6.

List of Abbreviations

Å	Angstrom (1×10^{-10} m)
AAFS	American Academy of Forensic Sciences
AED	atomic emission detector
APCI	atmospheric pressure chemical ionization
Ar	argon gas
b.p	boiling point
CE	capillary electrophoresis
CI	chemical ionization
CID	collision induced dissociation
COOH	carboxyl group
CSV	comma-separated values
Da	Daltons
DART	direct analysis in real time
DC	direct current
DESI	desorption electrospray ionization
DMISC	1,2-dimethylimidazole-4-sulfonyl chloride
EDC	1-ethyl-3-(3-dimethylaminopropyl)carbodiimide
EDT	1-[3-(Dimethylamino)propyl]-3-ethylcarbodiimide methiodide
EE	ethinylestradiol
EI	electron impact or electron ionization
ESI	Electrospray Ionization
FAB	fast atom bombardment
FAIMS	high-field asymmetric waveform ion mobility spectrometry
FIB	fast ion bombardment
FTICR	Fourier transform ion cyclotron resonance
FTIR	Fourier transform infrared
GC	gas chromatography
GC×GC	comprehensive two-dimensional gas chromatography
GQDs	graphene quantum dots
HPLC	high performance liquid chromatography
HTGC	high-temperature gas chromatography
ICP	inductively coupled plasma
IR	infrared
LC	liquid chromatography
LD/VUV	synchrotron vacuum ultraviolet photoionization mass spectrometry
LIAD	Laser induced acoustic desorption
L^2MS	two-step laser mass spectrometry
MALDI	matrix-assisted laser desorption ionization
MCP	micro-channel plate
MS	mass spectrometry/ mass spectrometer / mass spectrum
MS/MS	tandem mass spectrometry
Mol.Wt.	molecular weight
min	minute
MTBSTFA	*N*-methyl-*N*-(*t*-butyldimethylsilyl)trifluoroacetamide
M.W.	molecular weight

m/z	mass-to-charge ratio
NAC	naphthenic acids corrosion
NCD	nitrogen-specific detection
NCI	negative chemical ionization
NIST	National Institute of Standards
NMR	nuclear magnetic resonance
NPH	nitrophenylhydrazine
OH	hydroxy group
PAH	polycyclic aromatic hydrocarbon
PCI	positive chemical ionization
PEEK	poly ether ether ketone
PEGs	polyethylene glycols
PFTBA	perfluorotributylamine
$[PF_6]^-$	hexafluorophosphate
PSI	pressurized sample infusion
psi	pounds per square inch
PSS	programmable split/splitless
PTFE	polytetrafluoroethylene
PVC	polyvinyl chloride
Q-ToF	quadrupole-time-of-flight
rf	radio frequency
RLS	resonance light scattering
RT	room temperature
S/N	signal-to-noise ratio
SEC	size exclusion chromatography
SMB	supersonic molecular beam
TAN	total acid number
ToF	time-of-flight
TPA	tris(2-pyridyl-methyl)amine
$t_{1/2}$	half time
UV-Vis	ultraviolet visible
VGO	vacuum gas oil

Acknowledgments

I would like to appreciate Dr. J. Scott McIndoe giving me chance to work in his research group. He has encouraged me and gave me insightful research suggestions over the last two years. As a chemically timid grad student, he was always patient and gave me time and chance to try ideas I want to instead of hurrying me up. His guidance helps me to achieve distant goals bit by bit. Besides, I am extremely grateful for him sharing his life and teaching experience with me, which is very valuable for me on a person level.

I wish to thank all the past and present group members, Eric and James for teaching me in everything at the beginning of my grad life, Jingwei who helped me to make a huge breakthrough on my research, Rhonda and Robin, for their listening ears and giving me their hands whenever I needed help, Johanne and Harmen, for feeling appreciated to become friends with them, my other group members, Lars, Natalie, Kingsly, Landon, Jie, Peter, Darien, Issac, Anuj, and Jin and Roman in Lisa's group, make the lab a desirable place to work every day.

I also appreciate Dr. Ori Granot for helping me on all MS instrument issues, Christopher Barr for teaching me the NMR knowledge, and my TA instructors, Monica Reimer and Jane Browning, for sharing their advices and stories to make my teaching easy and enjoyable.

Last and foremost, I am so grateful to my parents, my cousin sister and all of my friends. Even though we are far away from each other, their support, accompanies and trust make me become a better man. "Pain is inevitable. Suffering is optional." As my favorite author said "The 'hurt' part is an unavoidable reality, but whether or not you can stand anymore is up to yourself."

Dedication

感谢爸爸妈妈给予我生命，感谢老顾十五年的陪伴，很珍贵。

Chapter 1 Introduction

1.1 A brief history of mass spectrometry

Mass spectrometry is an outstanding analytical tool that is available to both qualitative and quantitative chemistry. A mass spectrometer generates gas phase ions, separates these ions in a vacuum chamber based on their mass-to-charge ratio by using an electric or magnetic field and counts the number of ions.[1]

The first mass spectrometer dates back to the work of J.J Thomson in the early 20th century. He used the magnetic and electric fields successfully for separating the two isotopes of neon (^{20}Ne and ^{22}Ne).[2, 3] In addition, F.W. Aston systematically improved the apparatus of Thomson to make it more precise and versatile. Because of his contribution, he was awarded the Nobel Prize in 1922.[4] From then on, mass spectrometry took off.

There is no universal mass spectrometer. Over the last 110 years, a variety of designs and mechanics have been developed; each of them is intended for a specific use. However, there are three common components in most mass spectrometers: 1) the ion source, which has the function of producing ions and transferring them into the mass analyzer; 2) the mass analyzer, whose job is to separate ions on their mass-to-charge ratio (*m/z*); 3) the detector, whose role is to measure the abundance of ions at each mass-to-charge ratio (*m/z*).

The ion source is regarded as the heart of the mass spectrometer and is actually a chemical reaction vessel. The most commonly used and also the first ionization technique is electron ionization (EI) created by A.J. Dempster.[5] The EI source generates electrons by heating a metal filament. The energetic electrons interact with vaporised sample molecules to expel an electron from the analyte

molecules, which leads to the production of the molecular ions.[6, 7] However, its highly energetic ionization process makes the abundance of the molecular ions quite low, and fragments dominate the spectrum that often provides only limited information on the parent ion. The most widely used sample insertion method in EI-MS is gas chromatography (GC). The EI source is well-matched for the small, volatile and thermally stable molecules that can be separated by GC.[1]

Considering the importance of molecular weight for structural identification, scientists invented several "softer" ionization methods. The first soft ionization method was chemical ionization (CI) introduced by Munson and Field in 1966.[8] A reagent gas, ionized by electron beam, is applied to transfer charge to the molecular analytes. By avoiding direct ionization by electron beam, the molecular weight can be obtained. However, the application of CI is limited as the sample still needs to be thermally volatile and robust.[9]

Many other ionization techniques have been invented, such as field ionization, photoionization and plasma desorption etc.[10] Thanks to modern soft ionization techniques, intact molecules are able to be characterized by matrix assisted laser desorption ionization (MALDI) and electrospray ionization (ESI). Fenn[11] and Tanaka[12, 13]who developed them respectively, won the Nobel Prize in Chemistry in 2002. In MALDI, the analytes are co-crystalized with the matrix, and a laser beam energizes the matrix which is then blasted into the gas phase. The protons transfer occurs between matrix molecules and analyte molecules producing singly charged analytes. This technology has extensive applications it the study of large molecules, especially biomolecules.[14, 15] As for ESI, it is one of the softest ionization techniques that can be used to analyse large and thermally fragile polar molecules like proteins.[16]

Its high sensitivity, high accuracy and high mass range detection has gained tremendous popularity.

For the mass analyser, the magnetic sector, quadrupoles, ion traps, time-of-flight analyzers and Fourier transform ion cyclotron resonance are used according to the need. The detectors in most cases are electron multipliers and microchannel plates (MCP).[10]

Table 1.1 Historical Developments in mass spectrometry.[17]

Scientist(s)	Year	Contribution
Thomson*	1899-1911	First mass spectrometer
Dempster	1918	EI and magnetic focusing
Aston*	1919	Atomic weights using MS
Stephens	1946	Time of Flight (TOF) mass analysis
Hipple, Sommer and Thomas	1949	Ion Cyclotron Resonance
Paul and Steinwedel	1953	Quadrupole analyzers
Beynon	1956	High-resolution MS
Munson and Field	1966	CI
Dole	1968	ESI
Beckey	1969	Field Desorption MS of organic molecules
MacFarlane and Torgerson	1974	Plasma Desorption MS
Comisarow and Marshall	1974	FTICR MS
Yost and Enke	1978	Triple Quadrupole MS
Barber	1981	Fast Atom Bombardment (FAB)
Tanaka*, Karas and Hillenkamp	1983	MALDI
Mann and Wilm	1991	MicroESI

* Nobel Prize winner

1.2 ESI-QTOF-MS

1.2.1 Electrospray ionization

In the late 1960s, Dole and co-workers invented ESI to characterize non-volatile polymers in their research.[18] Yamashita and Fenn combined it with a quadrupole mass analyser, improved the design and applied it to biomolecules in the 1980s.[19]

The electrospray ionization process is shown in Figure 1.1. In ESI, a solution containing analyte ions is introduced into the source and directed through a charged capillary. The latter is either at a positive or negative charge of 2500 V to 5000 V. The charged capillary induces the solution to emerge from the capillary in a shape called a "Taylor Cone", as a spray of charged droplets forms. It is possible to generate a net positive (or a negative) charge, depending on oxidative (reductive) electrochemical process occurring at the capillary. The net charges of droplets repel each other, which results in their relocation on the surface of the fine droplet. These droplets are dried by a warm desolvation gas (usually nitrogen) and the evaporation of solvent leads to the increment of charge density. Once the charge density attains a certain threshold, ion evaporation and/or Coulomb explosion happens to generate desolvated analyte ions in the gas phase that move into the MS analyzer.[20, 21, 22]

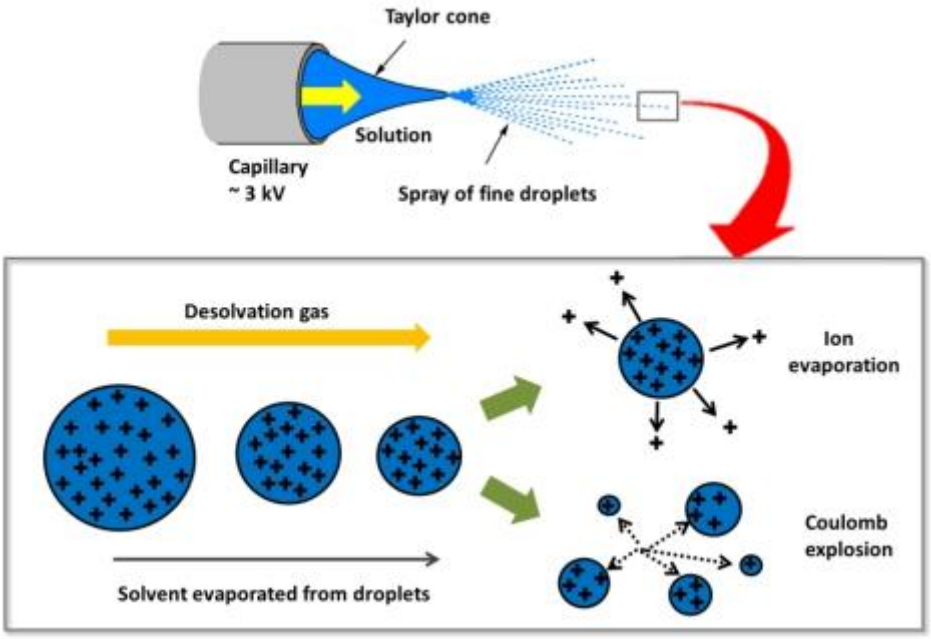

Figure 1.1 The desolvation process in electrospray ionization adapted from reference 1.

ESI is the softest ionization method,[23] which means little fragmentation is usually observed in the spectrum. Therefore, the intact molecule can be characterized. As only charged analytes are detectable in ESI-MS, all species of interest in reaction system must be charged. Reactions containing naturally charged intermediates allow for straightforward analysis. For example, in 1997, the intermediate $[Fe^{III}$-TPA(OOH)$]^{2+}$ in the hydroxylation of alkane by H_2O_2 (TPA= tris(2-pyridyl-methyl)amine) was reported investigated by ESI-MS.[24] Compounds of interest can also be charged adventitiously, for example, protonation of a basic group to form $[M+H]^+$ ions that can be captured in positive ion mode, or the addition of cations, such as Na^+ or K^+, gives $[M+Na]^+$ or $[M+K]^+$ ions. Deprotonation of an acidic group causes the formation of $[M-H]^-$ ions that can be detected in the negative ion mode.[1] Finally, targets can have charged or chargeable tags on them, where a charged or chargeable tag is purposefully installed on ions of interest. Our research group has developed charged tags for ESI-MS analysis and uses them frequently in the study of catalytic reactions in real time using ESI-MS. A designed charge-tagged alkyne and a

cationic rhodium catalyst were used to analyse alkyne hydrogenation.[25] Another example involves the charged analogue of Wilkinson's catalyst for olefin hydrogenation study.[26, 27] A new set of charged-tag imidazolium-type complex will be further discussed in Chapter 2.

1.2.2 Quadrupole-Time of Flight (Q-ToF)

The ESI source is under atmospheric pressure. From that point on, vacuum pumps decrease the pressure of the mass selectors through a series of pumped chambers (Figure 1.2). Voltage differences between the inside and outside of the sample cone draw ions into the spectrometer proper. At this point, some ions end up with the cleanable baffle and cannot get into the sample cone. Similarly, the remaining solvent is pumped out. As both of them cannot get into the sample cone, they can reduce the background noise and contamination among different trials.

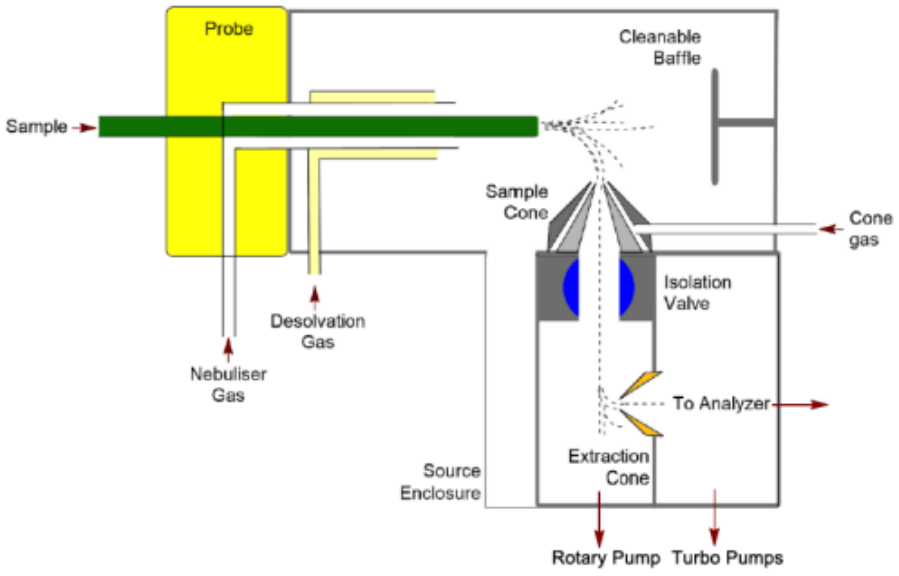

Figure 1.2 Ion path in the electrospray source of Q-ToF Micro adapted from reference 1.

After a right angle turning and passing through the extraction cone, ions come into the hexapole where the ions are focused by a radio frequency (rf) to fly into the first mass analyzer. Next, the ions fly through a quadrupole, the first mass analyser,

which is composed of four parallel metal rods. Each rod and its opposite one are electrically in pairs. A combination of DC voltage and radio-frequency potential is applied between each pair. The polarity of these pairs is opposite and changes rapidly back and forth. The ions are drawn toward an opposite charged rod, and then the field switches the polarity before the ions arrive at the rod, which causes the ions to undergo complex trajectories. Since only a certain mass to charge are transmitted by a specific frequency, the quadrupole can work as a mass filter.[28]

The next step for ions is to pass through collision gas cell where the pressure is ~ 1×10^{-3} torr, which contains Ar gas. In this part, the ions can hit the argon atoms and generate fragments by applying a higher voltage when being used for MS/MS mode. In MS mode, it works as an ion guide to pass through the ions.

After that, the ions enter the ToF analyser, which works as the second mass analyser. The ToF chamber is under a very low pressure and the vacuum system induces the ions into the ToF chamber. Incoming ions are given the same kinetic energy in the form of an electric pulse at the beginning of the process and then take varying amounts of time to reach the detector dependent on their mass. On the principle of the kinetic energy whose formula is

$$E_k = \tfrac{1}{2} mv^2 \qquad (1)$$

the velocity of the ions depends on its mass, so the ions with smallest *m/z* value reach firstly the detector followed by the ions with gradual increasing *m/z*. The device called the pusher provides the kinetic energy to form the electric pulse of the ions, and the energy can be described by the equation:

$$E_k = zeV \qquad (2)$$

where *z* is the charge on ions, *e* is the charge of an electron in coulombs, and *V* is the strength of the electric field in volts. Combine equation (1) with equation (2) to give:

$$zeV = ½\ mv^2 \qquad (3)$$

$$zeV = ½\ m\ (dx / dt)^2 \qquad (4)$$

$$m/z = 2eV(dt / dx)^2 \qquad (5)$$

Where *m* represents the mass in kilogram, *dt* is the time of flight in seconds, and *dx* is the path length of the ions traveling in meters. (Figure 1.3)

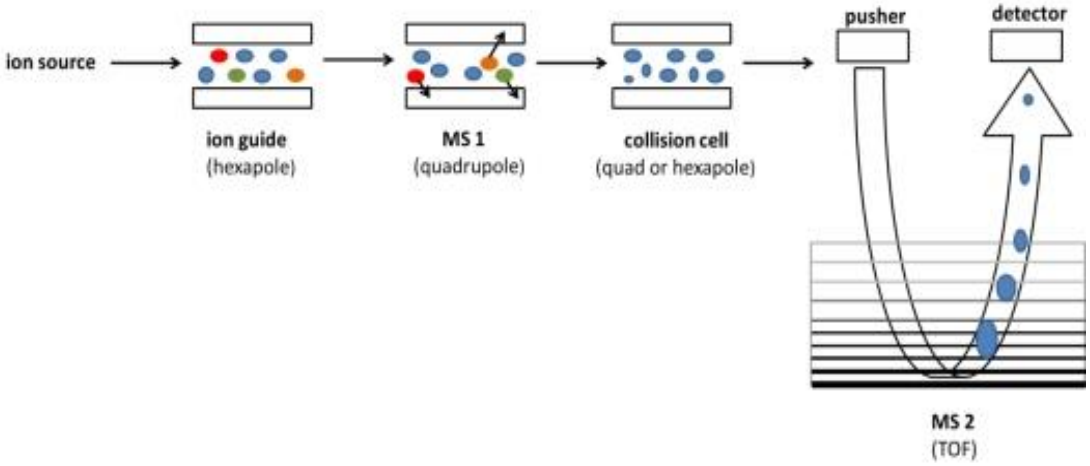

Figure 1.3 Ion path through the mass analyser to the ToF adapted from reference 1.

The good performance of ToF mass analysers depends on a high vacuum at 10^{-7} mbar. The requirement of very high vacuum can eliminate collisions, leading to transfer efficiencies.[29]

The ions leaving the ion source actually have slightly different starting times and kinetic energies. The reflectron as shown in Figure 1.4 is the device to fix the difference. It works as an ion mirror when the ions of the same *m/z* value travel into the reflectron with different kinetic energies. The ions with more kinetic energy go

deeper in the reflectron than those with less. Thus, it takes the ions the same time to travel through in the flight tube and therefore reach the detector at the same time. The application of a reflectron improves the resolution dramatically.

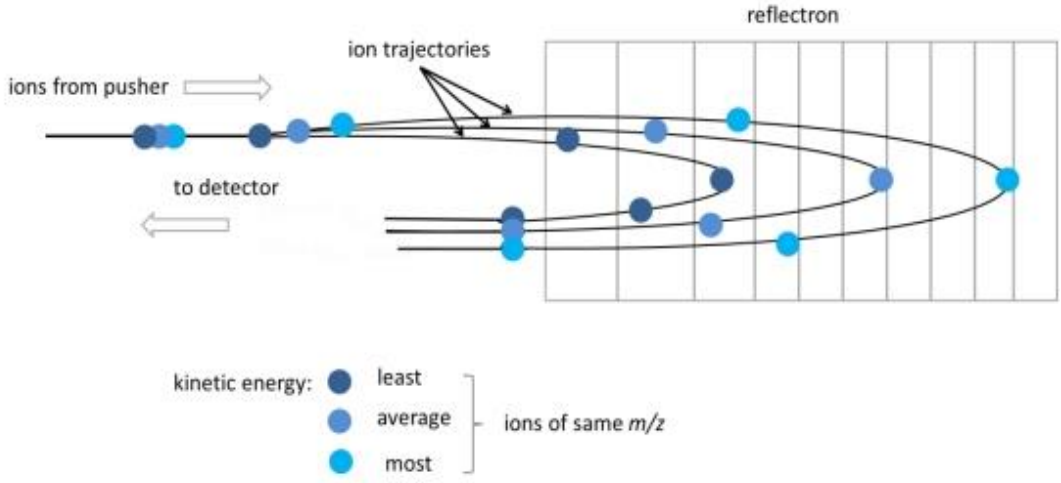

Figure 1.4 Path for ions with the same *m/z* but different initial kinetic energies through the reflectron in a ToF mass analyzer adapted from reference 1.

The detector is the destination for the ions. The detector used here is MCP, which contains thousands of electron multiplier tubes. A small current is generated when MCP is hit by an ion. And the more ions hit, the stronger current will be produced. Thus, the kinetic energy is converted into electronic signal for future data processing. User can get the information about the ion counts and *m/z* from the Water's software MassLynx.

1.2.3 PSI-ESI-MS

Pressurized sample infusion (PSI) is a simple method to inject the sample to the ESI-MS. It has the advantage that it can be applied to the real-time reaction monitoring.[30] Common lab materials are used in a PSI system: a Schlenk flask, rubber septum, rubber hose, PEEK tubing, PEEK chromatography fitting and regulated inert gas. The Schlenk flask containing the reaction solution is under inert gas atmosphere. The overpressure created by the gas (around 3 psi) can push the reaction solution into

the ESI source via a PEEK tubing. One end of the PEEK tubing is inserted through the septum into the reaction solution and the other end is connected to the ESI source.[31] (Figure 1.5)

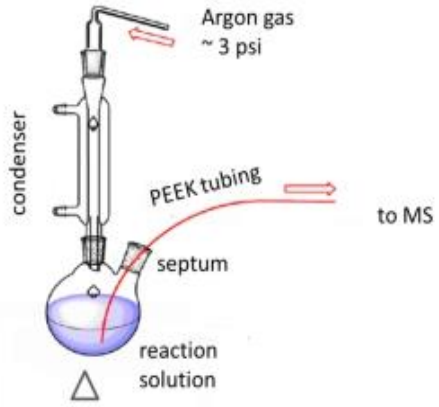

Figure 1.5 Pressurized sample infusion (PSI) setup adapted from reference 31.

The reaction solution is pushed into ESI-MS continuously via PEEK tubing. In some cases, the sample that needs to be analysed is the jet fuel that is a complex matrix and contains lots of insoluble components. Any insoluble particles in the reaction solution will increase the opportunity to block the pathway. Therefore, filtration is necessary before introduction into the MS system. Cotton filters are connected to one end of the PEEK tubing by Teflon tape, which will neither decrease the flow rate, nor form different concentration areas and interfere with the reaction.[32] (Figure 1.6)

Usually Schlenk glassware is used for a PSI setup but for the work presented in this thesis, sample vials were more suitable. Indeed, considering that a large quantity of samples needed to be analysed without interruptions and no specific treatment during the measurement was required (heat or reflex), a simplified PSI system has been used for the research project. Using sample vials made the whole

preparation and analysis processes more convenient. The PSI glassware applied here is the Agilent 15 mL sample vial. Two PEEK tubing are plugged into the vial through the septum, one for inducing gas pressure and another for connecting ESI-MS source. The septum is wrapped by Teflon tape to prevent any contamination from the antioxidant in the septum (Figure 1.6).

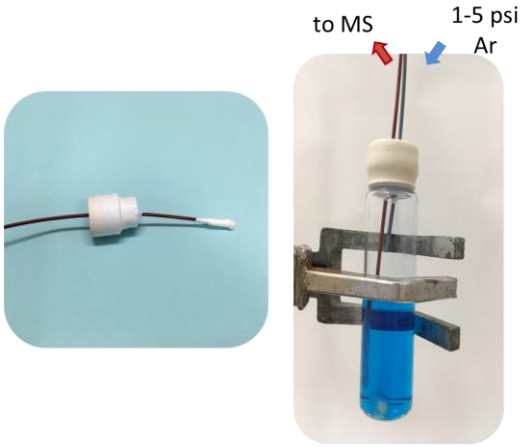

Figure 1.6 The left one is the cotton filter connected with PEEK tubing through septum wrapped by Teflon tape. The right one simplified PSI system applies Agilent 15 mL sample vial. Two PEEK tubes pierce through septum into the vial, the blue one is connected to Ar for supplying pressure and the red one is merged into the reaction solution for inducing the solution into the ESI-MS.

The Hagen-Poiseuille equation can illustrate the relationship between the flow rate in the tubing and the pressure applied to the flask:

$$\Delta P = (128\mu LQ) / (\pi d^4) \qquad (6)$$

where ΔP is the loss of pressure (Pa), μ is the dynamic viscosity, L is the tube length, Q is the volumetric flow rate and d is the inner diameter of the tube.[33]

1.3 Gas chromatography/mass spectrometry (GC/MS)

Gas chromatography/mass spectrometry (GC/MS) is a powerful technique that integrates gas chromatography and mass spectrometry into a single system. The GC provides the function for separating the components in a mixture, and MS has a feature of detection and identification of each component after the separation.[34]

The combination of GC and MS was developed during the 1950s after GC was introduced by James and Martin in 1952.[35] Roland Gohlke and Fred McLafferty made one of the first GC/MS instruments at Dow Chemical Company in the late 1950s (Figure 1.7).[36] However, the original GC/MS was too unwieldy and breakable for widespread use. Advancement in computer technology improved and simplified greatly the use of GC/MS. Under the leadership of Rober E. Finnigan, Electronic Associates, Inc. began to design a computer to control quadrupole mass spectrometer in 1964, because before that, scientists had to write their own computer programs to acquire data.[37] A few years later, in early 1968, the first prototype quadrupole GC/MS was set up in Stanford and Purdue University.[38] In 1996, it took no more than 90 seconds for the top-of-the-line high-speed GC/MS units to analyse fire accelerants, while the first-generation GC/MS would spend at least 16 minutes.[39]

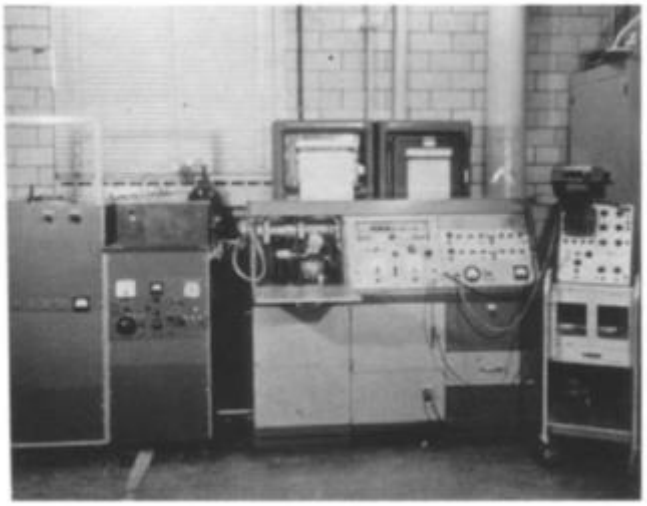

Figure 1.7 Dow gas chromatograph and Bendix TOF mass spectrometer in the Dow Spectroscopy Laboratory, 1957. [36]

By beginning of the 2000s, computerized GC/MS instruments in conjunction with quadrupole technology had become vital to chemical research, especially for organic analysis. Today, GC/MS has great versatility in its application, such as for environmental monitoring, food safety, and pharmaceutical analysis.[40, 41, 42]

1.3.1 Instrumentation

The GC/MS consists of two principal parts: the gas chromatograph and the mass spectrometer. GC separates components of a sample by specially prepared column. The carrier gas, applied to transfer the sample from the injector through the column into the detector, plays an important role on GC. The most common carrier gas is helium (He), but hydrogen (H_2) and nitrogen (N_2) are also used in certain conditions.[34]

Injectors are used to introduce the sample to the GC column. The split/splitless injection has become the model for GC injection. In the split mode, the vaporized sample mixes with the stream of carrier gas, and then goes through the column. The leftover of sample is expelled by splitter vent. Split ratios from 10:1 to 100:1 are common. 1-2 μl injected sample is often used for a split-mode injector, but larger

volumes (3-5 μl) can also be used. The splitless mode is mainly used for trace analysis because the entire analyte sample vaporized in the injector goes onto the column. In this method, the splitter vent closed at the beginning allows for transferring the entire sample to the head of the column. The splitter vent is then opened after a certain time to purge solvent on the head of the column. This step is called purge activation time. In order to obtain the best result, the optimization of some parameters such as column temperature and purge time is required.[43]

Separation occurs within the column. Two types of columns are commonly used: capillary or packed. Packed columns are typically a glass or stainless steel coil (usually 1-10 m in length and 2-4 mm inner diameter) that is filled with the stationary phase, or a packing coated with the stationary phase.[44] Capillary columns are a thin fused-silica (purified silicate glass) capillary (typically 10-100 m in length and 0.1-0.5 mm inner diameter) that has the stationary phase coated on the inner wall of the column.[45] Columns are selected for use in a particular application. All of the parameters, such as length, diameter, film thickness and type of packing have an impact on the separation. The difference in the chemical properties between different components of a sample and their relative affinity for the column stationary phase will affect their separations.[46] The time the molecules spend in a column is called retention time.[44]

After the molecules elute from the column, they go through the transfer line and are captured, ionized and detected by mass spectrometer. A number of ionization techniques are available to the mass spectrometer. However, the ionization method chosen for GC/MS is either CI or EI.

In positive chemical ionization (PCI), the reagent gas often exchanges a proton with the target molecule. This soft method allows for the observation of a more intense molecular ion and less fragmentation. In negative chemical ionization (NCI), negative ions are produced by electron capture, which is often used to analyse highly halogenated compounds.[34]

But by far the most commonly used ionization method is EI. The use of electron energy, typical 70 eV, creates more fragments of low *m/z* and few molecular ions are observed. Manufacturer-supplied software or National Institute of Standards (NIST-USA)-developed software provide established 70 eV EI library spectra. They are used as a reference for comparison. It is a powerful tool for sample identification. Sources of libraries contain NIST,[47] Wiley,[48] the AAFS,[49] and instrument manufacturers.

1.3.2 Cold EI GC/MS

As a "hard ionization" technique, the EI mass spectra are void of molecular ions information, and so the technique suffers from decreased confidence level for the identification of sample compounds. This is especially true when the principal content of some samples is heavy hydrocarbons or highly branched alkanes, because their similar fragmentation patterns result into the same EI mass spectra. Hence the molecular ion information is essential for the identification of measured compounds.[50] CI is capable of providing molecular ions information, but it lacks effectiveness on analysing some compounds such as aliphatics.[51] It is less sensitive and incompatible with library search relative to EI.[52] So this is where the cold EI come in.

In the last decade, a new type of GC/MS was developed with supersonic molecular beam (SMB), which is called "Supersonic GC/MS" ("cold EI"). In this

method, cooling the molecules before their ionization softens the “hard ionization”, leading to rich molecular ion information. After exiting the GC column, the molecules are mixed with the makeup gas (He gas at a high flow rate; typically 40 mL/min). They then expand into a vacuum chamber through a designed supersonic nozzle to form SMB (Figure 1.8). Collisions with the makeup gas cause the decrease of the internal vibrational energy of the molecules, therefore substantially reducing the degree of fragmentation and improving molecular ions intensity compared to a typical GC/MS. As the fragmentation pattern of cold EI is similar to EI, the library search can also be used to cold EI spectra.[53, 54] Kantrowitz and Grey suggested the idea of SMB in the first place,[55] and it is now widely used in various scientific fields such as environmental analysis[50] and food safety[52], etc.

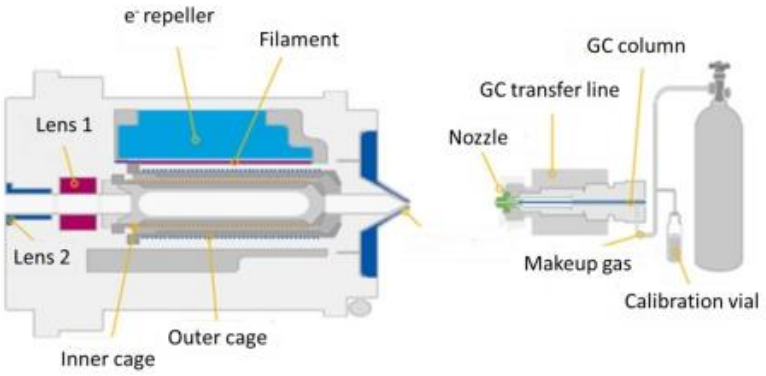

Figure 1.8 Cold EI ionization technique adapted from Axion iQT service manual.[56]

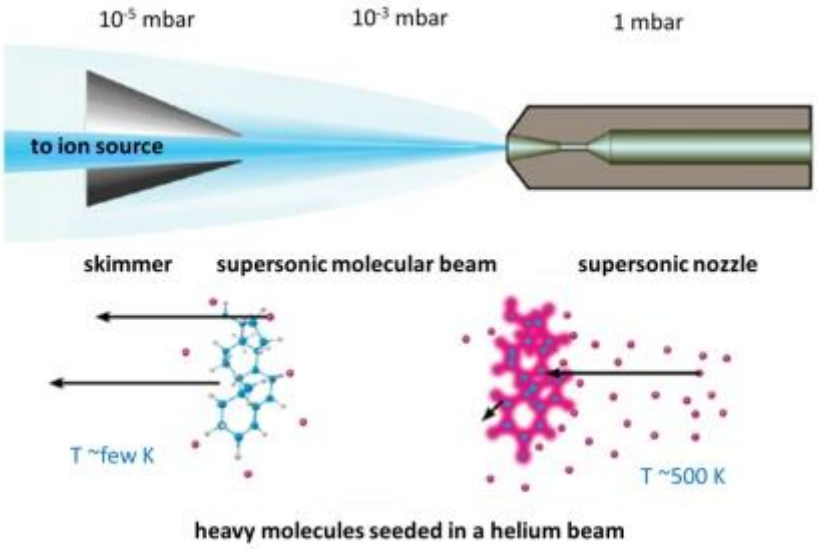

Figure 1.9 Cold EI ion source adapted from reference 56.

The supersonic GC/MS provides significant improvements through the use of SMB and its capability to handle high column flow rates (90 mL/min).[57] The boundary of GC/MS performance is redefined: 1) the sample identification is improved by enhancing molecular ion, its mass spectral isomer, and structural information;[50] 2) the range of identifiable compounds is extended;[58] 3) the speed of analysis is faster;[59] 4) the sensitivity for some compounds which are hard to detect in GC/MS is improved.[60]

Supersonic GC/MS is flexible to operate "classical EI" mode. Classical EI is operated by simply decreasing the makeup gas flow rate to reduce the SMB cooling efficiency.[61] The degree of sample cooling can be tuned in classical EI, hence increasing the probabilities to get excellent sample identification and great matching spectra to library spectra.

1.4 Analytical chemistry of petroleum

Petroleum (also called crude oil) is a complex mixture of hydrocarbons and other organic compounds extracted from the ground, land or under the oceans. It is

produced by the decomposition of animals and plants that are millions of years old.[62] Depending on the different molecular weight of the hydrocarbons, the states of petroleum may be gaseous, liquid or solid.[63] Some non-hydrocarbons containing sulphur (0.1-8% w/w), nitrogen (0.1-1.0% w/w), oxygen (0.1-3% w/w) and metals (ppm level) may also be present in petroleum.[64] Despite the fact that only small amounts of these non-hydrocarbons exist in petroleum, they have a significant impact on the characteristics of petroleum and its products, and should not be disregarded.

The composition and chemistry of petroleum is vast and complicated. Many research groups investigate petroleum through different viewpoints. Here we report one of these lines of action. Information on the composition of petroleum allows chemists to improve the production process of crude oil into high-quality petroleum products. The composition of petroleum also provides the geologists with evidence on plate tectonics, evolution of life and past climate change.[65] In addition, knowledge of the molecular components of petroleum offers the biologists to consider the biological impact of environmental exposure.[66] It is for these reasons that the measurement of physical and chemical properties of petroleum and its products as well as their compositions are extremely significant.

Analysis of petroleum and its products was developed on the second half of the 19th century. In 1857, the formation of barium salts of benzenesulfonic acids in conjunction with fractional crystallization was carried out to detect several aromatic hydrocarbons of petroleum.[60] Benjamin Silliman, Jr. reported that half of raw petroleum samples from western Pennsylvania could be distilled into a usable illuminant, and an analytical distillation of petroleum was applied in the 1870s.[67] In the last decade, the application of new analytical techniques, either qualitative or

quantitative, leads to the new knowledge and deep understanding of the petroleum industry.

It is not practical to apply most analytical techniques to petroleum analysis directly because of the complex composition of petroleum. Some separation techniques are usually employed before analysis, such as chromatography, fractionation, etc. GC is highly efficient at separating volatile components of mixtures and it can be applied into quantitative analysis of known components. For instance, *n*-paraffin distribution and its molecular weight could be obtained by high-temperature gas chromatography (HTGC).[68] Pyrolysis, followed by GC/MS of petroleum solved the problems about the distribution patterns of *n*-alkane.[69] Two-dimensional gas chromatography is a powerful tool to achieve high sensitivity and peak capacity. Organic acid extracts through a microwave extraction in conjunction with GC×GC-ToF-MS was applied to the identification of polar organic compounds.[70] The use of GC coupled with a different detector is a widespread application in detecting various species, for example GC×GC with nitrogen-specific detection (NCD) used for nitrogen compounds analysis.[71]

Beside GC techniques, non-aqueous capillary electrophoresis (CE) application was developed by Kok *et al*. to investigate the charge properties of asphaltenes.[72] High performance liquid chromatography (HPLC) system was used to do quantitative analysis of aromatic carbons in heavy crude oil distillates.[73] HPLC with silver-modified column in conjunction with GC×GC was first used to analyse oil pollution by Mao *et al*.[74] In addition, it is common to use Nuclear Magnetic Resonance (NMR) to offer the carbon and hydrogen structure information of petroleum fractions.[75, 76] Other techniques including fluorescence spectroscopy,[77] High-Q ultrasonic

spectroscopy,[78] X-ray photoelectron spectroscopy,[79] etc. were also reported sequentially.[80, 81]

It might be said that the development of petroleum analysis relates tightly to the advances of mass spectrometry. Fenn and his coworkers were the first to use ESI-MS to analyse petroleum materials in the late 1990s.[82] They combined it with high-resolution FTICR MS to detect the acidic and basic components in petroleum.[83] Desorption electrospray ionization (DESI) was introduced by Wu *et al*. to analyse saturated hydrocarbons in petroleum distillates.[84] FTICR mass spectrometer coupled with direct analysis in real time (DART) source was used to identify polycyclic aromatic hydrocarbon (PAH) of petroleum.[85] Laser induced acoustic desorption (LIAD) desorption of petroleum followed by CI and low-resolution ion trap detection was also applied.[86] In addition, other ionization techniques such as two-step laser mass spectrometry (L^2MS),[87] inductively coupled plasma (ICP) mass spectrometry,[88] and direct insertion probe-mass spectrometry[89] also exhibited good performance on petroleum analysis.

Let us now look more closely at the developments that are needed. Up to now, not a single technique can satisfy the increasing demand of petroleum analysis. Using just one technique is sometimes not sensitive and (or) selective enough to determine the final speciation. Mass spectrometry coupled with other methods, such as IR, UV-Vis and NMR are promising and can open up our dynamic range. We can benefit from respective merits of these techniques to achieve different purposes.

IR desorption coupled with tunable synchrotron vacuum ultraviolet photoionization mass spectrometry (LD/VUV PIMS) was a new attempt to detect petroleum atmospheric residue.[90] Volk and co-workers reported a combination of

online femtosecond laser ablation with GC/MS to analyse petroleum which was exploited from single rock/ mineral inclusions.[91] In addition, Wiwel *et al*. employed GC/MS, GC with atomic emission detector (AED) and NMR to identify nitrogen compounds in vacuum gas oil (VGO).[92] Lobinski's group also reported a pair of methods including size exclusion chromatography (SEC) and high-resolution ICP-MS to detect metal species in oil samples.[93, 94] An amide derivatization followed by LC separation and MS^n was applied by Rowland *et al.* to provide them structural information about polycyclic acids in oil sand samples.[95] There are many other similar examples, too numerous to list.

To sum up, the three key parameters in analytical chemistry are speed, selectivity, and sensitivity. They are the key metrics of performance in analytical chemistry and consequently in the analytical support arms of the petroleum industry. However, in reality, one or two parameters are often sacrificed in order to solve the problems (speed is often prioritized, for example). Thus, developments on analytical chemistry are always needed to meet the challenges of a fast changing petroleum industry.

Chapter 2 Phenol-selective mass spectrometric analysis of petroleum fractions

2.1 Introduction

Petroleum is an extremely valuable natural resource in the modern world, as petrochemicals play an important role in the manufacture of various petroleum products including fuels, solvents, plastics, detergents, fibres, rubbers, waxes, lubricants, dyes etc.[64] Petroleum remains a major contributor to the world's energy consumption. As the United States Annual Energy Review showed,[96] 91.5% of the transportation sectors energy consumption and 43.4% of the industrial sectors energy consumption was provided by petroleum in 2015.

The number of unique chemical constituents in petroleum is around 10^4 to 10^5.[97] As one of the most compositionally complex natural mixtures, the commercial value of raw petroleum is low. The different constituents of petroleum need to be separated to realize its benefits. Generally, after the petroleum is extracted from a well, it is sent to an oil refinery and goes through physical separation and chemical conversion process to produce the commercial products (Figure 2.1). Fractionation leads to the various petroleum products such as gasoline, kerosene, jet fuel etc.[63]

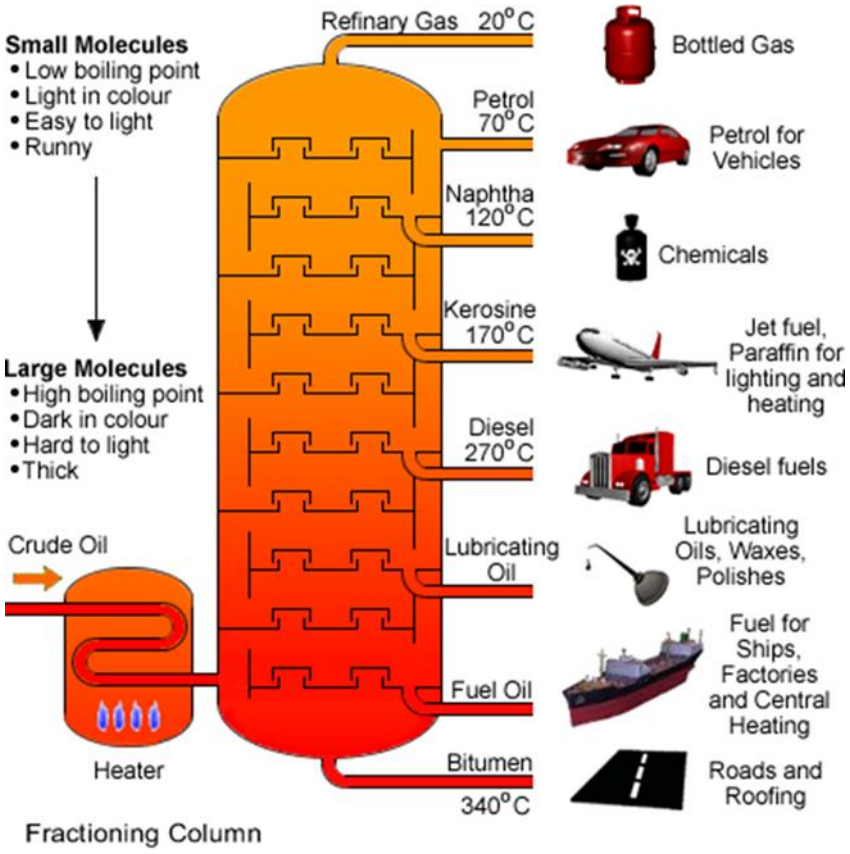

Figure 2.1 Petroleum fractionation column.[98]

As a type of petroleum distillate, jet fuel contains a large quantity of different hydrocarbons, and is used in gas-turbine engine aircraft. The carbon number of jet fuel is between 5 and 16. Naphtha-type jet fuel has carbon numbers from 5 to 15, and the carbon numbers of kerosene-type jet fuel distribute between around 8 and 16.[99] Jet fuel consists of straight (~32%) and branched (~31%) chain alkanes, cycloalkanes (~16%) and aromatic hydrocarbon (~21%).[100] However, these proportions may have great variation based on the provenance of the jet fuel. In addition, because of naturally occurring organic acids and acid treatment during the refining process, acid compounds including phenols are also found in jet fuel.[63]

It is well known that numerous undesirable components exist in petroleum products. For instance, sulfur compounds may lead to corrosion, generate unpleasant

smell and reduce the effect of some additives. Compounds including nitrogen can result in discoloration. Trace metals can have adverse effects on refinery catalysts. Oxygen compounds, especially acidic ones, are also undesirable components as they cause metal corrosion, impair the water separation characteristics of the fuel and cause problematic deposits.[101] Thus, these impurities are removed by a variety of treatments, including the addition of chemicals such as emulsifiers, wetting agents and surfactants.[63, 64] Some of these treatments result in unwanted contaminants in the fuel.

Alkylphenols are a class of compound occurring in crude oil with variable concentrations, depending on several factors such as biodegradation, origin of the crude oil and water washing. The distribution of hydrophilic compounds of crude oil such as carboxylic acids and alkylphenols is affected greatly due to their interaction with natural mineral deposits and groundwater during secondary migration, the movement of the petroleum through reservoir rock.[102] These compounds are also formed during cracking and present in all fractions of crude oil of appropriate boiling point range (the boiling point of phenol itself is 182℃). Jet fuel (b.p range 170-270℃) is one of the petroleum fractions that is most likely to suffer from phenol contamination.[103] In view of the similarity of structures of alkylphenols and their low relative abundance in jet fuel, the analysis of petroleum and its fractions is not simple.[104] An ideal method of identifying such impurities or molecules of interest should be both selective and sensitive. A wide variety of interesting approaches have been investigated to identify and monitor phenol and phenolic compounds in the most complex natural organic mixtures, including petroleum fractions.

As early as 1965 the Singleton-Rossi method (colorimetry with phosphomolybdic-phosphotungstic acid reagents) was developed to determine the

total phenolics in wines and other foods and beverages from plants.[105] Combined with electron capture gas chromatography, α-bromo-2,3,4,5,6-pentafluorotoluene derivatization method was carried out on river water to detect phenols and mercaptans in 1968.[106] UV/Vis spectroscopy has also been applied to detect phenols in wastewater.[107] Faced with highly complex mixtures, the application of separation techniques is typically applied to reduce the number of components and thus simplify the determination of phenols and phenolic compounds. Various extraction methods, such as two-trap tandem extraction[108] or two-step liquid-liquid extraction[109] combined with HPLC have been described for detecting phenols in water samples. In addition, an amperometric biosensor based on covalently immobilized tyrosinase on the surface of graphite electrode successfully performed selective analyses of phenol and several phenolic compounds in a flow system.[110] A resonance light scattering (RLS) method involving the use of graphene quantum dots (GQDs) was carried out on different types of industrial water to analyze phenols.[111]

Analysis of phenols by GC/MS has already offered good performance. Acidic compounds including phenols are usually pretreated by different derivation methods including silylation,[112] microwave-assisted silylation,[113] acylation,[114] alkylation[115] and esterification,[116] among others[117] to form sufficiently volatile compounds before GC/MS analysis. The extreme complexity of petroleum products leads to GC×GC methods being applied to their study.[118] However, GC×GC has limits in the analysis of non-volatile compounds and is time-consuming.

It was demonstrated that 1,2-dimethylimidazole-4-sulfonyl chloride (DMISC) had high selectivity towards phenols, and the improved sensitivity of its products was obtained in LC/ESI-MS.[119] The similar method with DMISC was researched and developed for the analysis of 1-hydroxypyrene in human urine.[120] Flow injection

analysis involving acetic anhydride acetylation of phenols in a K_2CO_3-buffered alkaline medium followed by membrane introduction mass spectrometry showed fast, accurate and sensitive quantitation.[121] The analytical performance of CO_2 laser ablation of a frozen water matrix, followed by resonance-enhanced multiphoton ionization coupled with reflection time-of-flight mass spectrometry was validated and the method was successfully employed in the determination of phenol molecules in polluted water.[122]

"Petroleomics" as a discipline describes the characterization of all of the chemical constituents of petroleum at molecular level.[123] This discipline appeared soon after Fenn and Zhan first demonstrated the efficiency of ESI-MS in analysing a petroleum sample.[124] Their research revealed the extreme complexity of the polar molecules in petroleum fraction and also inspired the application of high-resolution ESI-MS to petroleomics. Ultra-high resolution instruments ($m/\Delta m50\% \approx 400{,}000$), obtainable on high-field FTICR machines, have been subsequently employed and successfully identified thousands of polar and non-polar compounds present in petroleum.[62, 98, 123, 125] It is possible for these analyses to pick out all abundant components, including phenols, but not routine enough owing to the relatively rare accessibility of FTICR instruments. However, even if these analyses obtain certain success, different types of compound with the same *m/z* are hard to distinguish. For instance, something with the formula CxHyOz with 4 or more double bond equivalents might not be a phenol - it could be an alcohol, an ether or a carbonyl.

Exploitation of the acidity of the hydroxyl group is another common way to detect phenols in petroleum. Negative ion mode ESI-MS allows detection of phenolates, which can be produced by deprotonation by strong bases including

sodium and potassium hydroxide.[126] However, deprotonation of alcohols, thiols, and naphthenic acids present in the petroleum fraction happens as well owing to the use of strong base, and the lack of selectivity is problematic for this proposed mass spectrometric analysis approach.

Ultimately, several of these techniques have proven less selective than required for the analysis of phenolic species in the highly complex matrix of petroleum fractions.[127, 128] Trace impurities including thiols, naphthenic acids, alcohols and amines existing within finished product from a refinery[129] can have a considerably adverse influence on analysis of phenolic constituents. To sum up, the ideal method for the analysis of phenolic constituents of petroleum fractions should be robust to interaction with all manner of chemical moieties, along with high selectivity, sensitivity and quantitation. One reaction involving the use of dansyl chloride (5-(dimethylamino)naphthalene-1-sulfonyl chloride) in order to form a sulfonate with phenol species which then protonated under slightly acidic conditions has been reported to detect phenols by mass spectrometry.[130] However, dansyl chloride will also derivatize thiols, so the resulting mass spectrum would have to be interpreted carefully. Beyond this difficulty, because of the abundance of basic amines or other oxygen-containing molecules in petroleum fraction, the addition of acid alone may result in a highly complex spectrum. It has been reported that dansyl chloride derivatization of ethinylestradiol (EE) followed by sensitive and specific LC-MS/MS detection works effectively.[131] This method is highly sensitive and selective which allows to quantify the EE at picogram-per-milliter concentrations in plasma sample.

In order to facilitate the selective detection of phenols in petroleum fractions through derivatization, the reaction employed in this work is that of an O-alkylation of the phenol. This reaction is known to react fairly slowly with weak bases[132] but that

can be accelerated with stronger ones. As an example, the Williamson ether synthesis[133] is largely free from side reactions and its kinetics can be altered readily through manipulation of solvent and base. The mechanism of this reaction goes by S_N2 displacement of an alkyl halide by an alkoxide (in this case a phenoxide).

To study the overall reaction, we have applied the method of charge tagging, where a charged tag is remote from the reactive site (the C-Br bond) and unreactive towards base or any other competing side reactions. In the design of the charged tag, we need to consider the efficiency of the charged tag in the ESI process. Molecules associated with charged species show very different affinities. Thus, two molecules with the same quantities do not generate the same abundance of ions. In practice, polar solvents are usually employed in ESI-MS, and large greasy and hydrophobic ions are more likely to find themselves at the surface of droplets.[134] This phenomenon -that certain ions are more likely to find themselves at the surface of the droplet - is called surface activity.[135] As a result, molecules incorporating highly surface active charged species dominate the spectra, and all the ions associated with that charged tag show the similar response factors, which make possible to relate the relative intensities to concentrations.

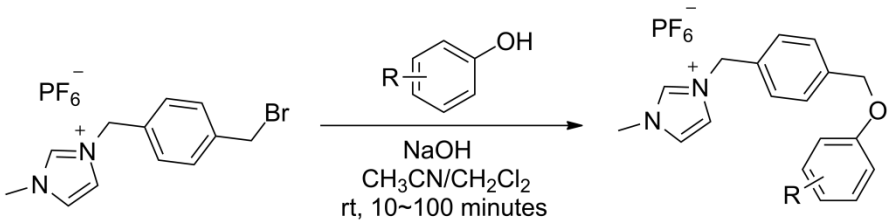

Scheme 2.1 The reaction between charged tag and substituted phenols (R=alkyl, aryl ring).

A new charge-tagged imidazolium-type complex was designed and used to react with phenols *in situ* for straightforward mass spectrometric detection in the positive ion mode (Scheme 2.1). This imidazolium-type charged tag exhibits high

surface activity as a result of its bulk and hydrophobicity, and we have paired it with a non-coordinating anion to reduce the strength of ion pairing. The Williamson ether synthesis is much faster for phenols than for alcohols, and as such acts as a selective reagent for the derivatization of phenols. The charge-tagged derivatization approach enhances analyte signal by producing very high ionization efficiency due to the intrinsic charge present on the derivatization agent.

2.2 Results and discussion

Prior to employ the charge-tagging approach on sample analysis, the samples of interest were studied by a well-established gas chromatography mass spectrometric approach. GC/MS is capable of separating components of a mixture by their physicochemical properties, and in the case of the jet fuel, the principal components are saturated hydrocarbons C_nH_{2n+2} (n = 9-16, Figure 2.2).

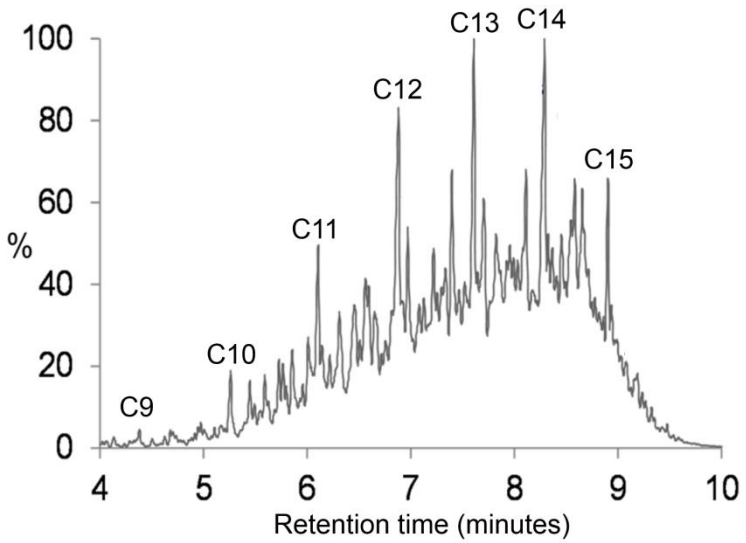

Figure 2.2 Cold EI GC/MS chromatogram of untreated jet fuel sample A. Major peaks are labelled with carbon number and correspond to the alkane (e.g. C13 = $C_{13}H_{28}$). Peak assignments were made using library matching. Phenols could not be identified in any of the sample studied.

Nonane boils at 151°C and pentadecane at 271°C, so we may expect other hydrocarbons boiling in that range to also be included in the distillation fraction.[103] It

is estimated that the mixture contains numerous other hydrocarbon products beyond isomers of the hydrocarbons themselves - substituted benzenes and naphthalenes. For example, trimethylbenzenes have boiling points around 170°C, and the boiling point of naphthalene is 218°C. At the highest elution times, we observe alkylated naphthalenes. If we consider the phenols likely to appear in the boiling point range 150-270°C as shown in Table 2.1, we would expect to see phenol itself (b.p. 182°C) and variously alkylated versions, such as 2,5-dimethylphenol (b.p. 212°C). Naphthol sublimes at 288°C, and its alkylated derivatives have boiling points higher than this as shown in Table 2.2.[103] However, the resulting GC/MS spectrum is sufficiently dominated by the hydrocarbons that the small amounts of phenols and naphthols could not be picked out in this simple analysis. The application of high resolution mass spectrometry or GC×GC methods would be required to distinguish them.

Table 2.1 The Boiling Points of alkylated phenols.

R group	Number of R group	Mol.Wt. of alkylated phenols	Boiling point (°C)
CH_3	0	94.1	182
CH_3	1	108.3	191~202
CH_3	2	122.2	204~218, 277
CH_3	3	136.1	213~249
CH_3	4	150.2	224~251
CH_3	5	164.2	127, 233~262
CH_3	6	178.3	138, 247~262
CH_3	7	192.3	NA

Table 2.2 The Boiling Points of alkylated naphthols.

R group	Number of R group	Mol.Wt. of alkylated naphthols	Boiling point (°C)
CH_3	0	144.2	286
CH_3	1	158.1	304
CH_3	2	172.1	315
CH_3	3	186.1	335
CH_3	4	200.2	341-343
CH_3	5	214.1	357

The cationic charged tag used in this study was prepared by alkylation of methylimidazole using 1,4-di(bromomethyl)benzene. It was paired with the hexafluorophosphate anion ($[PF_6]^-$) through salt metathesis with $NaPF_6$ of the resulting bromide, which generated the more soluble hexafluorophosphate salt. This compound can react with base and a phenol to produce an aryl ether (Scheme 2.1). Both the charged tag and the product of its reaction with phenol were fully characterized, including by X-ray crystallography (Figures. 2.3 and 2.4).

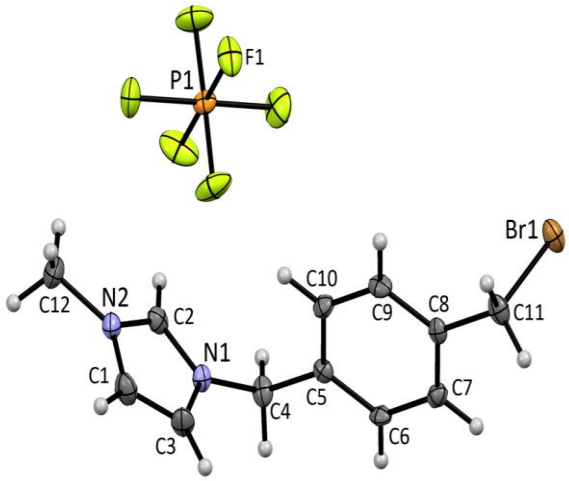

Figure 2.3 X-ray crystal structure of charged tag compound. Key bond lengths and angles: average P-F: 1.5908(18) Å; N1-C1: 1.327 (3)Å; N1-C2: 1.373(3) Å; N1-C4:1.462 (3)Å; N2-C1: 1.317(3) Å; N2-C3: 1.364(4) Å; N2-C12: 1.469(3) Å; Br1-C11: 1.971(3) Å; C8-C11-Br1: 109.88(17)°; N1-C4-C5: 112.0(2)°.

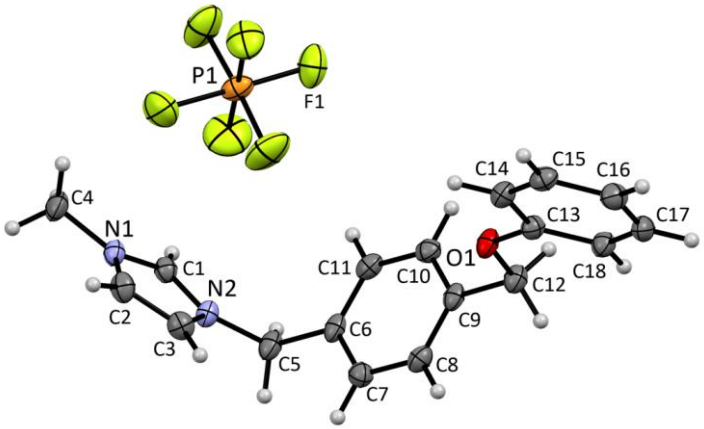

Figure 2.4 X-ray crystal structure of the product of the reaction between the charged tag and phenol. Key bond lengths and angles: average P-F: 1.5845(2) Å; N1-C1 :1.319(3) Å; N1-C2:1.372(4) Å; N1-C4: 1.459(4) Å; N2-C1: 1.325(4) Å; N2-C3: 1.380(4) Å; N2-C5:1.472(3) Å; O1-C13: 1.371(3) Å; O1-C12: 1.435(3) Å; O1-C13: 1.371(3) Å; C13-O1-C12: 117.6(2)° ; N2-C5-C6: 111.6(2)°.

The reactivity of the charged tag was studied by PSI ESI-MS in positive ion mode. They were done by adding the charged tag into a solution containing NaOH and phenols and monitoring the change in speciation by PSI ESI-MS. A variety of experiments were conducted with different phenols individually: phenol, o-cresol, 2,3-dimethylphenol, 1-naphthol and 2,4-dimethylphenol (Figure 2.5).

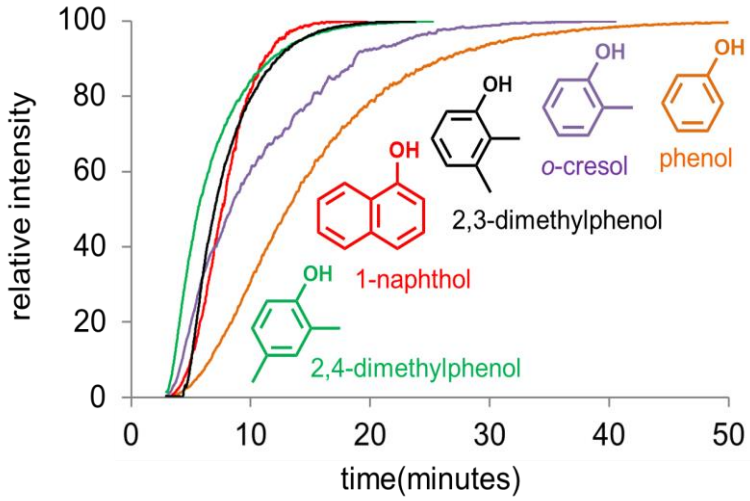

Figure 2.5 O-alkylation products relative intensity increases over time, monitored by PSI online monitoring (CH_3CN, RT). Five different experiments, all set to the same addition time (3 minutes).

What we observe is that 1-naphthol and the two dimethylphenols (2,3- and 2,4-) were the fastest reacting phenols. All three of these starting phenols turned into products completely within 10 minutes in what followed pseudo-first order kinetics. The *ortho*-cresol was slightly slower (first order, $t_{1/2}$ = 5.5 min) and phenol was the slowest (also first order, $t_{1/2}$ = 10.4 min). This evidence suggests that the electronic property exerts more influence on the reaction than steric bulk. The more electron-rich phenol, the faster the reaction, which is due to the basicity of the phenol paralleling its efficacy as a nucleophile.

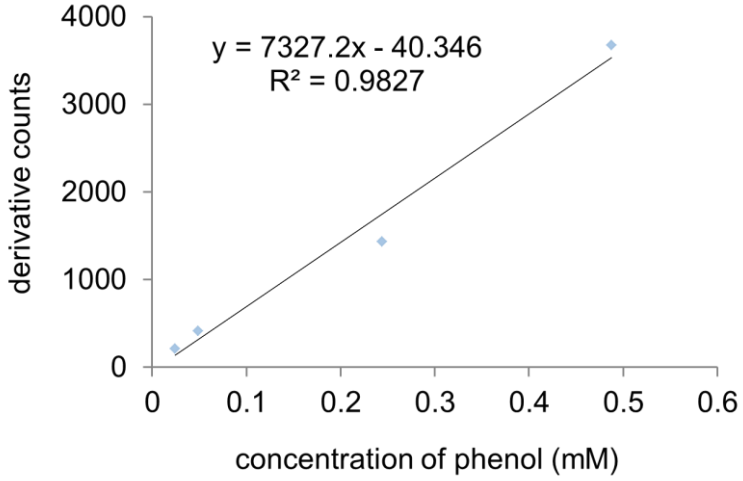

Figure 2.6 Response of derivative following the reaction between charged tag (0.488 mM) and phenol.

The method detection limit was then established on the noise present in a method blank sample including solvent and 0.488 mM of charged tag. The response of derivative compound was found to be linear to micromolar quantities of charged tag. The derivatization process is limited by reactivity and concentration of target analytes in addition to variation in the sample matrix; therefore, the method detection limit defined here is an approximation only and will vary between samples and matrices. The general method limit was established based on a reaction with 0.488 mM of charged tag and phenol (see Equation 1).[44] The response of the lowest

identifiable derivative was then used to establish the limit detection (3 times the signal-to-noise ratio) and quantitation (10 times the signal-to-noise ratio) for the jet fuel samples. The limit of detection for phenol product was examined and found to be 18 counts (8.0 µM) with a limit of quantitation of 60 counts (26.7 µM). (Figure 2.6)

Concerned about the complexity of jet fuel samples, we first mixed a quantity of a jet fuel sample with NaOH to examine the speciation under negative ion mode by ESI-MS and to see whether the phenol components were discernable or not *without* a charged tag. The resulting spectrum (Figure 2.7) is typically dominated by trace amounts of other anions (such as naphthenic acids, or the phenol antioxidants added to rubber septa), and the spectrum clearly shows that speciation contains no simple phenols (in ESI-MS, ions with even-numbered *m/z* values implicate the presence of atoms other than just C, H and O).

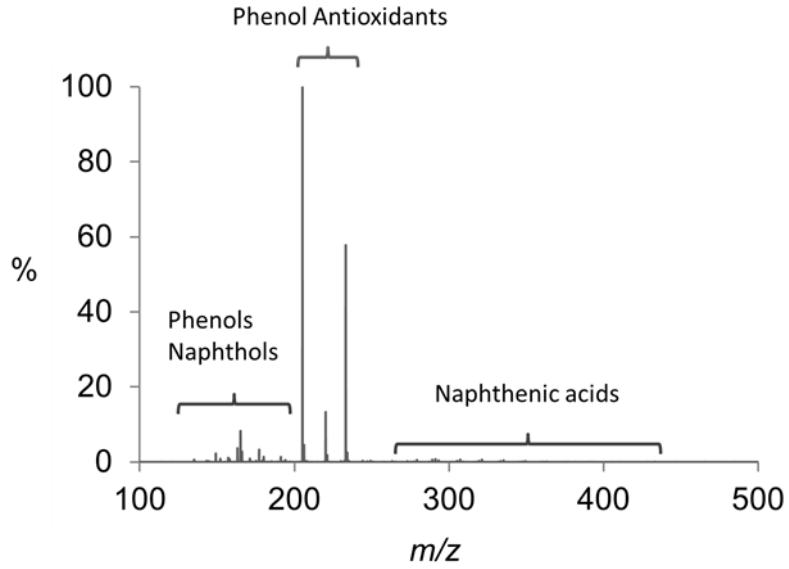

Figure 2.7 Negative ion mode ESI-MS (CH_3CN/CH_2Cl_2, v/v =1:3) of sample B after NaOH addition.

We then examined a solution of jet fuel in positive ion mode by ESI-MS. It unexpectedly showed the presence of polyethylene glycols (PEGs) in the range *m/z*

250-550, corresponding to the Na^+ and K^+ adducts of $H(OCH_2CH_2)_nOH$ (n = 3-13) (Figure 2.8). Addition of NaOH resulted in a decrease in intensity of the potassiated PEGs (Figure 2.9). We checked blanks and they contained no PEGs, which is proof that PEGs came from the sample itself, and they probably were introduced in low quantity at some stage during the extraction or refining process. Furthermore, no other peaks of note were observed, indicative of the low amount of basic material in the sample (aside from the PEGs).

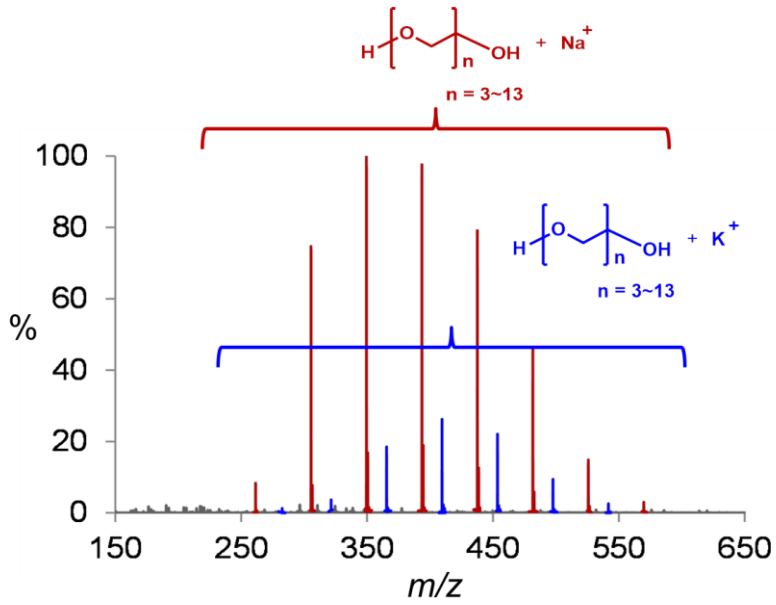

Figure 2.8 Positive ion mode ESI-MS (CH_3CN/CH_2Cl_2, v/v=1:3) of sample B after NaOH addition. By far the most prominent ions were based on polyethylene glycols.

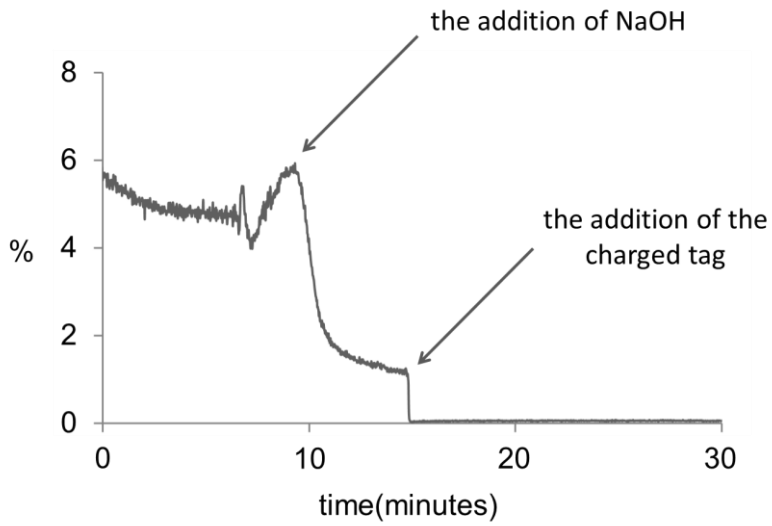

Figure 2.9 Relative intensity of PEG (K^+ adduct of $H(OCH_2CH_2)_5OH$) changes over time, monitored by PSI online monitoring. Sample B reacted with charged tag under the base condition, solvent is CH_3CN/CH_2Cl_2 (v/v =1:3). The addition of NaOH makes the K^+ adducts of PEGs decrease but increase the Na^+ adducts of PEGs, and because of the high surface activity of the charged tag, the addition of charged tag suppresses the appearance of PEGs.

Despite the apparent prominence of the peaks above (refer to Figure 2.8) and the good signal-to-noise ratio (S/N), PEGs plummet to the baseline when the charged tag is injected in this mixture. This occurrence is quite reasonable considering the purposefully-designed high surface activity of the charged tag. After the addition of the charged tag, it immediately begins reacting with the trace levels of phenols present to generate an assembly of different but related species (Figure 2.10). The most prominent of these are derived from variously alkylated phenols, of general formula $C_6H_5(CH_2)_nOH$ (where n = 2-9). This distribution reaches a maximum at n = 5. It is not possible for us to differentiate between isomers, so for example the n = 3 compound could include contributions from five different trimethyl phenols, ten ethylmethyl phenols, or three propyl phenols. In the same mass range, we also observe other two series of compounds with varying structural possibilities. All of these compounds are in a predictable mass range for jet fuel. However, there exists an additional pair of series of related compounds approximately 150 Da higher in mass

(from 450 Da to 550 Da). The combinatorial possibilities of these series are sufficiently high, but we still endeavored to make structural assignments for them.

The instrument used above has a QToF mass analyzer whose resolutions is up to 30000. In order to get more accurate *m/z* to help us find the formulae, the same sample was diluted with acetonitrile to 10 ppm and analysed by the Thermo Q-Exactive ESI-MS with an orbitrap mass analyzer which has very high resolution (upwards of 100 000). The accurate *m/z* of these five series, assumed compositions and relative accuracy were shown in the Table 2.3 to Table 2.7. Besides phenols, we observed a series of alkylated thiols of general formula $HS(CH_2)_nH$ (where n = 9-14) of varying isomeric composition. A related series of general formula $HS(CH)_2(CH_2)_n$ (where n = 6-11) was also observed, which may be alkylated thiols with one double bond equivalent. An additional pair of series of related compounds which are in range of 450 Da to 550 Da might correspond to $C_6H_4OHS(CH_2)_nH$ (n = 10-17) and $C_6H_4OHS(CH)_2(CH_2)_nH$ (n = 9-15). These compounds have 4 and 5 double-bond equivalents respectively, indicating that they may contain one aromatic ring. One of the most compositional possibilists is phenol with thiol group.

Table 2. 3 Experimental results from orbitrap experiment and relative assumption (black series).

Experimental *m/z*	Calculated *m/z*	Composition	Accuracy (ppm)
307.18045	307.18104	$C_{20}H_{23}N_2O$	-1.920691459
321.19610	321.19669	$C_{21}H_{25}N_2O$	-1.836880698
335.21160	335.21234	$C_{22}H_{27}N_2O$	-2.207555963
349.22735	349.22799	$C_{23}H_{29}N_2O$	-1.832613703
363.24297	363.24364	$C_{24}H_{31}N_2O$	-1.844492033
377.25875	377.25929	$C_{25}H_{33}N_2O$	-1.431376282
391.27431	391.27494	$C_{26}H_{35}N_2O$	-1.610121006
405.29011	405.29059	$C_{27}H_{37}N_2O$	-1.184335417

Table 2. 4 Experimental results from orbitrap experiment and relative assumption (blue series).

Experimental *m/z*	Calculated *m/z*	Composition	Accuracy (ppm)
345.23592	345.23645	$C_{21}H_{33}N_2S$	-1.53517973
359.25158	359.25210	$C_{22}H_{35}N_2S$	-1.447451525
373.26729	373.26775	$C_{23}H_{37}N_2S$	-1.232359345
387.28297	387.28340	$C_{24}H_{39}N_2S$	-1.11029804
401.29868	401.29905	$C_{25}H_{41}N_2S$	-0.922005671
415.31431	415.31470	$C_{26}H_{43}N_2S$	-0.939046944

Table 2. 5 Experimental results from orbitrap experiment and relative assumption (green series).

Experimental *m/z*	Calculated *m/z*	Composition	Accuracy (ppm)
329.20455	329.20514	$C_{20}H_{29}N_2S$	-1.79219559
343.22030	343.22080	$C_{21}H_{31}N_2S$	-1.456788167
357.23594	357.23645	$C_{22}H_{33}N_2S$	-1.427625876
371.25174	371.25210	$C_{23}H_{35}N_2S$	-0.969691485
385.26723	385.26775	$C_{24}H_{37}N_2S$	-1.349710688
399.28310	399.28340	$C_{25}H_{39}N_2S$	-0.751346036

Table 2. 6 Experimental results from orbitrap experiment and relative assumption (red series).

Experimental *m/z*	Calculated *m/z*	Composition	Accuracy (ppm)
451.27955	451.27831	$C_{28}H_{39}N_2OS$	2.747750053
465.29411	465.29396	$C_{29}H_{41}N_2OS$	0.322376847
479.30943	479.30961	$C_{30}H_{43}N_2OS$	-0.375540144
493.32497	493.32526	$C_{31}H_{45}N_2OS$	-0.587847458
507.34077	507.34091	$C_{32}H_{47}N_2OS$	-0.275948573
521.35629	521.35656	$C_{33}H_{49}N_2OS$	-0.51787974
535.37194	535.37221	$C_{34}H_{51}N_2OS$	-0.50432203

Table 2. 7 Experimental results from orbitrap experiment and relative assumption (purple series).

Experimental *m/z*	Calculated *m/z*	Composition	Accuracy (ppm)
463.27800	463.27831	$C_{29}H_{39}N_2OS$	-0.669144213
477.29366	477.29396	$C_{30}H_{41}N_2OS$	-0.628543466
491.30917	491.30961	$C_{31}H_{43}N_2OS$	-0.895565629
505.32479	505.32526	$C_{32}H_{45}N_2OS$	-0.930094015
519.34062	519.34091	$C_{33}H_{47}N_2OS$	-0.558400069
533.35642	533.35656	$C_{34}H_{49}N_2OS$	-0.262488569
547.37206	547.37221	$C_{35}H_{51}N_2OS$	-0.274036565

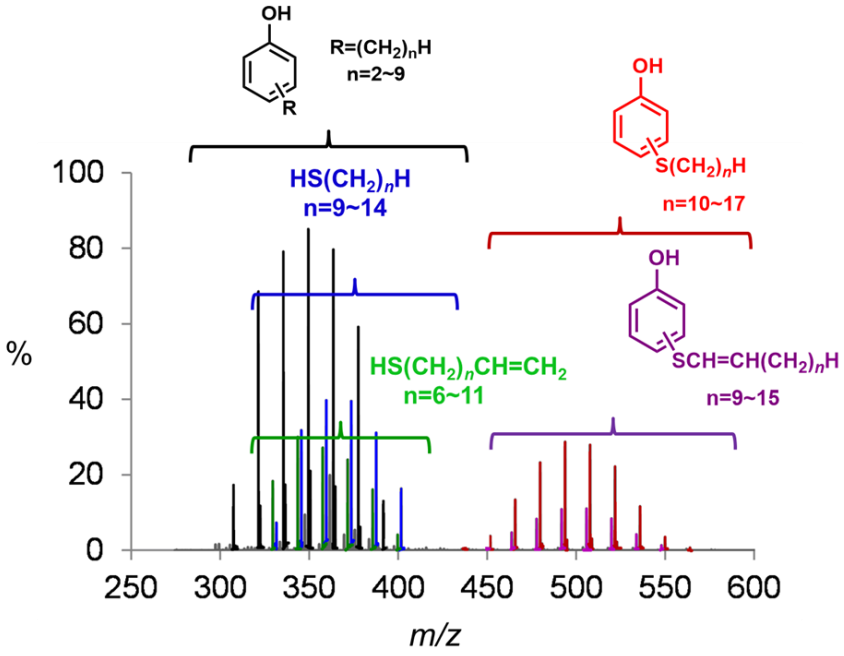

Figure 2.10 Positive ion mode ESI-MS (CH_3CN/CH_2Cl_2, v/v=1:3) of sample B after NaOH and charged tag addition. When reaction finished, the final spectrum contains the leftover charged tag after all phenol reacted. There are 5 different phenol products series. The series are all labeled in different colors. The relative intensity shown on the spectrum can reflect the phenol concentration in the jet fuel sample.

We also notice that the phenolic compounds and some carboxylic acids are main acidic oxygen-containing compounds that may present in the same distillated fraction of petroleum (< 350°C).[63] Meanwhile, the charged tag used in this study is the primary alkyl halide. Under the base condition, naphthenic acids give carboxylate as nucleophiles which replace an alkyl bromide on the charged tag to form esters. The mechanism here undergoes S_N2 reaction. From the above, even though the combinatorial possibilities of these *m/z* are sufficiently high, naphthenic acids are very likely to be present. The reaction between the charged tag and cyclohexaneacetic acid was conducted to find out the reaction conditions (Figure 2.11). The NaOH was mixed with naphthenic acids to get carboxylate anion. The addition of charged tag found that the reaction didn't happened under RT, then by increasing the reaction temperature to 60°C, the reaction occurred.

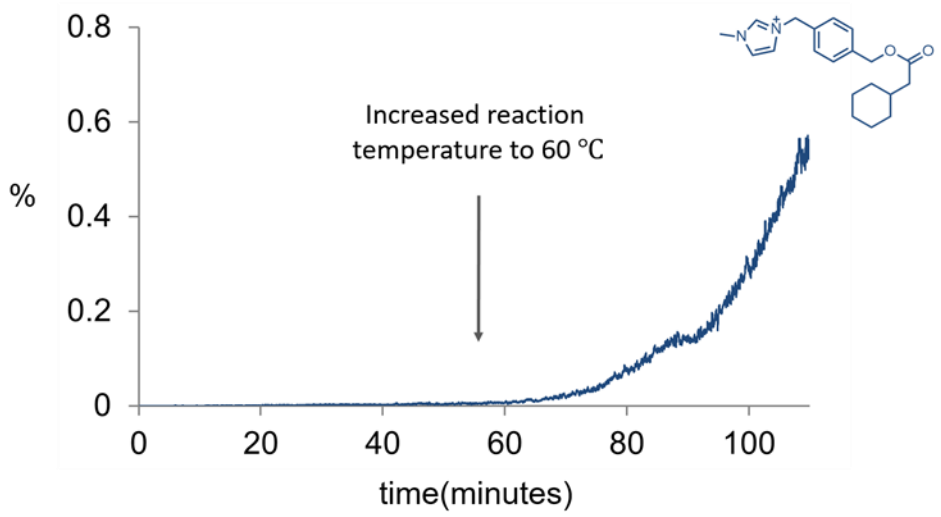

Figure 2.11 The substitution reaction between charged tag, cyclohexaneacetic acid and NaOH, monitored by PSI online monitoring (solvent: CH_3CN: CH_2Cl_2= 1:3) in positive ESI-MS mode. The reaction temperature was RT at the beginning and then increased to 60℃ at 55 minutes.

We conducted reactions between different naphthenic acids, charged tag and NaOH individually to study the reactivity of charged tag: cyclopentanecarboxylic acid, cyclohexanepentanoic acid and cyclohexaneacetic acid (Figure 2.12). None of the three naphthenic acids turned into products completely after the reaction reached equilibrium. The half time of cyclohexaneacetic acid is 8.1 minutes, cyclopentanecarboxylic acid is 14.2 minutes, and cyclohexanepentanoic acid is slowest which is 20.1 minutes. We also compared the reactivity of charged tag between phenol and naphthenic acid (Figure 2.13). The charged tag was added at the solution containing phenol, cyclohexaneacetic acid and NaOH. The reaction temperature was under 60℃. Phenol turned into product completely within 10 minutes and only 0.02% cyclohexaneacetic acid was turned into product after 40 minutes under 60℃. Reaction temperature is a crucial factor. Based on the study of reactivity of the reaction between and naphthenic acids and charged tag, we found these series of compounds that correspond to $C_{15}H_{13}(CH_2)_nOH$ (n = 2-12) and $C_{16}H_{13}(CH_2)_nOH$ (n = 2-12) don't behave chemically as naphthenic acids. We assume

instead that these compounds may contain two aromatic rings with at least one phenolic –OH group.

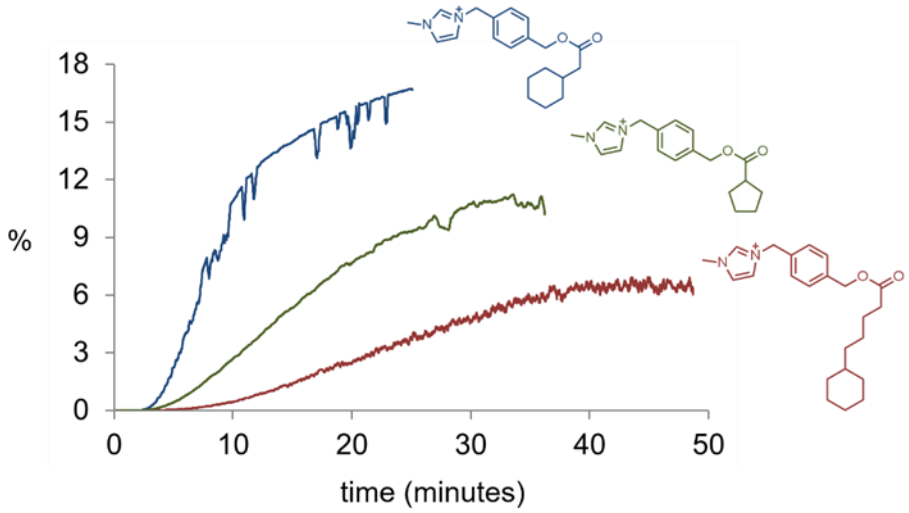

Figure 2.12 The substitution reaction products relative intensity increases over time, monitored by PSI online monitoring (solvent: CH_3CN: CH_2Cl_2= 3:1, 60°C) in positive ESI-MS mode. Three different experiments, all set to the same addition time (2 minutes).

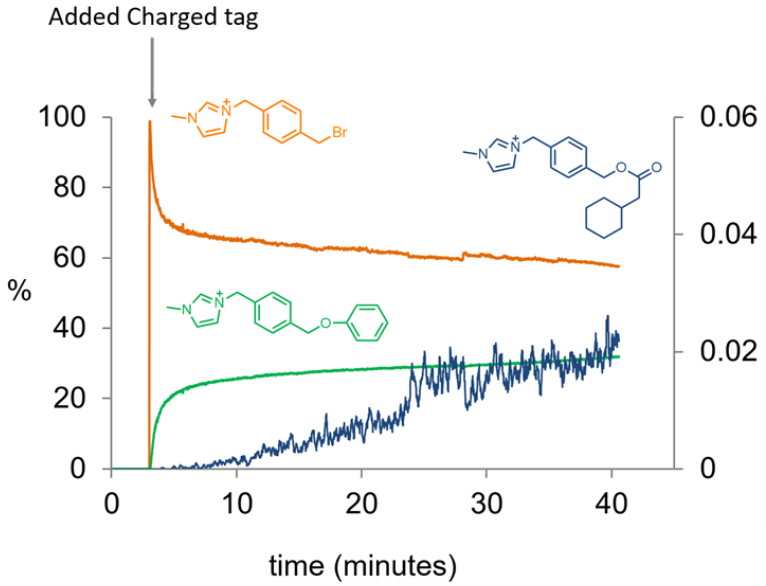

Figure 2.13 The reaction between charged tag, phenol, cyclohexaneacetic acid and NaOH, monitored by PSI online monitoring (solvent: CH_3CN: CH_2Cl_2= 3:1, 60°C) in positive ESI-MS mode.

In a refinery environment, petroleum streams undergo various processes to remove undesired contaminants, and phenols fall into this category of compound. Figure 2.14 outlines the changes in detected phenols depending on the treatment. Untreated sample C is the same as shown in Figure 2.10, but the unreacted charged

tag is also shown in the spectrum to provide an indication of the relative abundance of the products. Clay treatment (sample D) exhibits reduced phenol concentrations (by about 20-50%, depending on the phenol series being measured). Silica gel treatment (sample E) removes nearly all phenols as does lab clay (sample F). Washing the lab clay with pentane (sample G) removed some of the phenols from the clay, or in the case of toluene (sample H), a lot. None of the higher mass phenols were removed however, suggesting that these had a higher affinity for the lab clay than the lower mass phenols.

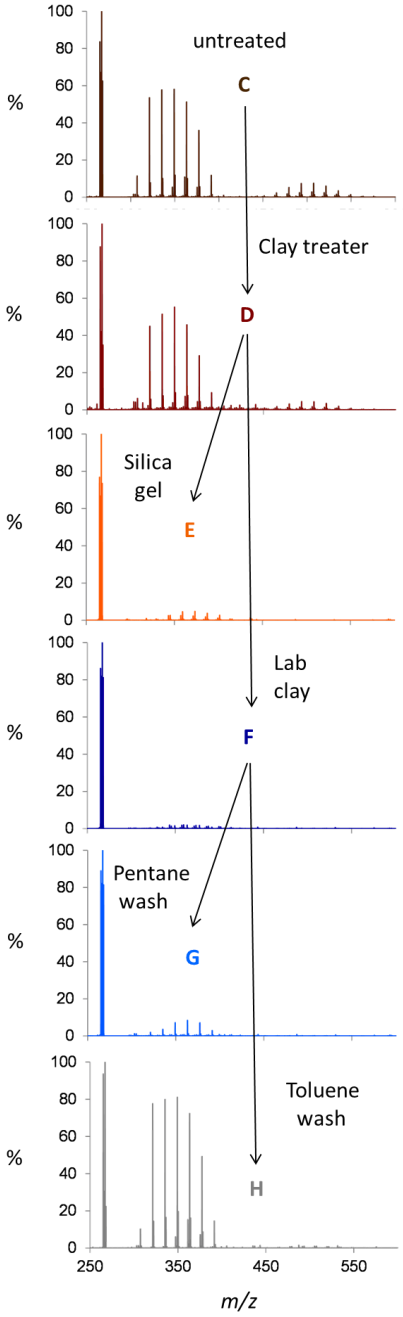

Figure 2.14 Positive ion mode ESI-MS of selective phenol analysis of a series of jet fuel samples. The untreated sample (C) starts with clay treatment, followed by treatment with either lab clay or silica gel. Then the lab clay is recovered by washing by pentane and toluene.

In order to test the efficiency of this methodology further, a variety of in-house experiments with the jet fuel were conducted. The jet fuel was left to stir for 40 hours in the presence of alumina and jet fuel samples were examined with and without alumina treatment. The comparison spectrum below (Figure 2.12) points to that

alumina treatment was able to remove nearly all of the higher mass phenols and about three quarters of the lower mass phenols.

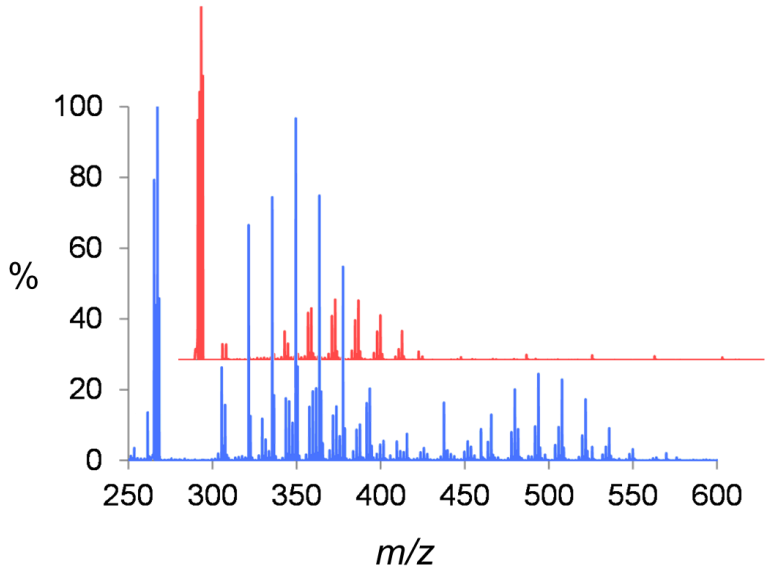

Figure 2.15 Positive ion mode ESI-MS of Jet fuel sample B before (blue) and after (red) stirring in the presence of alumina for 40 hours.

2.3 Conclusions

We have developed a rapid, selective and chromatography-free mass spectrometric analysis of a highly complex matrix. While derivation is common in ESI-MS, this methodology in petrolemics is less commonly explored. Additionally, we are looking to use relatively simple equipment, syntheses, and reactions. Specifically, it entails the selective identification of phenols in petroleum fractions using charged tags and electrospray-ionization mass spectrometry. The results from analysis of jet fuels at different treatment stages are consistent with these treatments being effective though not quantitative removers of phenols from the petroleum matrix.

This approach may be further extended and developed for other classes of compounds and applied to petroleum processing, rendering this technique a powerful

method to selectively identify impurities and contaminants. We will modify these reactions (if necessary, use different ones altogether) to make them amenable to a different solvent environment, and design new charge-tagged versions of the substrates.

2.4 Experimental

All solvents were HPLC grade. Acetonitrile and dichloromethane were purchased from Sigma-Aldrich, and hexane and tetrahydrofuran were obtained from fisher Chemicals and used as received. 1-methylimidazole, α,α′-dibromo-p-xylenesodium hexafluorophosphate were purchased from Sigma-Aldrich and used as received without further purification. All the jet fuel samples were provided by Esso Imperial oil company and used as received. 1H NMR spectra were recorded on a Bruker AVANCE 300 MHz operating at 300.13 MHz for ^{1}H. Chemical shifts are reported in ppm at ambient temperature. ^{1}H chemical shifts are referenced to residual protonated solvent peaks at 7.26 ($CHCl_3$) and 3.31 (CH_3OD). ESI-MS of synthetic products were collected in the positive ion mode on a Waters Micromass Q-ToF *micro* mass spectrometer using solutions prepared in acetonitrile and dichloromethane. Thermo Q-Exactive mass spectrometer contains an electrospray ionization source and an orbitrap mass analyzer. Waters Q-ToF-Micro tandem mass spectrometer contains an electrospray ionization source and involves both a quadrupole and a time-of-flight mass analyzer. Its detector is MCP. Capillary voltage, 3000 V; Cone voltage, 16 V; Extraction voltage, 0.5 V; Source temperature, 90°C; Desolvation temperature, 190°C; Cone gas flow rate, 100 L/h; Desolvation gas flow, 200 L/h; collision voltage, 2 V (for MS experiments); collision voltage, 2-80 V (for MS/MS experiments); MCP voltage, 2700 V. PSI experiments used identical instrument settings. For PSI experiments, the reaction vessel was pressurized using 3 psi of nitrogen gas. Reflux

was achieved via mechanical stirring provided by magnetic stirring hot plate and stir bar. Assignments were made with the help of chemcalc.org.[136] Cold EI GC/MS data were obtained on an AXION iQT GC/MS instrument from Perkin Elmer (Waltham, Massachusetts, USA) which equipped with a Clarus 680 gas chromatogram from Perkin Elmer (Waltham, Massachusetts, USA). The mass spectrometer was tuned using perfluorotributylamine (PFTBA) solution. The Clarus 680 GC was equipped with an autosampler with two injection systems (injector A & injector B). Injector B is programmable split/splitless (PSS) injector which is connected with a PerkinElmer EliteTM-5MS (Perkin Elmer, length 30 m, inner diameter 250 mm, film thickness 0.25 µm) capillary column which is a mid-polar with cross bonded with 5% diphenyl 95% dimethyl polysiloxane. The injector A is split/splitless (PSS) injector which is connected with a Rxi®-5HT (from RESTEK, length 15 m, inner diameter 320 mm, film thickness 0.1 µm) column which is cross bonded with diphenyl dimethyl polysiloxane. The carrier and makeup gas was helium (99.999% purity). The jet fuel sample A was diluted 100 times with hexane before analysis. After that the sample (0.5 µL) was analyzed through injector B, set at 220°C. The GC column oven temperature program was 40°C for 1 minute, which was followed by ramping at 20 °C/min to a final temperature of 260°C, which was held for 1 minute. The transfer line temperature was 250°C and source temperature was 200°C. Make up gas flow was 50 mL/min. Axion eCipher software was used for post processing data application for identification of compounds.

Synthesis of 3-(4-(bromomethyl)benzyl)-1-methylimidazolium hexafluorophosphate. [137] 1-methylimidazole (0.46 mL, 5.77 mmol) was reacted with excess α,α′-dibromo-p-xylene (2.049 g, 7.76 mmol) through reflux under argon about 14 hours in 50 mL of tetrahydrofuran. A white powder is recovered from acetonitrile

through vacuum filtration and vacuum dried for 1 day. The 3-(4-bromomethyl)benzyl)-1-methylimidazolium bromide (0.220 g) and 25 mL of 50% (v/v) aqueous methanol were added to a round bottomed flask, followed by sodium hexafluorophosphate (0.330 g). The solution was stirred for 12 hours. A white powder was recovered from the reaction solution via vacuum filtration. 0.686 g (28.9%) of final product was obtained. ^{1}H NMR (300 MHz, $CDCl_3$): δ ppm: 3.93 (s, 3H), 4.59 (s, 2H), 5.41 (s, 2H), 7.61-7.40 (m, 6H), 8.95 (s, 1H). QTOF ESI(+): $[M]^+$ *m/z* 265.1; ESI(-): $[M]^-$ *m/z* 145.1.

Synthesis of 1-methyl-3-(4-(phenoxymethyl)benzyl)-1H-imidazol-3-ium hexafluorophosphate(V). 3-(4-(bromomethyl)benzyl)-1-methylimidazolium hexafluorophosphate (0.100 g, 0.243 mmol) was reacted with excess phenol (0.0343 g, 0.365 mmol) and excess sodium hydroxide (0.194 g, 4.86 mmol) was in a round bottom flask at room temperature for 30 minutes in 5 mL acetonitrile. The reaction solution was filtered and the filtrate was vacuum dried and washed with ether and vacuum dried. The powder was redissolved in a minimum amount of acetonitrile and white crystals were precipitated after leaving the solution at 4 °C overnight. The crystals were recovered from reaction solution through vacuum filtration, 0.018g (17%) of final product obtained. 1H NMR (300 MHz, $CDCl_3$): δ ppm: 3.90 (s, 3H), 5.05 (s, 2H), 5.29 (s, 2H), 6.94-7.50 (m, 11H), 8.64 (s, 1H). QTOF ESI(+): $[M]^+$ *m/z* 279.4.

ESI-MS reaction monitoring using pressurized sample infusion. As described elsewhere,[30, 31] a 20 mL Agilent headspace vial was filled with 15 mL the mixture of acetonitrile and CH_2Cl_2 (v/v = 4:9) and between 20-30 equivalents of sodium hydroxide. The vial was equipped with a magnetic stirring bar, and rubber stopper wrapped by Taegaseal PTFE tape. PEEK tubing was fed from the vial to the ESI-MS

source and the headspace vial pressurized using 3 psi of nitrogen gas. The solution end of PEEK tubing was protected with a cotton filter system to avoid the tube being blocked by any insoluble substances in jet fuel. The solution was stirred at room temperature. The 2 mL analytes of interest were injected via syringe.

Chapter 3 Naphthenic acids-selective mass spectrometric analysis of petroleum fraction

3.1 Introduction

Most petroleum contains oxygen compounds in widely varying amounts from 0.1% by weight to around 3% by weight.[132] The structures of these compounds are complex and varied but a well-known unwanted component of the distillates of petroleum is alkyl-substituted acyclic and cycloaliphatic carboxylic acids, which are known as "naphthenic acids".[63] Although the definition used to describe this type of compounds in petroleum is very loose, the term "naphthenic acids" generally refers to a mixture of cycloaliphatic carboxylic and alkyl-substituted acids. They have the simplified chemical formula $C_nH_{2n+Z}O_2$, where n is the number of carbons and Z can be zero or a negative integer to show the hydrogen deficiency due to the presence of multiple rings. The carboxylic acid group (COOH) is often attached to side chains instead of the cycloaliphatic ring.[138] Some representative structures for naphthenic acids are shown in Figure 3.1.

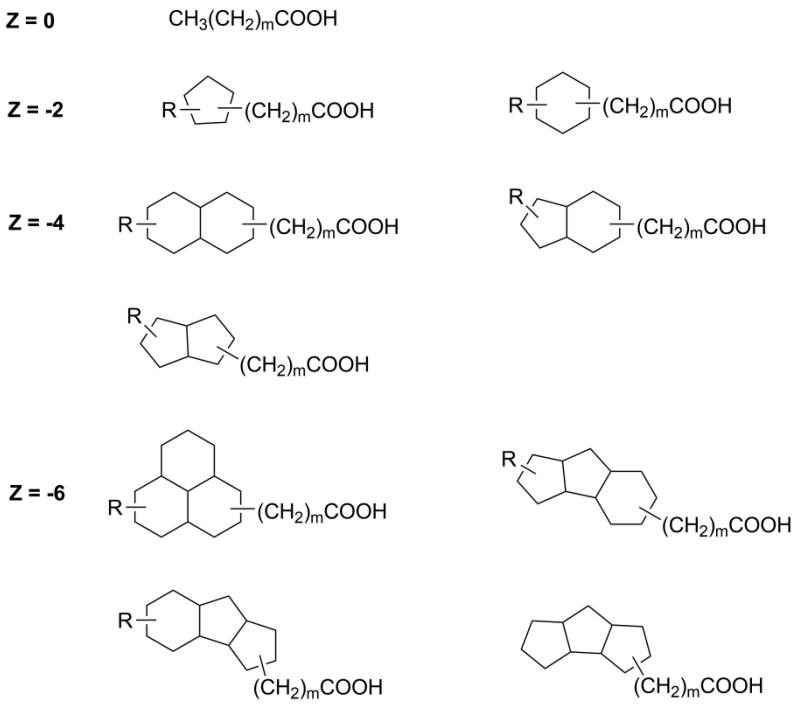

Figure 3.1 Sample naphthenic acid structures where R is an alkyl chain, Z is the hydrogen deficiency, and m is the number of CH_2 units.

Naphthenic acids are naturally present in petroleum.[139] However, the composition and concentration of naphthenic acids varies considerably depending on the source of crude oil. These acids are highly corrosive and special steel alloys need to be applied to refining equipment to avoid corrosion damage.[64] Slavcheva *et al.* reported the phenomenon of naphthenic acids corrosion (NAC). Increasing total acid number (TAN) usually increases the rate of corrosion. The TAN value is a measurement of total acidity, but naphthenic acids are not the only acid present in petroleum.[140] The alkyl chain length of naphthenic acids is also a factor to influencing corrosiveness according to the research performed by the Turnbull group.[141] However, the NAC process is still not completely understood.

During the extraction of petroleum, it is possible for naphthenic acids to enter surface water. Wastewater from petroleum refineries may also contain naphthenic acids;[142] for instance, tailing pond waters in the Athabasca oil sands contains naphthenic acids at around 81 mg/L due to the extraction of bitumen from Athabasca

oil sands.[143] It is well known that naphthenic acids are toxic to fish and other organisms.[142] Their low aqueous solubility and medium soil sorption result in low bioavailability in aquatic environment which can be used to identify the extent of maturation of the oil source.[144] In addition, naphthenic acids have good weathering resistance, so they are well suited for use in marking fuel spills.[145]

Naphthenic acids also have some commercial value. Naphthenic acids are formed following extraction and acidification of petroleum distillates. However, the composition and purity of their commercial products are largely based on different oil sources and various processing methods. The salts of naphthenic acids, naphthenates, have industrial applications including use as corrosion inhibitors and oil drying agents for painting. Napalm is the combination of palmitic acid, aluminium naphthenate and petroleum that was widely used as an incendiary device during World War II and the Vietnam War. Cobalt salts of naphthenic acid are used as an adhesion promoter in the tire industry. In addition, naphthenic acid esters have a variety of applications such as surfactants, lubricants and plasticizers for polyvinyl chloride (PVC) resins. The reduction products of naphthenic acids or naphthenic acids esters, naphthenic alcohols, can be used as surfactants and components of lubricants.[146]

Crude oil is an incredibly confounding matrix. Characterization and analysis of naphthenic acids in petroleum is not only extremely necessary but highly complicated. Pyrroles, thiophenes and phenols are also found in addition to naphthenic acids in fractions obtained from petroleum.[147] To date, some methods have proven to be insufficient for the identification of individual naphthenic acids. However, various analytical methods have been developed to enable a better understanding of the composition of naphthenic acids in petroleum.

The standard approach for quantitative analysis of naphthenic acids in oil sand industry is Fourier transform infrared (FTIR) spectroscopic analysis.[148] This method involves quantitatively extracting the naphthenic acids into dichloromethane and measuring the absorbance of the carboxylic groups in the extract using FTIR spectroscopy.[149] The other common method is GC analysis. In this method, naphthenic acids in laboratory cultures were derivatized into their methyl esters and stearic acid was used as an internal standard for GC analysis.[150] This GC method was improved by Jones *et al*., and they successfully applied their method to analyse naphthenic acids within crude oil.[151] HPLC methods are also currently used to detect naphthenic acids in natural environments. By adding 1-ethyl-3-(3-dimethylaminopropyl)carbodiimide (EDC), naphthenic acids were derivatized to form 2-nitrophenylhydrazine (NPH) which are detected by HPLC with a UV-Vis detector.[152, 153, 154] Yen *et al.* improved this HPLC method.[155] In this modified method, the detection limit was reduced from 15 mg/L to 5 mg/L (for naphthenic acids). In addition, they compared the modified HPLC method with the standard FTIR method, which showed the greater efficiency of the HPLC method.

The methods mentioned above are generally employed to determine the total naphthenic acid concentration. Unfortunately, it is not sufficient to illustrate the corrosiveness and toxicity of naphthenic acids in the petroleum. A variety of studies using sophisticated MS methods have been attempted to order to determine the molecular structure and composition of the naphthenic acids mixtures.

EI ionization was used by Seifer *et al.* in an early attempt to characterize naphthenic acids and it provided evidence for the complexity of naphthenic acids as there were about 1500 acids detected.[147] However, hard ionization techniques produce similar fragments for naphthenic acid mixtures leading to very complicated spectra.

Soft ionization methods are a powerful tool to simplify the mass spectra. For instance, CI mass spectrometry with fluoride ions was demonstrated as an efficient approach to detect naphthenic acids in crude oils and refinery wastewaters.[156] A method based on FAB-MS has also been employed to analyse naphthenic acids from crude oil.[157] Bunce and co-workers used ESI-MS in negative ion mode to study naphthenic acids from oil sands tailing water.[158] CI, fast ion bombardment (FIB), atmospheric pressure chemical ionization (APCI), and ESI (in both negative and positive ion modes) methods were compared for determining the molecular distribution in naphthenic acids extracted from crude oil and commercial preparations.[159] Gabryelski and Froese in 2003 coupled negative ion ESI ionization to high-field asymmetric waveform ion mobility spectrometry (ESI-FAIMS) with either quadrupole or ToF MS to analyse naphthenic acids in oil sands tailing water.[160] In their method, the detection limit was 1 mg/L naphthenic acid in methanol.

To date, GC/MS approaches have been the most common. Although complete separation of naphthenic acid mixtures has not been achieved by GC before mass spectrometric detection, the strategy of derivation of naphthenic acids followed by GC/MS analysis has been used successfully to reveal the molecular structures of some naphthenic acids. For example, combined with GC/MS, *N*-methyl-*N*-(*t*-butyldimethylsilyl)trifluoroacetamide (MTBSTFA) derivatisation was carried out to analyse naphthenic acids in wood decay fungicides.[161] Similarly, Caramão and co-workers applied liquid-liquid extraction, solid-phase extraction and ultrasound desorption to isolate the acid fraction from heavy gas oil, and the naphthenic acids analysis was accomplished by GC/MS after MTBSTFA derivation.[162] In contrast to the partial separation obtained by GC/MS, GC×GC-MS has the capability to separate and identify some components of naphthenic acids at the isomer level. A method

based on GC×GC in conjunction with ToF-MS was employed to characterize two commercial naphthenic acid mixtures and an oil sand mixture.[163] Even though GC×GC-MS might not characterize all individual components in naphthenic acids, there is still dramatic potential for the development of this technique. What's more, there are several examples detailing the application of liquid chromatography mass spectrometry (LCMS) application. Anion exchange chromatographic separation, followed by ESI-MS analysis was applied to detect the toxicity of naphthenic acids in oil sands extract.[164] A dilute-and-shoot reversed-phase capillary HPLC combined with QToF-MS was also developed to provide structural information on each naphthenic acid isomer class.[165]

As mentioned in Chapter 2, ultra-high mass accuracy and ultra-high resolution of FTICR-MS make it an attractive instrument to identify different ions in complex mixtures, which is also true for naphthenic acids analysis in petroleum industry. Qian *et al*. combined off-line HPLC with ESI-FTICR-MS to analyse acids fractions in crude oil and this method was able to distinguish 15 different chemical formulas of naphthenic acids.[166] Barrow *et al.* applied FTICR-MS to perform a study on the degradation of naphthenic acids in the environment.[167] FTICR-MS in their method not only provided unambiguous assignments of signals but was also able to detect the naphthenic acids with a high hydrogen deficiency. However, the ultra-high resolution FTICR spectra of naphthenic acid mixtures can be extremely complicated as shown in Figure 3.2.[168] There might be thousands of peaks in the resulting spectra and each peak represents chemically distinct compounds.[147] It is still a challenge to understand the spectra. Meanwhile, a very expensive instrument is needed in order to run experiments in high mass accuracy, which is also a disadvantage of FTICR-MS application.

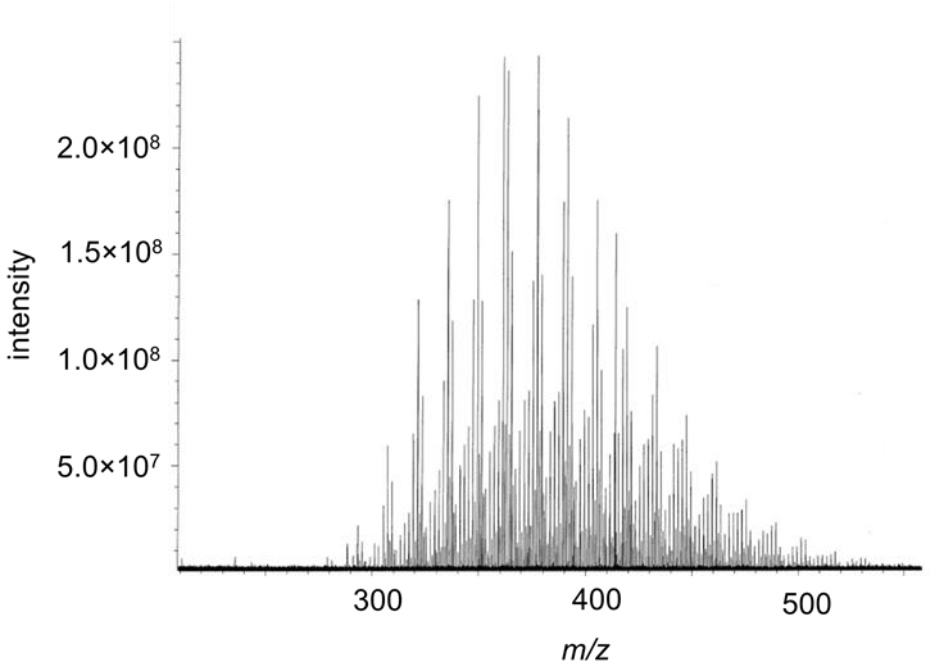

Figure 3.2 Nanospray negative-ion mode FTICR mass spectrum of a crude oil extract, containing naphthenic acids adapted from reference 33.

3.2 Attempted Fischer esterification of naphthenic acids

Based on previous results in Chapter 2, we wanted to develop a rapid, selective, inexpensive and chromatography-free mass spectrometric analysis of naphthenic acids in petroleum. The reaction we attempted first in this work was Fischer esterification of carboxylic acids, which is a simple and well-known reaction of carboxylic acids. A new charge-tagged alcohol was designed and reacted with naphthenic acids, allowing the mass spectrometric characterization of the ester derivatives (Scheme 3.1).

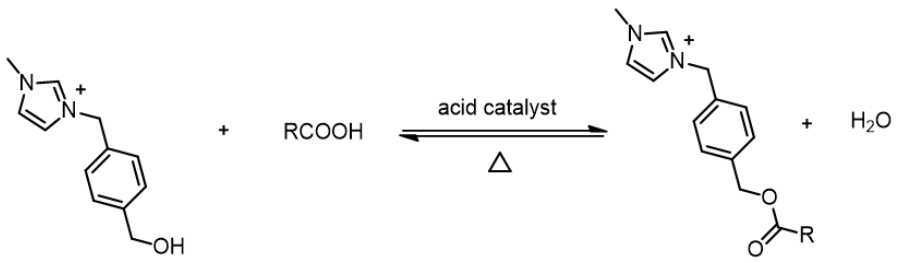

Scheme 3.1 The Fischer esterification of carboxylic acids (R= alkyl group).

Fischer esterification of carboxylic acids is however slow and reversible. Thus, esters are produced when the reaction involves heating with alcohol and the use of an acid catalyst to speed up the reaction. The alcohol is usually used as the solvent and is present in large excess. The acid catalyst must be strong enough to protonate the carbonyl oxygen of the carboxylic acid. The common acid catalysts are concentrated sulphuric acid and tosic acid. Dry HCl gas is also employed in some cases, but this method results in aromatic esters.[169] Protonation of carboxylic oxygen promotes electrophilicity of the carbonyl carbon, thus facilitating attack on the primary carbon by the oxygen of a hydroxyl group. The reaction then undergoes 1,2-addition by alcohol whose proton is transferred to one of the OH groups. 1,2-elimination of water subsequently occurs leading to the protonated water, and the ester is then deprotonated.

Before we took this charge-tagging alcohol into practice, we were fully aware of the disadvantages of the esterification of carboxylic acids. The first issue surrounding this reaction is the reversibility.[170] Water is formed during the reaction and it may attack the protonated ester derivatives, effectively reversing the reaction. Crude oil samples may contain some residual water, which would hamper the progress of the reaction to some extent. One solution to this problem is to use a large excess of charge-tagging alcohol to push the reaction forward. Furthermore, concentrated sulfuric acid or 4Å molecular sieves may be applied to extract water from the mixture to drive the reaction forward. The second complication to the esterification reaction may be the redundant transesterification. The esters formed from naphthenic acids in petroleum samples meet the attack from other alcohols in this mixture forming some different esters, and the charge-tagging ester derivatives

decrease. This transesterification side reaction can also be catalyzed by acid,[169] so the addition of an acid catalyst may exacerbate this problem.

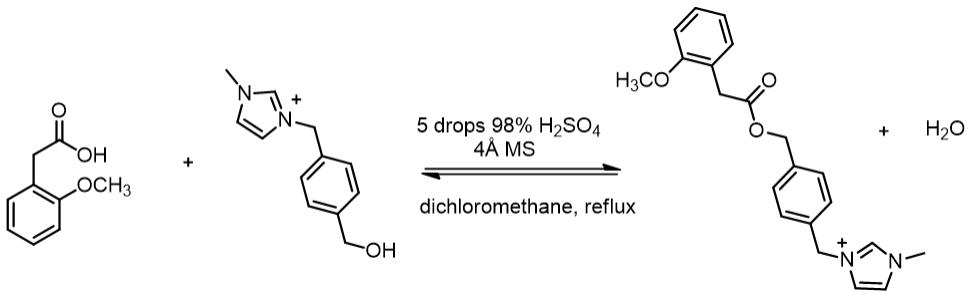

Scheme 3.2 The esterification reaction between charged-tagging alcohol and 2-methoxyphenylacetic acid.

The cationic charged tag used in this work was prepared by alkylation of methylimidazole using 1,4-di(bromomethyl)benzene and then hydrolysis using NaOH. It was paired with anion $[PF_6]^-$ through salt metathesis of the resulting alcohol with $NaPF_6$, which generated the final charge-tagging alcohol, 3-(4-(hydroxymethyl)benzyl)-1-methylimidazolium hexafluorophosphate. The charged tag mixture contains impurities and the purification doesn't process, because other impurities such as NaBr and the designed product have similar solubility which leads to the difficulty of isolation. (See Experimental in Section 3.5)

Prior to applying the charge-tagging alcohol to a sample, the efficiency of the charged tag was tested with a known naphthenic acid, 2-methoxyphenylacetic acid, in positive ion ESI-MS (Scheme 3.2). 2-methoxyphenylacetic acid was reacted with more than five equivalents of the charged tag and concentrated sulphuric acid as a catalyst through gentle reflux under argon about 3 hours in 50 mL of dichloromethane with the presence of activated 4Å molecular sieves. The charged tag was analysed by MS before the reaction and small amounts of innocent/unreactive impurities were detected. (Figure 3.3). The final reaction solution was analysed by MS (Figure 3.4).

The same experiment was conducted three times and each experiment had similar results.

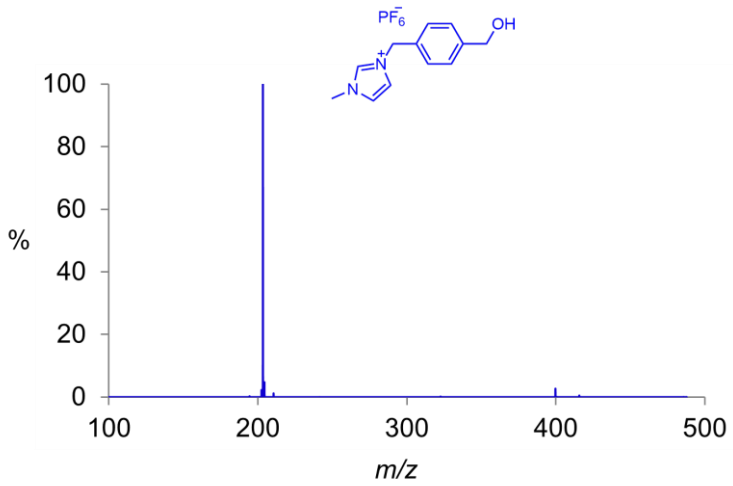

Figure 3.3 Positive ion mode ESI-MS of charged tag mixture prior to esterification reaction.

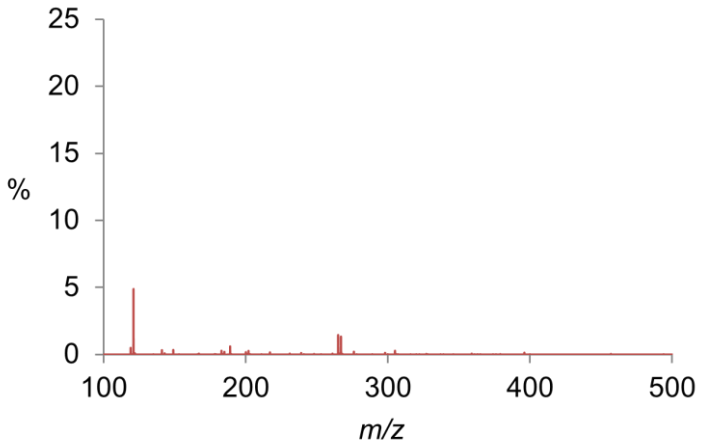

Figure 3.4 Positive ion mode mass spectrum after 3-hour esterification reaction.

As the above spectra show, the alcohol charged tag was unexpectedly decomposed and product with *m/z* 351.2 could not be observed after 3 hours, or put another way, the esterified naphthenic acid was not of sufficient intensity to be easily identified. The low efficiency of charge-tagging alcohol, long reaction time, solvent restrictions (both charged tag and analyte need to be soluble), harsh reaction conditions of esterification and problems on purification required us to move forward and find another solution to naphthenic acids analysis.

3.3 1-[3-(Dimethylamino)propyl]-3-ethylcarbodiimide methiodide (EDT) derivatization followed by ESI-MS for naphthenic acids analysis

Preliminary investigation of esterification of naphthenic acids leads us to attempt other new derivatization methods. A variety of chemical derivatizations of naphthenic acids are designed to facilitate GC-based analysis, most of them involve MTBSTFA derivative reagent application coupled with GC/MS.[149, 161, 171, 172] For LC based applications, the use of oxalyl chloride was reported to react with naphthenic acids to form acyl chlorides, which gave derivatives with ammonium hydroxide, followed by LC-MS/MS analysis.[173] An innovative method used EDC as a derivative reagent and involved liquid chromatographic separation followed by positive mode ESI-MS analysis of common fragments for derivatized carboxylate group.[174] These methods are quantitative and sensitive, but the sample pre-treatment and chromatographic separation make the whole process expensive and time-consuming. Accurate and quantitative analysis without chromatographic separation for naphthenic acids is still a challenge. The goals of the present work are to demonstrate derivatization method coupled with ESI-MS as a technique for the rapid analysis of naphthenic acids from petroleum samples, to apply the method to obtain *m/z* profiles of naphthenic acids and to realize sample characterization. Derivatization of naphthenic acids using EDT results in derivatives that can be subjected to straightforward mass spectrometric detection in the positive ion mode. (Scheme 3.3)

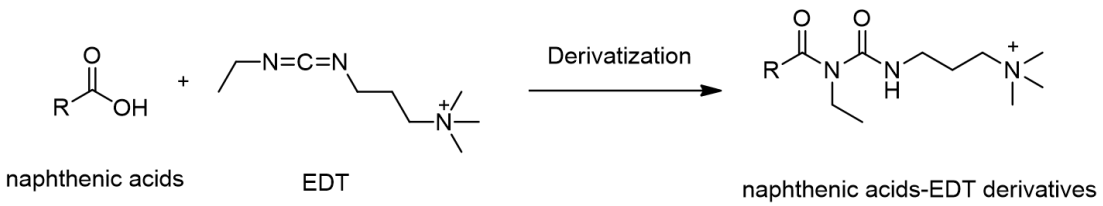

Scheme 3.3 The derivatization reaction between EDT and naphthenic acids (R= alkyl group).

A carbodiimide is a functional group involving the formula RN=C=NR.[175] Compounds containing the carbodiimide functionality are generally used as a dehydrating agent to activate carboxylic acids for the coupling with primary amines to yield amide compounds.[176] Meanwhile, carbodiimide is a well-known tool in the field of bioconjugation,[177] peptide synthesis[178] and modifications of polysaccharides[179]. EDT is one of the most common carbodiimides. Similar derivatization methods mentioned before were employed by Yen *et al.*[152] and Miwa *et al.*[155]. In their studies, EDC was used to react with carboxylic acids and 2-nitrophenylhydrazine hydrochloride (2-NPH·HCl) to form carboxylic acid hydrazides. However, this reaction has several side reactions complicating the study (Scheme 3.4).[180] EDT can react with a carboxylic acids group to give an active intermediate: the *O*-acylisourea **2** which will easily react with primary amine in the reaction mixture to form corresponding amide **3**. Meanwhile, the *O*-acylisourea **2** can react further with an additional carboxylic acid to form an acid anhydride **5**. The *O*-acylisourea **2** can also undergo rearrangement of stable *N*-acylurea **6**. In order to reduce the number of by-products and enhance analyte signal under positive ESI mode, we modified the derivatisation method such that 2-NPH·HCl is not used and the reaction is allowed to proceed to the formation of the intermediate with positive charge.

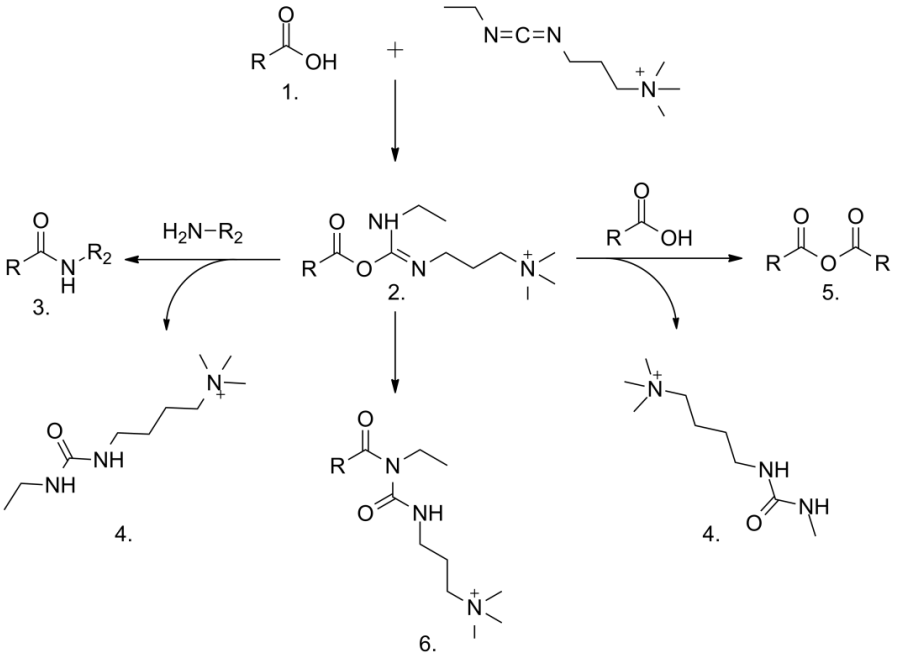

Scheme 3.4 EDT crosslinking reaction scheme. Carboxyl-to-amine crosslinking using the carbodiimide EDT (R= alkyl group).

EDT is commercially available. The reactivity of EDT was studied by PSI ESI-MS in positive ion mode. This was done by adding the mixture of different acids (cyclopentanecarboxylic acid, cyclohexanepentanoic acid and cyclohexaneacetic acid in the same molar amount) into a solution containing the EDT. (Figure 3.5).

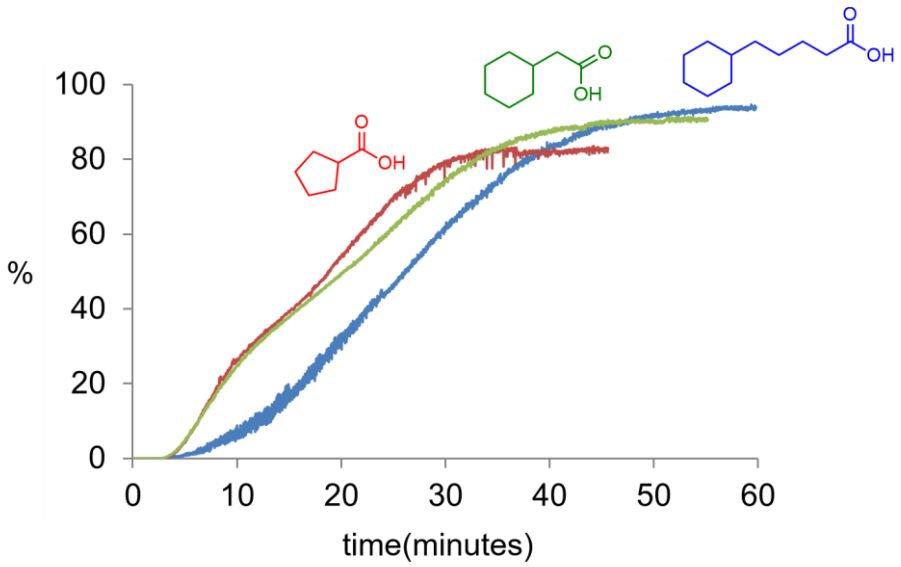

Figure 3.5 The positive ion mode ESI-MS of the reaction between EDT and the mixture of three standard acids (cyclopentanecarboxylic acid, cyclohexamepentanoic acid and cyclohexaneacetic acid). Solvent is CH_3OH and the reaction temperature is RT. EDT derivative products relative intensity increases over time, monitored by PSI online monitoring.

What we observe is that cyclopentanecarboxylic acid (red) is fast ($t_{1/2}$= 14.1 minutes). The half time of cyclohexanepentanoic acid (blue) is 20.1 minutes and cyclohexaneacetic acid (green) is 25.2 minutes. All of these three reactions finished within 45 minutes. The longer the chain length, the less reactivity.

Considering the complexity of jet fuel samples, we first mixed a quantity of a jet fuel sample with NaOH to examine the speciation in negative ion mode by ESI-MS and to see whether the naphthenic acids components were discernible or not without a charged tag. The resulting spectrum (Figure 3.6) presumably contains naphthenic acids and phenols according to their *m/z* or the second series may be the aggregation of the first species. However, the information provided does not allow us to figure out the exact speciation only based on their deprotonation behavior.

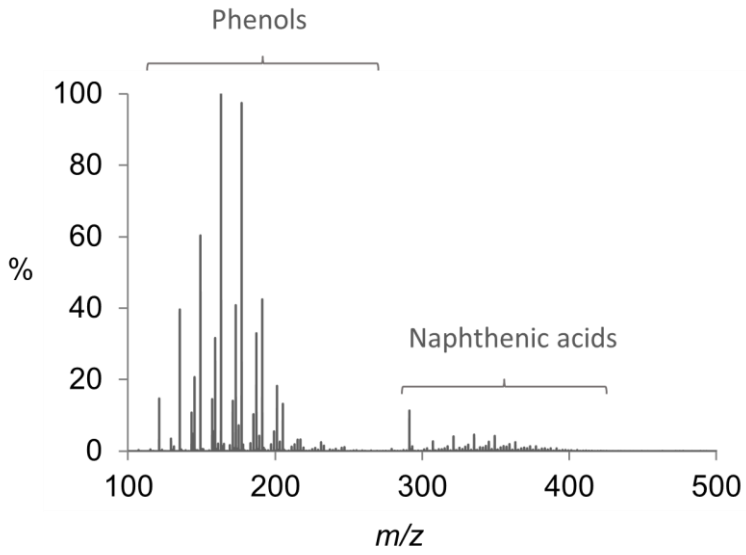

Figure 3.6 Negative ion mode ESI-MS (CH_3CN/CH_2Cl_2, v/v = 1:3) of sample A after NaOH addition.

The next step for us is to apply the EDT derivatization method to jet fuel samples.

3.4 Conclusions

Fischer esterification was proved to be low efficient in detecting naphthenic acids because of long reaction time, solvent restrictions (both charged tag and analyte need to be soluble), harsh reaction conditions of esterification and problems on charged tag purification. The current study on EDT and its reaction with standard naphthenic acids provide us with clues for future work, which provides us the reactivity of EDT.

Next step, we would like to figure out the detection limit of EDT, apply this method to jet fuel samples and figure out the matrix effects occurring in a complex mixture. This application would tell us the selectivity of this method in petroleum fractions by using EDT charged tag and ESI-MS, and provide us information about the its efficiency on quantitative analysis.

3.5 Experimental

All solvents were HPLC grade. Acetonitrile, methanol and dichloromethane was purchased from Sigma-Aldrich and used as received. EDT, cyclopentanecarboxylic acid, cyclohexanepentanoic acid and cyclohexaneacetic acid were purchased from Sigma-Aldrich and used as received without further purification. For PSI experiments, the reaction vessel was pressurized using 3 psi of nitrogen gas. Assignments were made with the help of chemcalc.org.[136] ESI-MS of the reaction was collected in the positive ion mode on a Waters Micromass Q-ToF *micro* mass spectrometer using solutions prepared in acetonitrile, dichloromethane and methanol. Capillary voltage, 3000 V; Cone voltage, 20 V; Extraction voltage, 0.5 V; Source temperature, 80°C; Desolvation temperature, 140°C; Cone gas flow rate, 100 L/h; Desolvation gas flow, 200 L/h; collision voltage, 2 V (for MS experiments); MCP voltage, 2700 V.

Synthesis of 3-(4-(hydroxymethyl)benzyl)-1-methylimidazolium hexafluorophosphate. 3-(4-(bromomethyl)benzyl)-1-methylimidazolium hexafluorophosphate (0.65 g, 1.59 mmol , see chapter 2 experimental section 2.4) was reacted with NaOH (6 g, 0.15 mol) solution in 50 mL distilled water at 70°C stirring for 10 hours, which caused the solution to turn orange. The reaction solution was filtered and the filtrate was vacuum dried. The powder was redissolved in a minimum amount of methanol and white precipitation was precipitated after leaving the solution at 4°C overnight. The white precipitation was recovered from reaction solution through vaccum filtration. The mass spectrum of this white crystals shows it is NaBr.

ESI-MS reaction monitoring using pressurized sample infusion. Standard stock solutions were prepared by individually dissolving the pure standard with methanol. The concentration for each stocking solution were EDT (1 mmol/L), cyclohexaneacetic acid (1 mmol/L, 2 mmol/L, 5 mmol/L, 10 mmol/L, 20 mmol/L), cyclopentanecarboxylic acid (20 mmol/L) and cyclohexanepentanoic acid (20 mmol/L). These solutions were stored at 4°C. As described elsewhere,[30, 31] a 20 mL Agilent headspace vial was filled with 10 mL acetonitrile and 5 mL EDT stock solution. The vial was equipped with a magnetic stir bar, and rubber stopper wrapped by Taegaseal PTFE tape. PEEK tubing was fed from the vial to the ESI-MS source and the headspace vial pressurized using 3 psi of nitrogen gas. The solution end of PEEK tubing was protected with a cotton filter system to avoid the tube being blocked by any insoluble substances in reaction solution. The solution was stirred without heat using a magnetic stirrer. The 2.5 mL of cyclohexaneacetic acid, cyclopentanecarboxylic acid and cyclohexanepentanoic acid stock solution were injected via syringe.

Chapter 4 A new dimension to cold EI GC/MS analyses of complex matrices with Python data processing

4.1 Application of cold EI and classical EI GC/MS

Cold EI GC/MS is a powerful and information-rich technique for qualitative characterization and quantitative analysis of compounds in a mixture (see Chapter 1). The strength of cold EI GC/MS is the low fragmentation rate of the compounds giving rise to a mass spectrum with an intense molecular ion peak. This signal is a unique for each analyte. There are numerous examples of Cold EI GC/MS applications. Fialkov *et al.* demonstrated that some thermally labile and low volatility compounds such as large polycyclic aromatic hydrocarbons (PAHs), metalloporphyrin and carbamates were easily analysed by Cold EI GC/MS, that otherwise could not be detected by standard GC/MS.[58] The same approach was also effective for characterization of straight chain alkanes with a general formula of C_8H_{18}-$C_{40}H_{82}$.[181] These and others examples show that Cold EI GC/MS has extended the range of compounds amenable for GC/MS analysis. Pesticide analysis in complex agricultural products is vital for our food safety. A new approach combined with cold EI GC/MS achieved fast, highly sensitive and quantitative analysis of all 88 pesticides in agricultural products whereas only 36 were detected with standard GC/MS techniques.[182]

By modifying certain parameters of the instrument, such as reducing the make-up gas flow, cold EI gives rise to classical EI mass analysis. Several experimental factors can influence the classical spectra: ion source temperature, electron energy, difference mass analysers and so on.[61] As shown in Figure 4.1, cold EI spectra are characterized by enhanced molecular ion abundance and decreased

fragment ions abundance whereas the classical EI spectra gives a slightly enhanced molecular ion over that in the NIST library spectrum with a high matching factor.

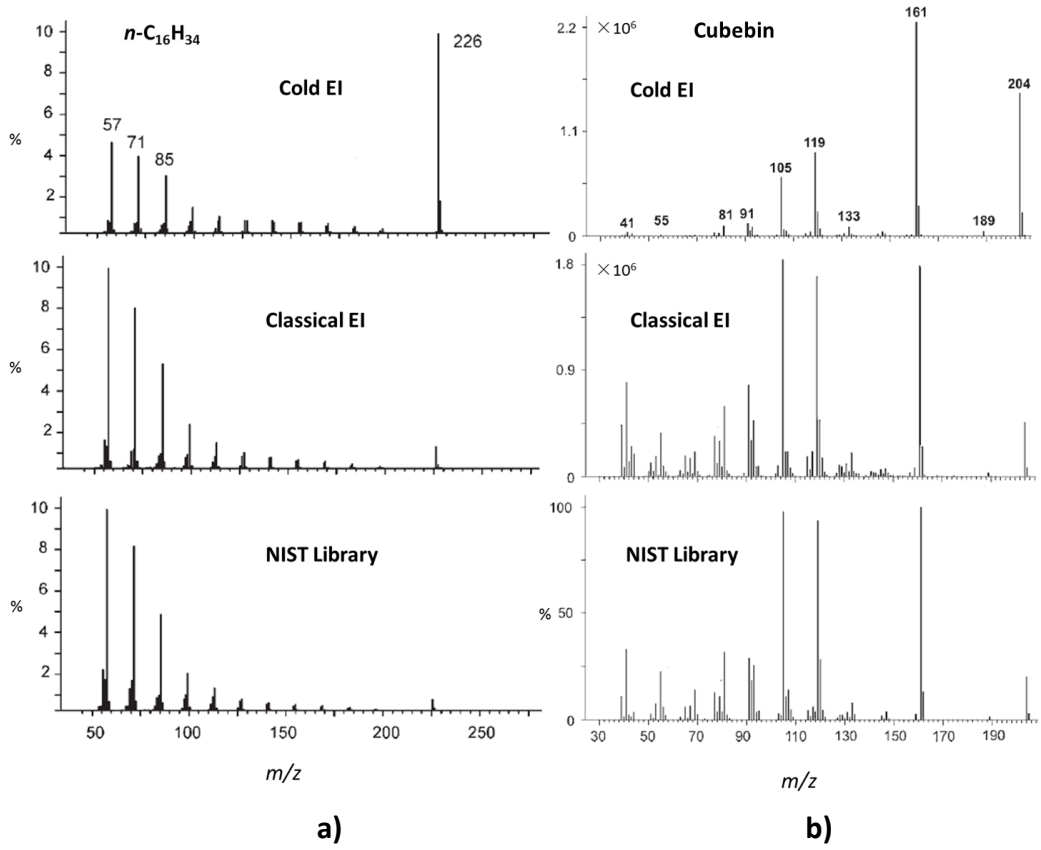

Figure 4.1 a) Cold EI, classical EI and NIST library EI mass spectra of linear chain hexadecane (n-$C_{16}H_{34}$). b) Cold EI, classical EI and NIST library EI mass spectra of Cubebin adapted from reference 63.

The principle content of petroleum distilled fraction is heavy hydrocarbons or highly branches alkenes, because their similar fragmentation patterns result into the similar EI spectra. Hence, the molecular ion information is essential for the identification of measured compound. Our goal is to combine the information from cold EI spectra and classical EI spectra by subtracting the cold EI mass spectra to the classical EI mass spectra revealing the molecular ion peaks, then combine the information on spectra and their corresponding retention time (Figure 4.2).

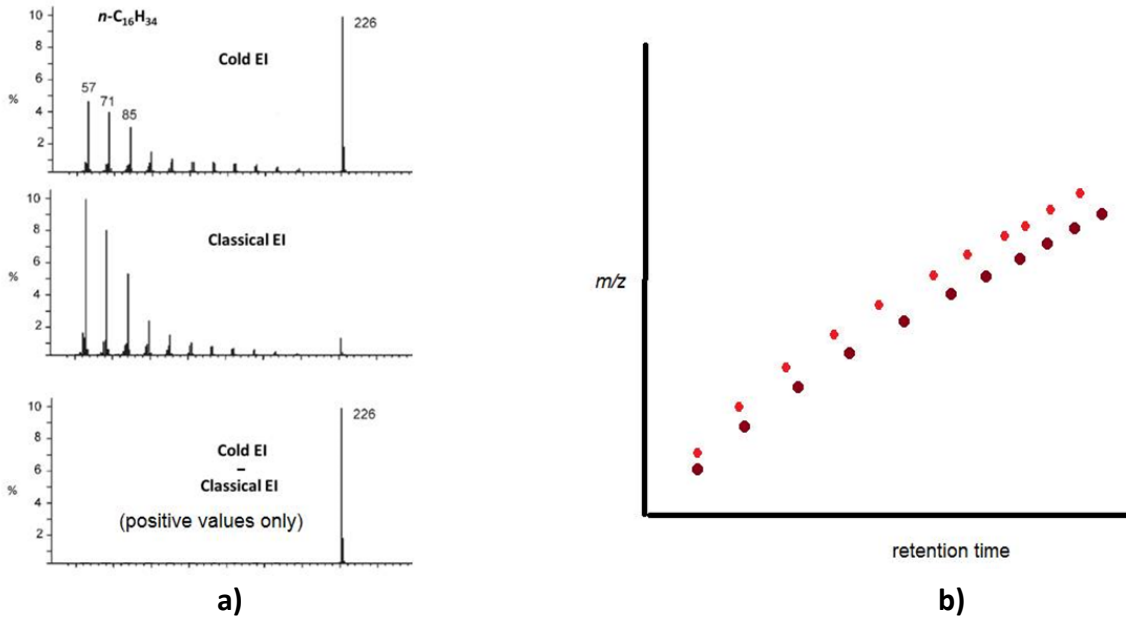

Figure 4.2 a) Mass spectrum from cold EI method, classical EI method and resulting mass spectrum by subtracting the cold EI mass spectra to the classical EI mass spectra; b) The expected resulting spectrum of this project which can give us the molecular weight of main products in each retention time. Red points stand for alkene series, pink points stand for alkane series in different retention time.

4.2 Current results and discussion

This chapter describe some preliminary work that was carried out when the department secured a new Cold EI instrument. Because my project involved selective analysis of petroleum, and the Cold EI has some unusual new abilities, we looked into ways of exploiting this for the analysis of complex mixtures. Because we did not have access to a functioning instrument for some time and some of the testing broke the instrument, we did not actually find suitable settings to enable the methodology. However, to keep this idea alive, and to pass on the Python code we developed for the analysis of the spectra, progress to date it reported here.

In our present work, we examined a jet fuel sample by both cold EI GC/MS and classical EI GC/MS approach. The cold EI source mode was chosen and the flow rate of make-up gas was set to 40 mL/min. The classical EI mode of operation with

the instrument is simply obtained through the reduction of helium make-up gas flow rate to 8 mL/min and the switch of the source mode to classical EI source mode (Figure 4.3). The same retention time was chosen for both runs to get the mass spectra, and then the python program was applied to do the mass spectra subtraction. Lars Yunker, a PhD student in the McIndoe group, has developed a program that allows for comparison of the two analysis methods. The program is unique in that it can compare the related mass spectra of cold and classical EI at a specific/ defined retention time. The program subtracts the cold EI mass spectra to the classical EI mass spectra revealing the molecular ion peak. Because peaks eluting at the same time in GC/MS are likely to have different molecular weights, we expect to be able to resolve different series of compounds by this approach.

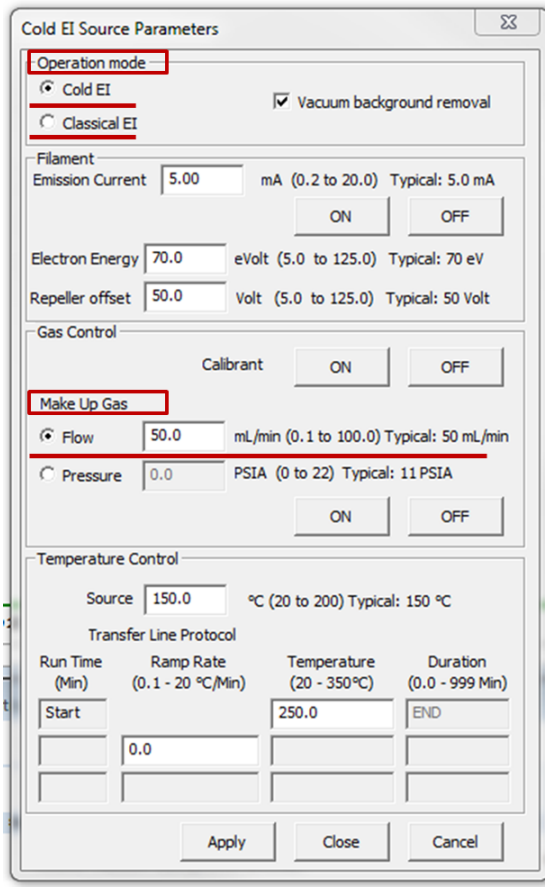

Figure 4.3 The cold EI source parameters window. Red marks for operation mode and make up gas modification.

The GC chromatograms (Figure 4.4) show our preliminary investigation of jet fuel sample A. The retention time of each peak in these two-run is unexpectedly slightly different. One reason to explain deference in retention time is the make-up gas flow which has an effect on retention time by changing the pressure on the end of the column and therefore, a high make-up gas flow gives shorter retention time for a defined compound.[183]

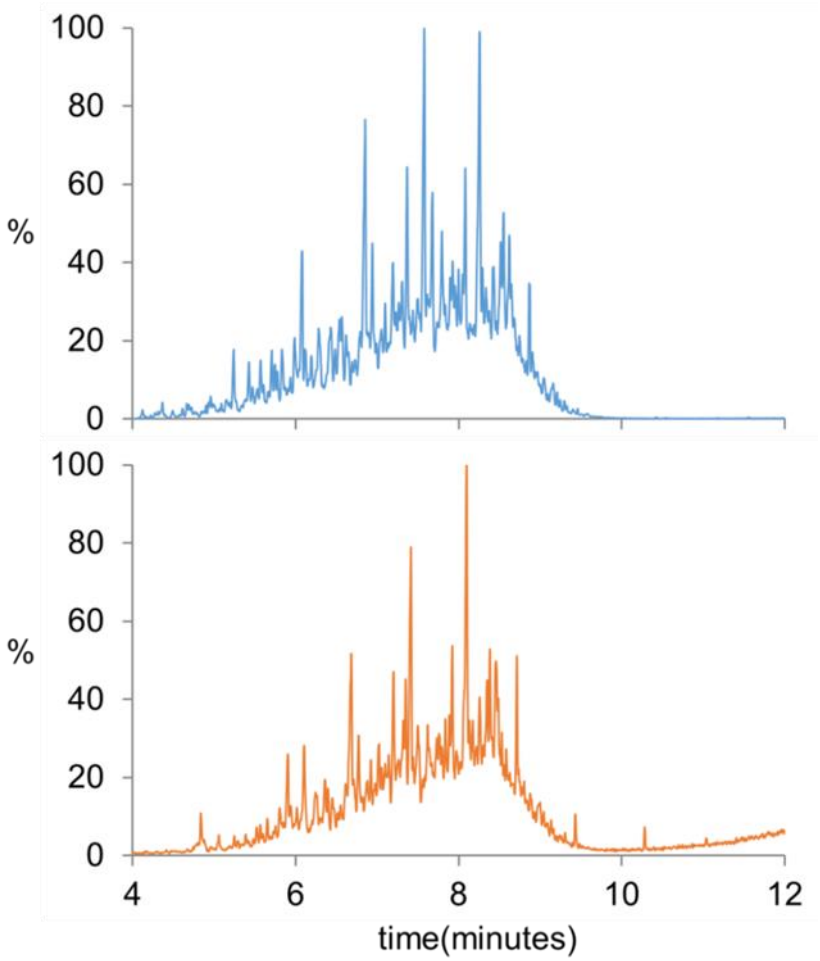

Figure 4.4 Top: cold EI GC/MS chromatogram of jet fuel sample A; Bottom: classical EI GC/MS chromatogram of jet fuel sample A.

For cold EI/classical EI comparison, we chose to focus on the retention time that is related to the most predominant peak in the chromatogram, 8.2 min. Figure 4.5 shows the classical EI and cold EI mass spectrum for jet fuel sample A at 8.2 min, and their subtracted spectrum. The mass spectrum at 8.2 min for cold EI displays a parent ion peak at 198 Da (specific for C_{14}). However, the molecular ion peak in the classical

EI mass spectrum is unidentified and the spectrum could not be fully interpreted. As mentioned before, carrier gas flow rate could affect the retention time. Therefore, it was problematic to align two comparable spectra from classical and cold EI.

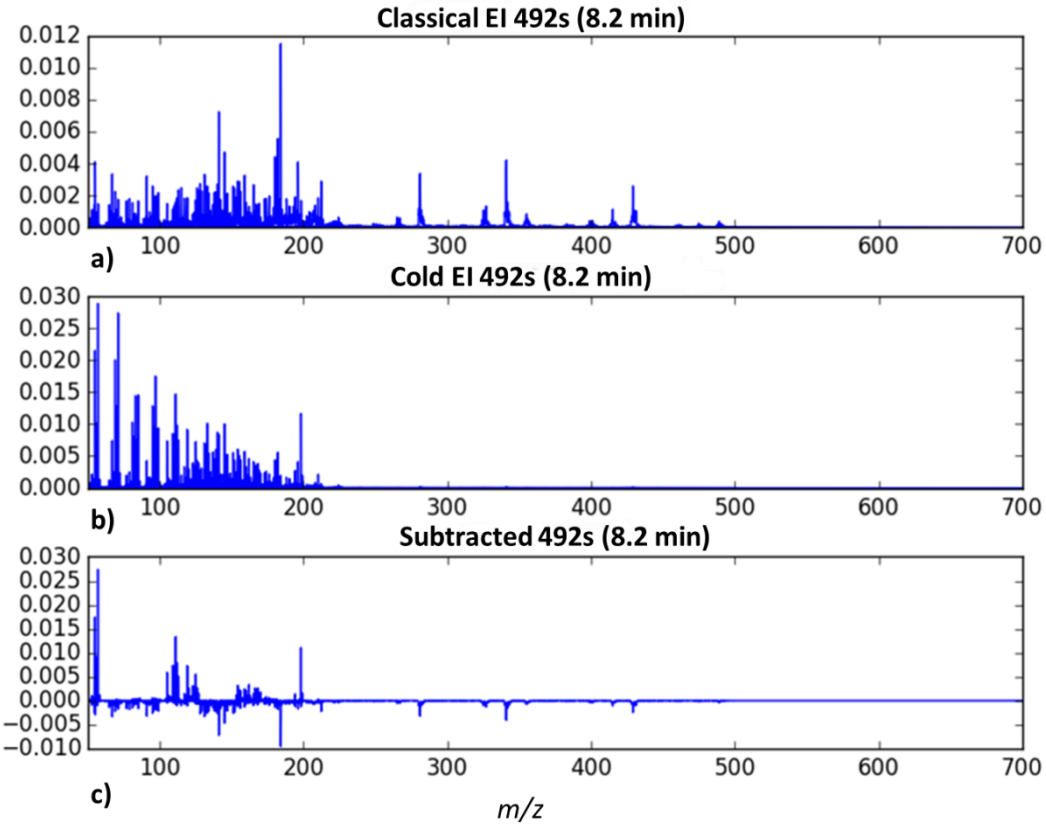

Figure 4.5 a) the mass spectrum of classical EI at 8.2 min; b) the mass spectrum of cold EI at 8.2 min; c) the subtracted spectrum from a) and b).

4.3 Conclusions

The preliminary study of this project offers us lots of information for our future work. Carrier gas is a main factor to affect the retention time, and the classical EI mode is obtained by modifying the make-up gas flow. Thus, the incomparable retention time of classical and cold EI is the main problem we need to solve. Meanwhile, the incomparable retention time makes the identification on the same compound's mass spectra far more challenging. The less complicated sample such as standard C_8~C_{20} will be studied instead of jet fuel sample so that the pattern of

retention time shifting can be obtained. The simpler mass spectra may offer us some clue to improve the Python script for data processing. In addition, the classical EI mass spectra can have a degree of tunable abundance of the molecular ion and fragment ions for obtaining optimal subtracted spectrum.[37]

4.4 Introduction for Python data processing

The development of computer technology has driven much of GC/MS improvement.[37] Commercial software including MassLynx (Waters Corporation, Milford, MA), ChromaTOF (Leco Corporation, St.Joseph, MI), and ChemStation (Agilent Technologies, Santa Clara, CA) as well as free data processing software for GC/MS has been developed by many academic groups, and open source licenses are also provided.[184, 185, 186, 187, 188]

The McIndoe group has also worked in the area of MS data processing [LPE Yunker, D Yeung, JS McIndoe, unpublished]. Based on this work, PyColdEI is a novel python code package for the processing of raw data from new AxioniQT Cold EI GC/MS instrument (PerkinElmer Clarus 680), particularly suitable for rapid screening of GC chromatographs of different samples and for quick comparison of mass spectra.

4.5 Results and Discussion

Here we report the functions of PyColdEI developed in Python.[189] GC/MS data is collected as a time series of mass spectral scans, where each scan contains a series of (*m/z*, intensity) pairs. PyColdEI has three functions: 1) Output GC chromatograms; 2) Output mass spectra of the same retention time from different files, which means users can check the retention time shifting when the instrument parameters change; 3) Output mass spectra of multiple retention times for one sample.

Each function has an independent piece of code including ColdEI-GCchroma, ColdEI-MSpart1(1RT) and ColdEI-MSpart2(nRT) (Figure 4.6).

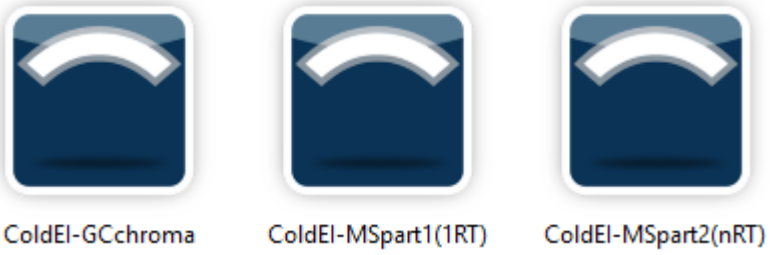

Figure 4.6 The icons for three independent PyColdEI code.

PyColdEI supports two data formats for data input, comma delimited CSV files for GC chromatographs and raw MS text files for mass spectra. In order to get GC chromatograph users can open the data analysis window in Axion eCipher software, copy the chromatogram lists, then paste into excel and save as *.csv files (Figure 4.7). Moreover, Users can open the data analysis window to select “home”, then select “Export Data File” and choose “As Txt” to get raw MS text files so as to obtain the mass spectra in PyColdEI package (Figure 4.8). When all the data files are ready, Figure 4.9 is an example to show how to input these data files obtained on Axion eCipher in PyColdEI package.

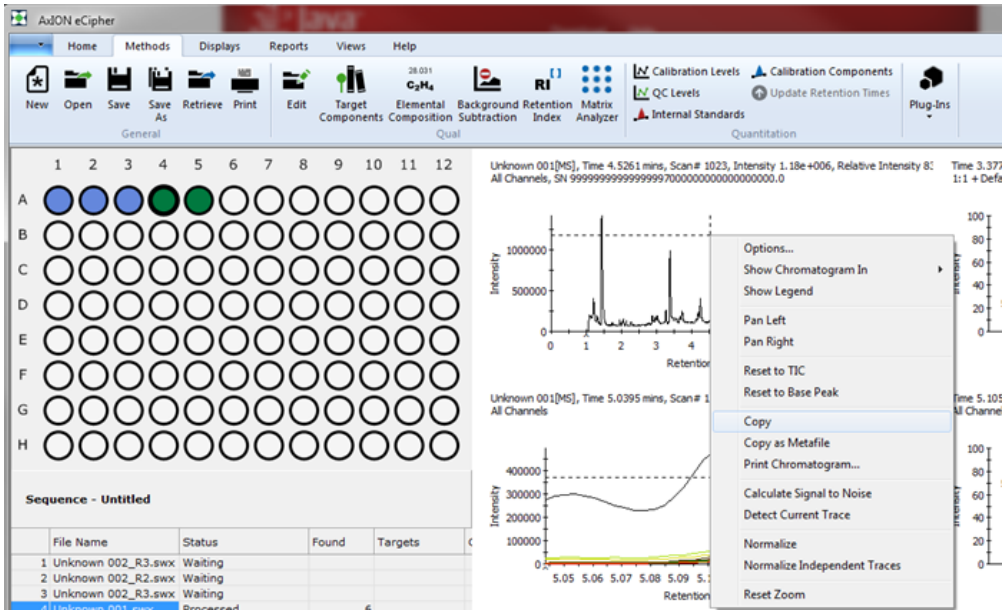

Figure 4.7 Data analysis window in Axion eCipher software, and the way to copy chromatogram list.

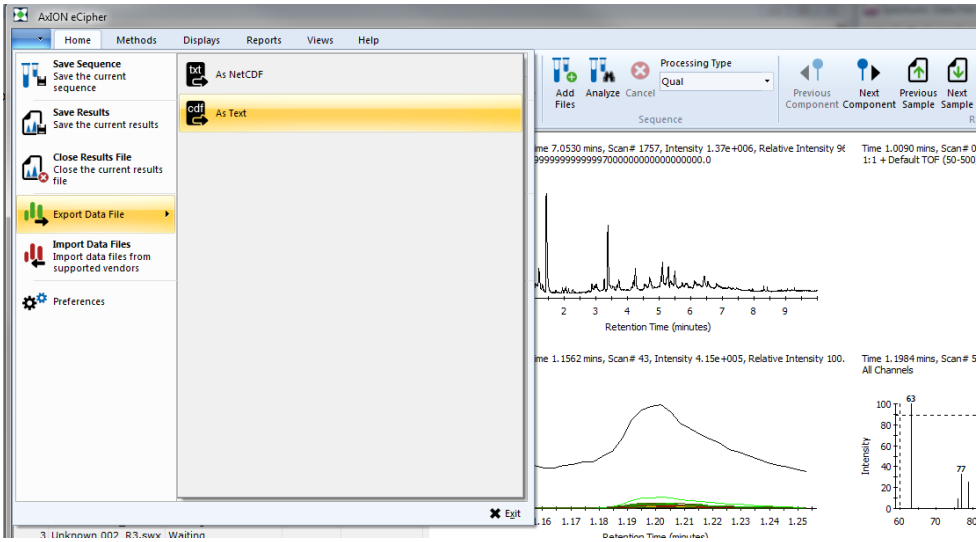

Figure 4.8 Data analysis window in Axion eCipher software, and the way to get text raw file.

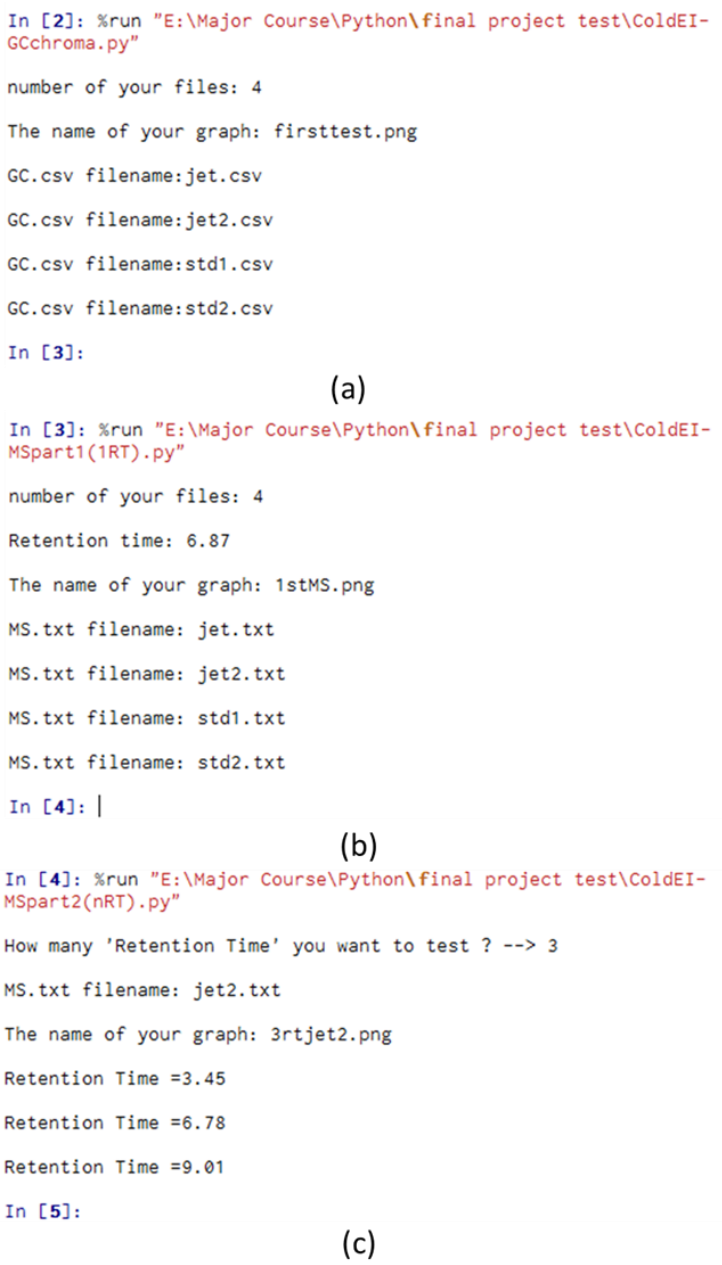

Figure 4.9 Examples of reading raw files from the Python command. (a) Input information for ColdEI-GCchroma program; (b) Input information for ColdEI-MSpart1(1RT) program; (c) Input information for ColdEI-MSpart2(nRT) program.

The GC chromatograms show the total ion chromatogram over time in minutes (Figure 4.10). The vertical arrangement of chromatograms and the same range of time make the observation on retention time shifting straightforward. Figure 4.11 and Figure 4.12 are the mass spectra at the same retention time for different samples, which is outperformed by ColdEI-MSpart1(1RT) in PyColdEI package. It is

a convenient and rapid way to compare the mass spectra at the same retention time but for different runs, partically suitable for comfirmation of retention time shifting made by instrument parameters. Figure 4.13 outperformed by ColdEI-MSpart2(nRT) in PyColdEI package is the mass spectra at different retention times for a single run. This function offers an easy access to mass spectra under multiple retention times for one sample and avoid on repetitive operation. All the mass spectra show the normalized intensity (to the max intensity) over the *m/z*. If retention time chosen for samples has no mass scan, the resulting spectrum would be blank such as the first spectrum in Figure 4.12 and Figure 4.13.

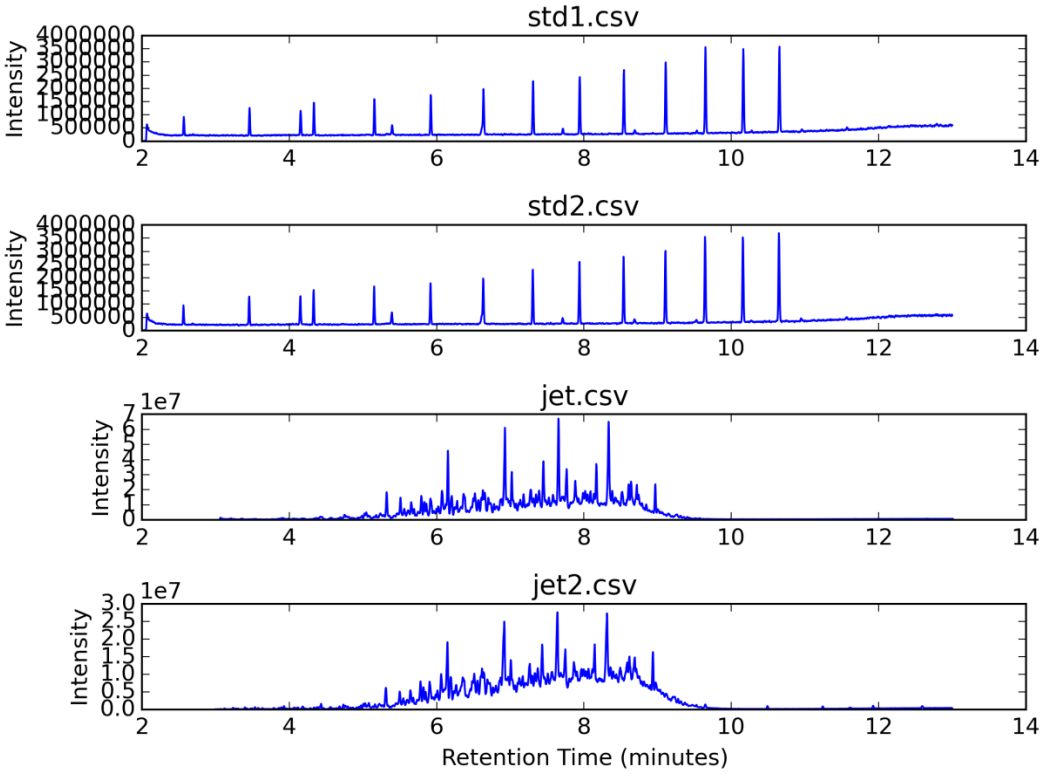

Figure 4.10 The GC chromatograms for four different samples: std1, std2, jet, and jet2. Output by ColdEI-GCchroma.

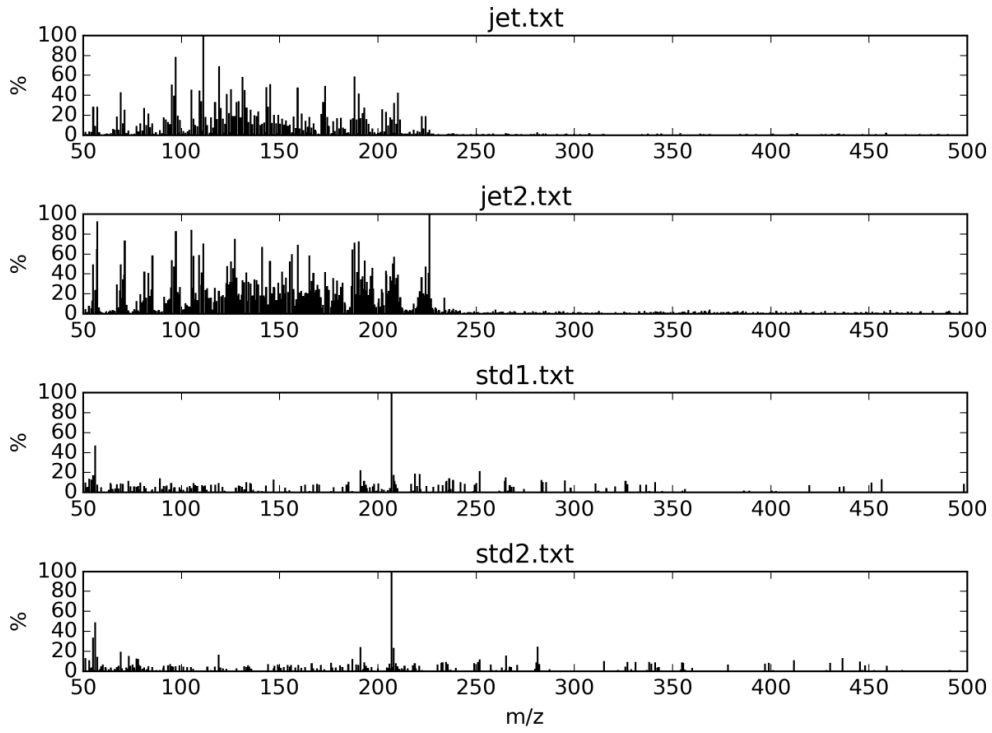

Figure 4.11 The mass spectra at the same retention time (9.78 min) for four different samples: jet, jet2, std1, and std2). Output by ColdEI-MSpart1(1RT).

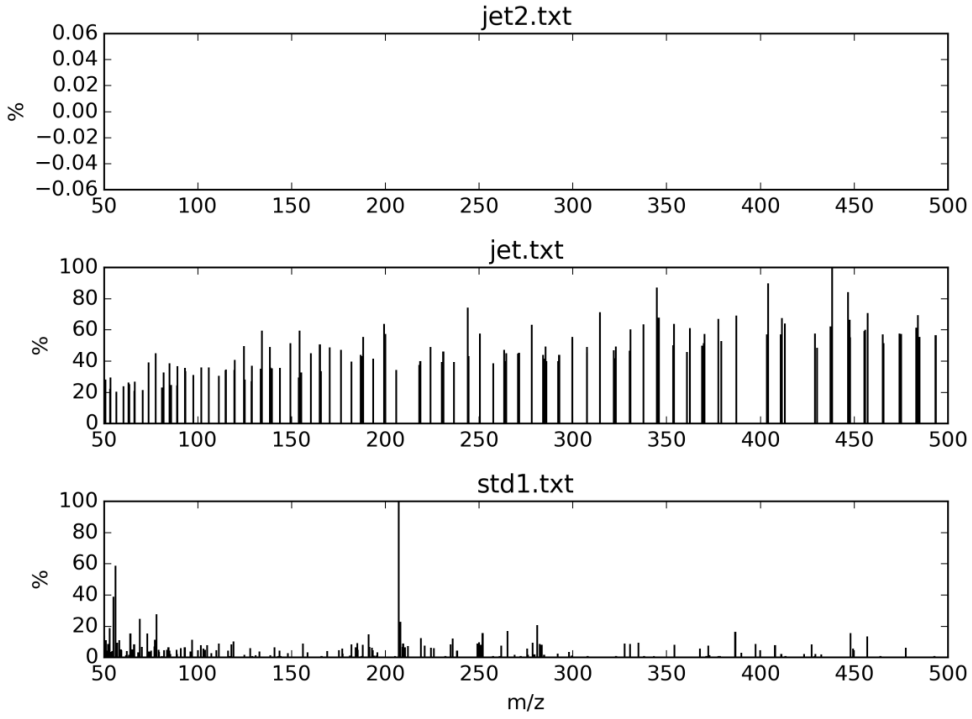

Figure 4.12 The mass spectra at the same retention time (5.34 min) for three different samples: jet2, jet, and std1). Output by ColdEI-MSpart1(1RT).

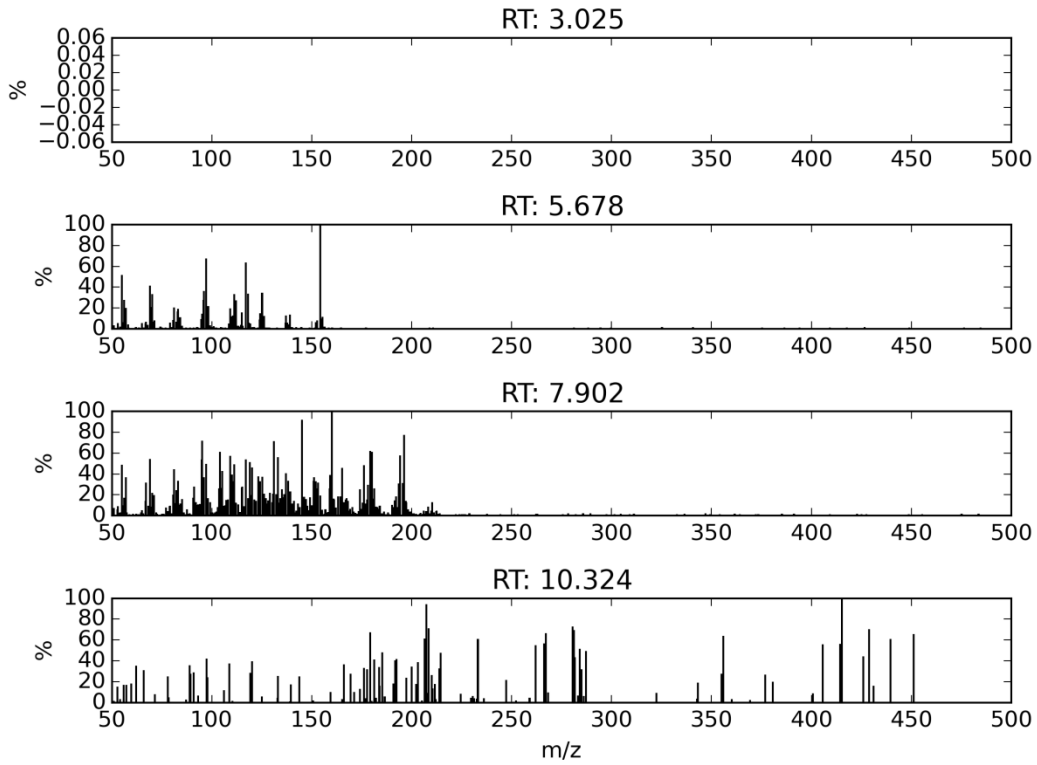

Figure 4.13 The mass spectra of four different retention times one sample: jet. Output by ColdEI-MSpart2(nRT).

4.6 Conclusions

The PyColdEI package contains some small programs that are easy to operate. It provides a rapid and direct way to obtain the GC chromatograms and mass spectra and the resulting graphics are straightforward and clear. At present, the PyColdEI is only used for rapid screening of cold EI GC/MS data for day-to-day tasks in our group, and the quality of the resulting graphics need to be improved. When making plots with such a long aspect ratio, reasonable spacing for the y-ticks should be considered. Otherwise, they are too close together and the numbers are overlapping. This problem can be tackled by specifying the tick position manually. The high-quality graphics is our future goal.

4.7 Experimental

All solvents were HPLC grade. Hexane was obtained from Fisher Chemicals used as received. Sample information see Chapter 2 experimental section. Cold EI GC/MS data were obtained on an AXION iQT GC/MS instrument from Perkin Elmer (Waltham, Massachusetts, USA) which was equipped with a Clarus 680 gas chromatogram from Perkin Elmer (Waltham, Massachusetts, USA). Make up gas flow for cold EI method was 40 mL/min under the cold EI operation mode and for classical mode was 8 mL/min in classical EI method. Other instrument parameters see chapter 2 experimental section. Axion eCipher software was used for post processing data application for identification of compounds.

Bibliography

[1] Henderson, W.; McIndoe, J. S. *Mass Spectrometry of Inorganic and Organometallic Compounds: Tools -Techniques – Tips.* John Wiley and Sons: New York, 2005.

[2] Thomson, J. J. *Rays of positive electricity and their application to chemical analyses.* London, New York [etc.] Longmans, Green and Co., 1913.

[3] Thomson, J. J. *Philosophical Magazine and Journal of Science Series 6.*, **1912**, *24*, 209–253.

[4] Aston, F. W. *Philos. Mag. Series 6.,* **1919**, *38*, 707–714.

[5] Dempster, A. J. *Phys. Rev.*, **1918**, *11*, 316.

[6] Dempster, A. J. *Philos. Mag*., **1916**, *31*, 438-443.

[7] Traeger, J. C. *The Encyclopedia of Mass Spectrometry, 1st ed.* M. L. G. a. R. M. Caprioli, Elsevier Ltd.: Amsterdam, 2007.

[8] Munson, M. S. B.; Field, F. H. *J. Am. Chem. Soc.*, **1966**, *88*, 2621-2630.

[9] El-Aneed, A.; Cohen, A.; Banoub, J. *Appl. Spectrosc. Rev*., **2009**, *44*, 210–230.

[10] Gross, J. H. *Mass Spectrometry: A Textbook,* 2nd ed. Springer Science & Business Media: Heidelberg University, 2011.

[11] Tanaka, K.; Waki, H.; Ido, Y.; Akita, S.; Yoshida, Y.; Yohida, T. *Rapid Commun. Mass Spectrom.,* **1988**, *2,* 151-153.

[12] Yamashita, M.; Fenn, J. B. *J. Phys. Chem.*, **1984**, *88*, 4451-4459.

[13] Fenn, J. B.; Mann, M.; Meng, C. K.; Wong, S. F.; Whitehouse, C. M. *Science.*, **1989**, *246*, 64-71.

[14] Karas, M.; Bahr, U.; Ingendoh, A.; Hillenkamp, F. *Angew. Chem., Int. Ed. Engl.,* **1989**, *28,* 760-761.

[15] Bahr, U.; Karas, M.; Hillenkamp, F. *Z. Anal. Chem.,* **1994**, *348,* 783-791.

[16] De, l. M. J. F.; Van, B. G. J.; Enke, C. G.; Cole, R. B.; Martinez-Sanchez, M.; Fenn, J. B. *J. Mass Spectrom.,* **2000**, *35,* 939-952.

[17] Borman, S.; Russell, H.; Stuzdak, G. *Today's Chemist At Work.,* **2003**,47-49.

[18] Dole, M.; Mack, L. L.; Hines, R. L.; Mobley, R. C.; Ferguson, L. D.; Alice, M. B. *J. Phys. Chem.,* **1968**, *49,* 2240-2249.

[19] Yamashita, M.; Fenn, J. B. *J. Phys. Chem.,* **1984**, *88,* 4451-4459.

[20] Cech, N. B.; Enke, C. G. *Mass Spectrom. Rev.,* **2001**, *20,* 362–387.

[21] Mora, J. F. de la; Van Berkel, G. J.; Enke, C. G.; Cole, R. B.; Martinez-Sanchez, M.; Fenn, J. B. *J. Mass Spectrom.,* **2000**, *35*, 939–952.

[22] Iribarne, J. V.; Thomson, B. A. *J. Phys. Chem.,* **1976**, *64*, 2287–2294.

[23] Cole, R. B. *J. Mass Spectrom.,* **2000**, *35,* 763-772.

[24] Kim, C.; Chen, K.; Kim, J.; Que, L, Jr. *J. Am. Chem. Soc.,* **1997**, *119,* 5964-5965.

[25] Luo, J.; Theron, R.; Sewell, L. J.; Hooper, T. N.; Weller, A. S.; Oliver, A. G.; McIndoe, J. S. *Organometallics.,* **2015**, *34,* 3021-3028.

[26] Chisholm, D. M.; Oliver, A. G.; McIndoe, J. S. *Dalton Trans.,* **2010**, *39,* 364-373.

[27] Jackson, S. M.; Chisholm, D. M.; McIndoe, J. S.; Rosenberg, L. *Eur. J. Inorg. Chem.,* **2011**, *2011*, 327-330.

[28] Dawson, P. H. *Quadrupole Mass Spectrometry and Its Applications.* American Inst. of Physics.: Maryland, 1997.

[29] Hoffmann, E. de.; Stroobant, V. *Mass Spectrometry: Principles and Applications, 3rd ed.* John Wiley & Sons Ltd., Chichester, 2007.

[30] Vikse, K. L.; Woods, M. P.; McIndoe, J. S. *Organometallics.,* **2010,** *29,* 6615–6618.

[31] Vikse, K. L.; Ahmadi, Z.; Luo, J.; van der Wal, N.; Daze, K.; Taylor, N.; McIndoe, J. S. *Int. J. Mass Spectrom.,* **2012**, *323–324*, 8–13.

[32] Luo, J. *Mechanistic investigation of catalytic organometallic reactions using ESI-MS. Diss.* University of Victoria, 2014.

[33] Sutera, S. P.; Skalak, R. *Annu. Rev. Fluid Mech.,* **1993**, *25*, 1–20.

[34] Kitson, F. G.; Larsen, B. S.; McEwen, C. N. *Gas Chromatography and Mass Spectrometry: A Practical Guide.* Elsevier Inc.: San Diego, 1996.

[35] James, A. T.; Martin, A. J. *Biochemical. J.*, **1952**, *50*, 679–690.

[36] Gohlke, R. S.; McLafferty, F. W. *J Am Sot Mass Spectrom.*, **1993**, *4*, 367-371.

[37] Chemical Heritage Foundation, Critical mass: A history of mass spectrometry, available from: <https://www.chemheritage.org/>, 2012.

[38] Finnigan, R. E. *Anal. Chem.*, **1994**, *66*, 969A–975A.

[39] Kataria, S.; Beniwal, P.; Middha, A.; Sandhu, P.; Rathore, D. *IJPBA.*, **2011**, *2*, 1544-1560.

[40] Ramaswamya, B. R.; Shanmugama, G.; Velua, G.; Rengarajana, B.; Larssonb, J. D. G. *J Hazard Mater.*, **2011**, *186*, 1586–1593.

[41] Herrero, M.; Simó, C.; García-Cañas, V.; Ibáñez, E.; Cifuentes, A. *Mass Spectrom. Rev.*, **2012**, *31*, 49-69.

[42] Aleksa, K.; Walasek, P.; Fulga, N.; Kapur, B.; Gareri, J.; Koren, G. *Forensic Sci Int.*, **2012**, *218*, 31–36.

[43] Grob, K. *Classical split and splitless injection in capillary gas chromatography*. Huethig Publishing Ltd.: London, 1988.

[44] Willard, H. H.; Merritt, L. L., Jr.; Dean, J. A.; Settle, F. A., Jr. *Instrumental Methods of Analysis, 7th ed*. Wadworth Pub Co.: California, 1988.

[45] Agilent Technologies, Capillary GC columns, available from: <https://www.chem.agilent.com/cag/cabu/capgccols.htm>.

[46] McMaster, K.; McMaster, C. *GC/MS: A Practical User's Guide*. Wiley: New York, 1998.

[47] Standard Reference Data. Available from: <http://www.nist.gov/srd/>.

[48] Wiley's Scientific, Technical, and Medical Databases: Home. Available from: <http://ca.wiley.com/WileyCDA/Section/id-823660.html>.

[49] Mass Spectrometry Database Committee. Available from: <http://ca.wiley.com/WileyCDA/Section/id-823660.html>.

[50] Fialkov, A. B.; Gordin, A.; Amirav, A. *J. Chromatogr. A.*, **2008**, *1195*, 127-135.

[51] Kochman, M.; Gordin, A.; Alon, T.; Amirav, A. *J. Chromatogr. A.*, **2006**, *1129*, 95-104.

[52] Kochman, M.; Gordin, A.; Goldshlag, P.; Lehotay, S. J.; Amirav, A. *J. Chromatogr. A.*, **2002**, *974*, 185-212.

[53] Amirav, A.; Gordin, A.; Poliak, M.; Fialkov, A. B. *J. Mass Spectrom.*, **2008**, *43*, 141–163.

[54] Alon, T.; Amirav, A. *Rapid Commun. Mass Spectrom*., **2006**, *20*, 2579–2588.

[55] Isreal, G. W.; Friedlander, S. K. *J. Colloid Interface Sci*., **1967**, *24*, 330-337.

[56] Western Canada Trace Organics Workshop, Calgary 2015. Available from: <http://www.traceorganic.com/2015/presentations/Enhanced%20Molecular%20Ion%20in%20GCMS%20by%20Cold%20EI%20WCTOW%202015.pdf>

[57] Fialkov, A. B.; Steiner, U.; Jones, L.; Amirav, A. *Int. J. Mass Spectrom*., **2006**, *251*, 47-58.

[58] Fialkov, A. B.; Gordin, A.; Amirav, A. *J. Chromatogr. A.*, **2003**, *991*, 217-240.

[59] Amirav, A.; Dagan, S.; Shahar, T.; Tzanani, N.; Wainhaus, S. B. *Adv. Mass Spectrom*., **1998**, *14*, 529-562.

[60] Fialkov, A. B.; Steiner, U.; Lehotay, S. J.; Amirav, A. *Int. J. Mass. Spectrom*., **2007**, *260*, 31-48.

[61] Gordin, A.; Fialkov, A. B.; Amirav, A. *Rapid Commun. Mass Spectrom*., **2008**, *22*, 2660–2666.

[62] Barrow, M. P. *Biofuels.*, **2010**, *1*, 651-655.

[63] Royal Dutch/Shell Group of Companies. *Petroleum Handbook, 6th ed*. Elsevier Science: Amsterdam, 1983.

[64] Speight, J. G. *Handbook of petroleum analysis, 2nd ed*. John Wiley and Sons Inc.: New York, 2001.

[65] Hunt, J. M. *Petroleum Geochemistry and Geology, 2nd ed*. W.H. Freeman & Co: San Francisco, 1996.

[66] Van Hamme, J. D.; Singh, A.; Ward, O. P. *Microbiol. Mol. Biol. Rev*., **2003**, *67*, 503-549.

[67] Silliman, B. Jr. *Report on the Rock Oil, or Petroleum, From Venango Co., Pennsylvania, with Special Reference to its Use for Illumination and other Purposes*. J.H. Benham's Steam Power Press: New Haven CT, 1855.

[68] Coto, B.; Coutinho, J. A.; Martos, C.; Robustillo, M. D.; Espada, J. J.; Pena, J. L. *Energy Fuels*., **2011**, *25*, 1153–1160.

[69] Sarmah, M. K.; Borthakur, A.; Dutta, A. *Petr. Sci. Technol*., **2010**, *28*, 1068–1077.

[70] Freitas, L. S.; Von Muehlen, C.; Bortoluzzi, J. H.; Zini, C. A.; Fortuny, M.; Dariva, C.; Couttinho, R. C. C.; Santos, A. F.; Caramao, E. B. *J. Chromatogr., A.,* **2009**, *1216*, 2860–28605.

[71] Adam, F.; Bertocini, F.; Dartiguelongue, C.; Marchand, K.; Thiebaut, D.; Hennion, M. C. *Fuel.,* **2009**, *88*, 938–946.

[72] Kok, W. T.; Tudos, A. J.; Grutters, M.; Shepherd, A. G. *Energy Fuels*., **2011**, *25*, 208–214.

[73] Robbins, W. K. *J. Chromatogr. Sci.,* **1998**, *36*, 457–466.

[74] Mao, D.; Van De Weghe, H.; Diels, L.; De Brucker, N.; Lookman, R.; Vanerman, G. *J. Chromatogr., A.,* **2008**, 1179, 33–40.

[75] Solum, M. S.; Pugmire, R. J.; Grant, D. M. *Energy Fuels.,* **1989**, *3*, 187–193.

[76] Storm, D. A.; Edwards, J. C.; DeCanio, S. J.; Sheau, E. Y. *Energy Fuels*., **1994**, *8*, 561–566.

[77] Ryder, A. G. *Analysis of Crude Petroleum Oils Using Fluorescence Spectroscopy. In Reviews in Fluorescence 2005.* Springer- Science + Business Media, Inc.: New York, 2005.

[78] Sirota, E. B. *Energy Fuels.*, **2005**, *19*, 1290–1296.

[79] Xing, C.; Hilts, R. W.; Shaw, J. M. *Energy Fuels*., **2010**, *24*, 2500-2513.

[80] Andrews, A. B.; Guerra, R. E.; Mullins, O. C.; Sen, P. N. *J. Phys. Chem. A*., **2006**, *110*, 8093–8097.

[81] Sheu, E. Y. *J. Phys.: Condens. Matter*., **2006**, *18*, S2485–S2498.

[82] Zhan, D.; Fenn, J. B. *Int. J. Mass Spectrom*., **2000**, *194*, 197–208.

[83] Qian, K.; Rodgers, R. P.; Hendrickson, C. L.; Emmett, M. R.; Marshall, A. G. *Energy Fuels*., **2001**, *15*, 492–498.

[84] Wu, C.; Qian, K.; Nefliu, M.; Cooks, R. G. *J. Am. Soc. Mass Spectrom*., **2010**, *21*, 261–267.

[85] Rummel, J. L.; McKenna, A. M.; Marshall, A. G.; Eyler, J. R.; Powell, D. H. *Rapid Commun. Mass Spectrom.,* **2010**, *24*, 784–790.

[86] Gao, J.; Borton, D. J., II; Owen, B. C.; Jin, Z.; Hurt, M.; Amundson, L. M.; Madden, J. T.; Qian, K.; Kenttamaa, H. I. *J. Am. Soc.Mass Spectrom*., **2011**, *22*, 531–538.

[87] Pomerantz, A. E.; Hammond, M. R.; Morrow, A. L.; Mullins, O. C.; Zare, R. N. *J. Am. Chem. Soc*., **2008**, *130*, 7216–7217.

[88] Maryutina, T. A.; Soin, A. V. *Anal. Chem*., **2009**, *81*, 5896–5901.

[89] Flego, C.; Zannoni, C. *Energy Fuels*., **2010**, *24*, 6041–6053.

[90] Guo, W.; Bi, Y.; Guo, H.; Pan, Y.; Qi, F.; Deng, W.; Shan, H. *Rapid Commun. Mass Spectrom.*, **2008**, *22*, 4025–4028.

[91] Volk, H.; Fuentes, D.; Fuerbach, A.; Miese, C.; Koehler, W.; Baersch, N.; Barcikowski, S. *Org. Geochem.*, **2010**, *41*, 74–77.

[92] Wiwel, P.; Hinnemann, B.; Hidalgo-Vivas, A.; Zeuthen, P.; Petersen, B. O.; Duus, J. O. *Ind. Eng. Chem.*, **2010**, *49*, 3184–3193.

[93] Caumette, G.; Dural, J.; Vorapalawut, N.; Merdrignac, I.; Lienemann, C. P.; Carrier, H.; Grassl, B.; Bouyssiere, B.; Lobinski, R. J. *Anal. At. Spectrom.*, **2010**, *25*, 1123–1129.

[94] Pohl, P.; Dural, J.; Vorapalawut, N.; Merdrignac, I.; Lienemann, C. P.; Carrier, H.; Grassl, B.; Bouyssiere, B.; Lobinski, R. J. *Anal. At. Spectrom.*, **2010**, *25*, 1974–1977.

[95] Smith, B. E.; Rowlan, S. J. *Rapid Commun. Mass Spectrom.*, **2008**, *22*, 3909–3927.

[96] U.S. Energy Information Administration, Annual Energy Review 1949-2016, Available from: <http://www.eia.gov/totalenergy/data/annual/#consumption>, 2015.

[97] Marshall, A. G.; Rodgers, R. P. *Acc. Chem. Res.*, **2004**, *37*, 53−59.

[98] Matthieu Théry, Available from: <http://www.matthieuthery.com/energy/fossil-energy/crude-oil/oil-exploitation/>, 2009.

[99] Chevron, Aviation fuels technical review, Available from: <https://www.cgabusinessdesk.com/document/aviation_tech_review.pdf>, 2007.

[100] ABB, ABB Environmental report 1990, Available from: <http://www.abb.com/>, 1990.

[101] Commodo, M.; Fabris, I.; Groth, C. P. T.; Gülder, Ö. L. *Energy Fuels*., **2011**, *25*, 2142–2150.

[102] Taylor, P.; Bennett, B.; Jones, M.; Larter, S. *Org. Geochem.,* **2001**, *32*, 341-358.

[103] Haynes, W. M. *CRC Handbook of Chemistry and Physics, 96th ed.;* CRC Press, Taylor & Francis Group, Inc.: Abingdon, 2015.

[104] Striebich, R. C.; Contreras, J.; Balster, L. M.; West, Z.; Shafer, L. M.; Zabarnick, S. *Energy Fuels.*, **2009**, *23*, 5474–5482.

[105] Slinkard, K.; Singleton, V. L. *Am. J. Enol. Vitic*., **1977**, *28*, 49-55.

[106] Kawahara, F. K. *Anal. Chem*., **1968**, *40*, 1009–1010.

[107] Martin, F.; Otto, M. *Fresenius J. Anal. Chem*., **1995**, *352*, 451-455.

[108] Corcia, A. D.; Marchese, S.; Samperi, R. *J. Chromatogr. A*., **1993**, *642*, 175-184.

[109] Saraji, M.; Marzban, M. *Anal Bioanal Chem*., **2010**, *396*, 2685-2693.

[110] Ortega, F.; Domínguez, E.; Jönsson-Pettersson, G.; Gorton, L. *J. Biotech*., **1993**, *31*, 289-300.

[111] Sun, R.; Wang, Y.; Ni, Y.; Kokot, S. *Talanta*., **2014**, *125*, 341-346.

[112] Kovácsa, A.; Mörtlb, M.; Kendea, A. *Microchem. J*., **2011**, *99*, 125–131.

[113] Chu, T.; Chang, C.; Liao, Y.; Chen, Y. *Talanta*., **2001**, *54*, 1163-1171.

[114] Dobos, A.; Hidvégi, E.; Somogyi, G. P. *J Anal Toxicol*., **2012**, *36*, 340-344.

[115] Schummer, C.; Delhommea, O.; Appenzeller, M.R. B.; Wennig, R.; Millet, M. *Talanta*., **2009**, *77*, 1473-1482.

[116] Pietrogrande, M. C.; Bacco, D.; Mercuriali, M. *Anal Bioanal Chem*., **2010**, *396*, 877-885.

[117] Harynuk, J. J.; Rossé, A. D.; McGarvey, G. B. *Anal. Bioanal. Chem*., **2011**, *401*, 2415–2422.

[118] Frysinger, G. S.; Gaines, R. B. *J. High Resolut. Chromatogr.,* **1999**, *22*, 251–255.

[119] Salomonsson, M. L.; Bondesson, U.; Hedeland, M. *Rapid Commun. Mass Spectrom*., **2008**, *22*, 2685-2697.

[120] Xua, Li.; Spink, D. C. *J. Chromatogr. B*., **2007**, *855*, 159-165.

[121] Alberici, R. M.; Sparrapan, R.; Jardim, W. F.; Eberlin, M. N. *Environ. Sci. Technol*., **2001**, *35*, 2084–2088.

[122] Alimpiev, S. S.; Mlynski, V. V.; Belov, M. E.; Nikiforov, S. M. *Anal. Chem*., **1995**, *67*, 181–186.

[123] Rodgers, R. P.; Schaub, T. M.; Marshall, A. G. *Anal. Chem*., **2005**, *77*, 20 A–27 A.

[124] Zhan, D.; Fenn, J. B. *Int. J. Mass Spectrom.,* **2000**, *194*, 197–208.

[125] Marshall, A. G.; Rodgers, R. P. *Proc. Nat. Ac. Sci.*, **2008**, *105*, 18090-18095.

[126] Schobert, H. H.; Song, C. *Fuel.*, **2002**, *81*, 15-32.

[127] Rolfes, J.; Andemson, J. T. *Anal. Commun.,* **1996**, *33*, 429-432.

[128] Lochte, H. Louis. *The petroleum acids and bases*; Chemical Pub. Co, Inc.: New York, 1955.

[129] Speight, J. G. *Petroleum Refinery Processes. Kirk-Othmer Encyclopedia of Chemical Technology*.; John Wiley & Sons, Inc. 2005.

[130] Quirke, J. M. E.; Adams, C. L.; Van Berkel, G. *J. Anal. Chem*., **1994**, *66*, 1302-1315.

[131] Noestheden, M.; Noot, D; Hindle R. *J. Chromatogr. A.*, **2012**, *1263*, 68-73.

[132] Brieger, G.; Hachey, D.; Nestrick, T. *J. Chem. Eng. Data.,* **1968**, *13*, 581-582.

[133] Williamson, W. J. *Chem. Soc*., **1852**, *106*, 229.

[134] Pape, J.; Vikse, K. L.; Janusson, E.; Taylor, N.; McIndoe, J. S. *Int. J. Mass Spectrom*., **2014**, *373*, 66–71.

[135] Cech, N. B.; Enke, C. G. *Mass Spectrom. Rev*., **2001**, *20*, 362–387.

[136] Patiny, L.; Borel, A. *J. Chem. Inf. Model.*, **2013**, *53*, 1223-1228.

[137] Dzyuba, S. V.; Kollar, K. D.; Sabnis, S. S. *J. Chem. Educ.*, **2009**, *86*, 856.

[138] Headley, J. V.; Peru, K. M.; Barrow, M. P. *Mass Spec Rev*. **2009**, *28*, 121–134.

[139] Seifert, W.K.; Teeter, R.M. *Anal. Chem.* **1969**, *41*, 786–795.

[140] Slavcheva, E.; Shone, R.; Turnbull, A. *Brit. Corrosion J*. **1999**, *34*, 125–131.

[141] Turnbull, A.; Slavcheva, E.; Shone, B. *Corrosion*. **1998**, *54*, 922–930.

[142] Allen, E. W. *Journal of Environmental Engineering and Science*. **2008**, *7*, 123-128.

[143] Rogers, V. V.; Liber, K.; MacKinnion, M. D. *Chemosphere*. **2002**, *48*, 519–527.

[144] Meredith, W.; Kelland, S. J.; Jones, D. M. *Org Geochem*. **2000**, *31*, 1059–1073.

[145] Rostad, C. E.; Hostettler, F. D. *Environ Forensics*. **2007**, *8*, 129–137.

[146] Nora, A., Szczepanek, A. and Koenen, G. *Metallic Soaps. Ullmann's Encyclopedia of Industrial Chemistry*. John Wiley & Sons, Inc.: New York, 2001

[147] Seifert, W. K.; Teeter, R. M.; Howells, W. G.; Cantow, M. J. R. *Anal. Chem*.**1969**, *41*, 1638-1647.

[148] Jivraj, M. N.; MacKinnon, M.; Fung, B. *Naphthenic acid extraction and quantitative analysis with FT-IR spectroscopy. Syncrude Analytical Manuals, 4th ed*. Research Department, Syncrude Canada Ltd.: Edmonton, AB, 1995.

[149] Holowenko, F. M.; MacKinnon, M. D.; Fedorak, P. M. *Water Res*. **2001**, *35*, 2595–2606.

[150] Herman, D. C.; Fedorak, P. M.; MacKinnon, M. D.; Costerton, J. W. *Can. J. Microbiol*. **1994**, *40*, 467–477.

[151] Jones, D. M.; Watson, J. S.; Meredith, W.; Chen, M.; Bennett, B. *Anal. Chem*. **2001**, *73*, 703–707.

[152] Miwa, H.; Hiyama, C.; Yamamoto, M. *J. Chromatogr*. **1985**, *321*, 165–174.

[153] Miwa, H.; Yamamoto, M. *J. Chromatogr*. **1986**, *351*, 275–282.

[154] Miwa, H., Yamamoto, M. *J. Chromatogr*. **1987**, *416*, 237–245.

[155] Yen, T. W.; Marsh, W. P.; MacKinnon, M. D.; Fedorak, P. M. *J. Chromatogr. A*. **2004**, *1033*, 81–88.

[156] Dzidic, I.; Somerville, A. C.; Raia, J. C.; Hart, H. V. *Anal. Chem*. **1988**, *60*, 1318–1323.

[157] Fan, T. P. *Energy Fuels*. **1991**, 5, 371–375.

[158] Lo, C. C.; Brownlee, B. G.; Bunce, N. J. *Anal. Chem*. **2003**, *75*, 6394–6400.

[159] Hsu, C. S.; Dechert, G. J.; Robbins, W. K.; Fukuda, E. K. *Energy Fuels*. **2000**, *14*, 217–223.

[160] Gabryelski, W.; Froese, K. L. *Anal. Chem*. **2003**, *75*, 4612–4623.

[161] St. John, W. P.; Righani, J.; Green, S. A.; McGinnis, G. D. *J. Chromatogr. A.* **1998**, *807*, 241–251.

[162] de Campos, M. C. V.; Oliveira, E. C.; Sanches, P. J.; Piatnicki, C. M. S.; Caramao, E. B. *J Chromatogr A.* **2006**, *1105*, 95–105.

[163] Hao, C. Y.; Headley, J. V.; Peru, K. M.; Frank, R.; Yang, P.; Solomon, K. R. *J Chromatogr A.* **2005**, *1067*, 277–284.

[164] Lo, C. C.; Brownlee, B. G.; Bunce, N. J. *Water Res.* **2006**, *40*, 655– 664.

[165] Bataineh, M.; Scott, A. C.; Fedorak, P. M.; Martin, J. W. *Anal Chem.* **2006**, *78*, 8354–8361.

[166] Qian, K.; Robbins, W. K.; Hughey, C. A.; Cooper, H. J.; Rodgers, R. P.; Marshall, A. G. *Energy Fuels*. **2001**, *15*, 1505–1511.

[167] Barrow, M. P.; Headley, J. V.; Peru, K. M.; Derrick, P. J. *J Chromatogr A.* **2004**, *1058*, 51–59.

[168] Barrow, M. P.; McDonnell, L. A.; Feng. X.; Walker, J.; Derrick, P. J. *Anal. Chem.* **2003**, *75*, 860–866.

[169] Ahiuwalia, V. K.; Aggarwal, R. *Comprehensive practical organic chemistry: preparation and quantitative analysis;* Universities Press (India) Private Limited: Hyderguda, 2000.

[170] Clayden, J.; Greeves, N.; Warren, S.; Wothers, P. *Organic Chemistry*. Oxford University Press: United Kingdom, 2001.

[171] Merlin, M.; Guigard, S. E.; Fedorak, P. M. *J. Chromatogr. A.* **2007**, *1140*, 225–229.

[172] Moreira, A. P. D.; Teixeira, A. M. R. F. *Brazilian journal of petroleum and gas*. **2009**, *3*, 57-65.

[173] Smith. B. E.; Rowland, S. J. *Rapid Commun. Mass Spectrom*. **2008**, *22*, 3909–3927.

[174] Woudneh, M. B.; Hamilton, M. C.; Benskin, J. P.; Wang, G. *J. Chromatogr. A*. **2013**, *1293*, 36–45.

[175] Fox, M. A.; Whitesell, J. K. *Organic Chemistry, 3rd ed*. Jones and Bartlett Publishers, Inc.: London, 2004.

[176] Hermanson, G. T. *Bioconjugate Techniques*, *2nd ed*. Elsevier Inc.: London, 2008.

[177] Hoffman, C.; Faure, A. C.; Vancaeyzeele, C.; Roux, S.; Tillement, O.; Pauthe, E.; Goubard, F. *Anal Bioanal Chem*. **2011**, *399*, 1653-1663.

[178] Wang, D.; Li, L.; Zhang, P. *Sci. Sin. Ser. B*. **1987**, *30*, 449-459.

[179] Darr, A.; Calabro, A. *J Mater Sci: Mater Med*. **2009**, *20*, 33-44.

[180] Nakajima, N.; Ikada, Y. *Bioconjugate Chem.* **1995**, *6*, 123-130.

[181] Dagan, S.; Amirav, A. *J Am Soc Mass Spectrorn*. **1995**, *6*, 120-131.

[182] Kochman, A.; Gordin, A.; Goldshlag, P.; Lehotay, S. J.; Amirav, A. *J. Chromatogr. A*. **2002**, *974*, 185-212.

[183] Klein, K. J.; Larson, P. A.; Breckenridge, J. A. *Journal of High Resolution Chromatograph*. **1992**, *15*, 615-619.

[184] Smith, C. A.; Want, E. J.; O'Maille, G.; Abagyan, R.; Siuzdak, G. *Anal Chem.* **2006**, *78*, 779–787.

[185] Katajamaa, M.; Miettinen, J.; Oresic, M. *Bioinformatics*. **2006**, *22*, 634–636.

[186] Bunk, B.; Kucklick, M.; Jonas, R.; Munch, R.; Schobert, M.; Jahn, D.; Hiller, K. *Bioinformatics*, **2006**, *22*, 2962–2965.

[187] Hiller, K.; Hangebrauk, J.; Jager, C.; Spura, J.; Schreiber, K.; Schomburg, D. *Anal Chem*. **2009**, *81*,3429–3439.

[188] Wenig, P.; Odermatt, J. *BMC Bioinforma*. **2010**, *11*, 405–413.

[189] The RedMonk programming language rankings: June 2015 - tecosystems, available from <http://redmonk.com/sograde/2015/07/01/language-rankings-6-15/>, 2015.

Appendix

A NMR Spectra

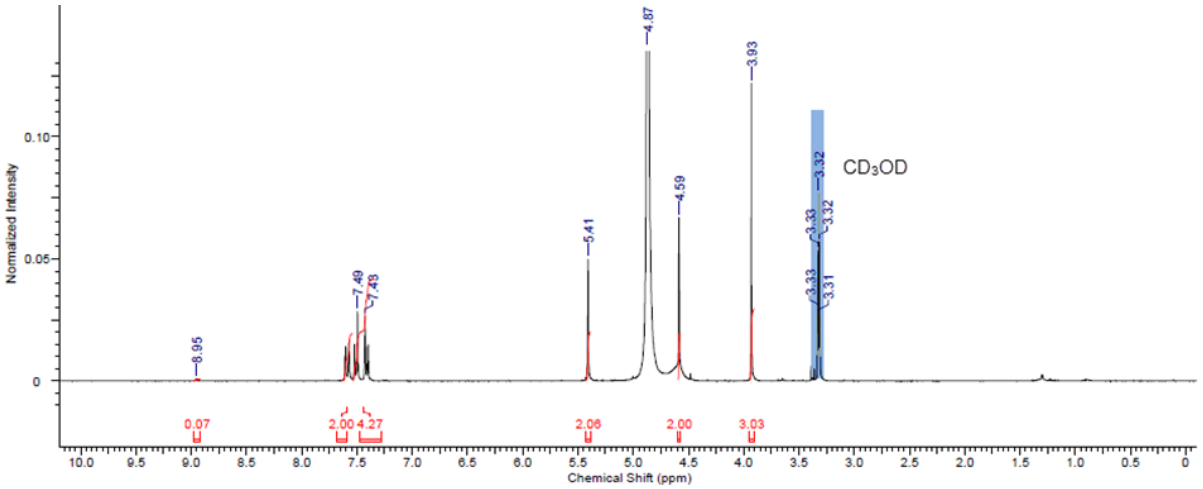

Figure A. 1 1H NMR (300 MHz, CD_3OD) spectra of 3-(4-(bromomethyl)benzyl)-1-methylimidazolium hexafluorophosphate, CD_3OD solvent. 298 K.

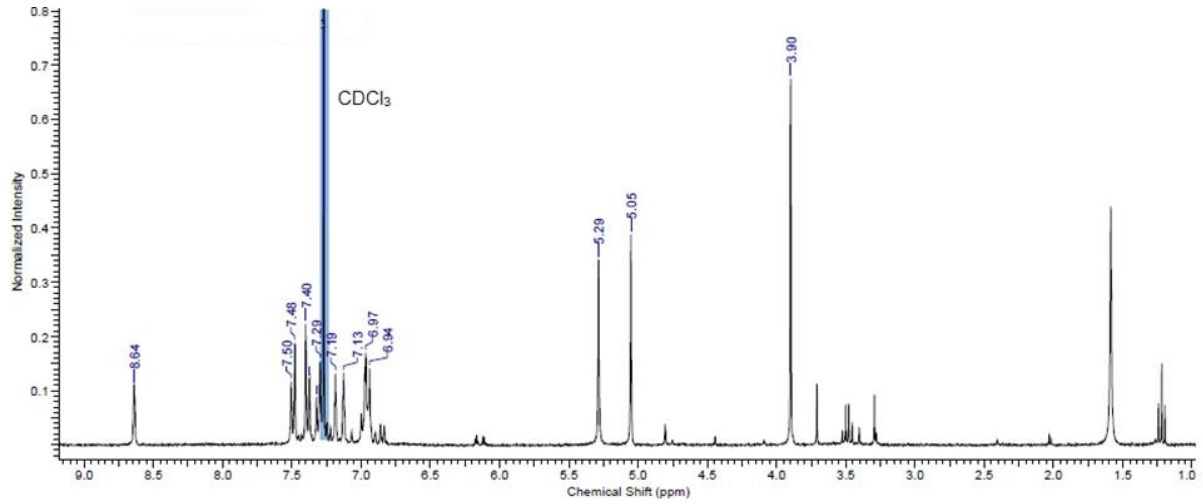

Figure A. 2 1H NMR (300 MHz, $CDCl_3$) spectra of 1-methyl-3-(4-(phenoxymethyl)benzyl)-1H-imidazol-3-ium hexafluorophosphate(V), $CDCl_3$ solvent. 298 K.

B Crystallography data

DISCUSSION

The diazole crystallizes as colourless tablet-like crystals from an acetonitrile / acetone solution. There are four molecules of the compound diazole and associated PF_6 anion in the unit cell of the primitive, acentric, orthorhombic space group $P2_12_12_1$. Although the molecules are achiral, the space group is chiral. Comparison of intensities of Friedel pairs of reflections was ultimately utilized to determine the correct enantiomorph of the space group, which is reported here. Two techniques were employed yielding a Flack *x* parameter = 0.008(3) [3] and a Hooft *y* parameter = 0.006(6) [4]. Values close to zero indicate the correct enantiomorph while a value of one for both analyses would indicate the inverted enantiomorph of the space group.

The structure of the diazole is as expected (see Figures). Bond distances and angles within the molecules are as expected.

CRYSTAL SUMMARY

Crystal data for $C_{12}H_{14}BrF_6N_2P$; M_r = 411.13; Orthorhombic; space group $P2_12_12_1$; *a* = 8.3093(6) Å; *b* = 10.6750(8) Å; *c* = 16.8309(13) Å; α = 90°; β = 90°; γ = 90°; V = 1492.93(19) $Å^3$; Z = 4; T = 120(2) K; λ(Mo-Kα) = 0.71073 Å; μ(Mo-Kα) = 2.922 mm^{-1}; d_{calc} = 1.829g.cm^{-3}; 26499 reflections collected; 3765 unique (R_{int} = 0.0348); giving R_1 = 0.0221, wR_2 = 0.0505 for 3516 data with [I>2σ(I)] and R_1 = 0.0255, wR_2 = 0.0516 for all 3765 data. Residual electron density (e^-.$Å^{-3}$) max/min: 0.326/-0.208.

An arbitrary sphere of data were collected on a colourless tablet-like crystal, having approximate dimensions of 0.200 × 0.090 × 0.060 mm, on a Bruker Kappa

X8-APEX-II diffractometer using a combination of ω- and φ-scans of 0.5° [1]. Data were corrected for absorption and polarization effects and analyzed for space group determination. The structure was solved by intrinsic phasing methods and expanded routinely [2]. The model was refined by full-matrix least-squares analysis of F^2 against all reflections. All non-hydrogen atoms were refined with anisotropic thermal displacement parameters. Unless otherwise noted, hydrogen atoms were included in calculated positions. Thermal parameters for the hydrogens were tied to the isotropic thermal parameter of the atom to which they are bonded (1.5 × for methyl, 1.2 × for all others).

REFERENCES

[1] Bruker AXS. (2008). *APEX-2*. Bruker-Nonius AXS, Madison, Wisconsin, USA.

[2] G. M. Sheldrick, *Acta Cryst.*, **2008**, *A64*, 112.

[3] S. Parsons, H. D. Flack & T. Wagner, *Acta Cryst*., **2013**, *B69*, 249.

[4] R. W. W. Hooft, L. H. Straver & A. L. Spek, *J. Appl. Cryst.*, **2008**, *41*, 96.

Table B. 1 Crystal data and structure refinement for uvic1410.

Identification code	uvic1410
Empirical formula	$C_{12}H_{14}BrF_6N_2P$
Formula weight	411.13
Temperature	120(2) K
Wavelength	0.71073 Å
Crystal system	Orthorhombic
Space group	$P2_12_12_1$
Unit cell dimensions	a = 8.3093(6) Å α = 90°
	b = 10.6750(8) Å β = 90°
	c = 16.8309(13) Å γ = 90°
Volume	1492.93(19) $Å^3$
Z	4
Density (calculated)	1.829 $g.cm^{-3}$
Absorption coefficient (μ)	2.922 mm^{-1}
F(000)	816
Crystal color, habit	colourless, tablet
Crystal size	0.200 × 0.090 × 0.060 mm^3
θ range for data collection	2.259 to 28.493°
Index ranges	$-10 \le h \le 11$, $-14 \le k \le 14$, $-22 \le l \le 21$
Reflections collected	26499
Independent reflections	3765 [R_{int} = 0.0348]
Completeness to θ = 25.242°	100.0 %
Absorption correction	Numerical
Max. and min. transmission	0.9363 and 0.7187
Refinement method	Full-matrix least-squares on F^2
Data / restraints / parameters	3765 / 0 / 200
Goodness-of-fit on F^2	1.036
Final R indices [I>2σ(I)]	R_1 = 0.0221, wR_2 = 0.0505
R indices (all data)	R_1 = 0.0255, wR_2 = 0.0516
Absolute structure parameter	0.008(3)
Extinction coefficient	n/a
Largest diff. peak and hole	0.326 and -0.208 $e^-.Å^{-3}$

Table B. 2 Atomic coordinates and equivalent isotropic displacement parameters ($Å^2$) for uvic1410. U(eq) is defined as one third of the trace of the orthogonalized U_{ij} tensor.

	x	y	z	U(eq)
Br(1)	-0.18657(3)	0.60389(3)	0.43860(2)	0.026(1)
N(1)	0.5857(3)	0.2976(2)	0.57922(12)	0.017(1)
N(2)	0.6362(3)	0.2148(2)	0.69274(13)	0.020(1)
C(1)	0.5663(3)	0.1959(2)	0.62354(16)	0.019(1)
C(2)	0.6706(3)	0.3844(2)	0.62240(16)	0.024(1)
C(3)	0.7020(4)	0.3319(3)	0.69358(16)	0.026(1)
C(4)	0.5201(3)	0.3184(3)	0.49966(15)	0.020(1)
C(5)	0.3869(3)	0.4139(2)	0.49992(14)	0.015(1)
C(6)	0.3694(3)	0.4941(2)	0.43569(15)	0.017(1)
C(7)	0.2439(3)	0.5791(2)	0.43408(15)	0.018(1)
C(8)	0.1345(3)	0.5859(2)	0.49608(14)	0.015(1)
C(9)	0.1523(3)	0.5057(2)	0.56048(15)	0.019(1)
C(10)	0.2777(3)	0.4208(2)	0.56229(15)	0.018(1)
C(11)	-0.0002(3)	0.6777(3)	0.49382(16)	0.022(1)
C(12)	0.6420(4)	0.1238(3)	0.75815(18)	0.034(1)
P(1)	0.13988(8)	0.19007(6)	0.75326(4)	0.018(1)
F(1)	0.0167(2)	0.26263(17)	0.80875(10)	0.031(1)
F(2)	0.2477(2)	0.31241(15)	0.74599(10)	0.036(1)
F(3)	0.0354(2)	0.06624(16)	0.76073(11)	0.037(1)
F(4)	0.2403(2)	0.14986(15)	0.83029(10)	0.031(1)
F(5)	0.0405(2)	0.23068(18)	0.67689(9)	0.036(1)
F(6)	0.2634(2)	0.11642(19)	0.69785(11)	0.041(1)
H(1A)	0.5113	0.1219	0.6079	0.023
H(2A)	0.7014	0.4658	0.6054	0.029
H(3A)	0.7591	0.3694	0.7363	0.031
H(4A)	0.4784	0.2382	0.4785	0.024
H(4B)	0.6073	0.3473	0.4640	0.024
H(6A)	0.4436	0.4906	0.3928	0.020
H(7A)	0.2325	0.6336	0.3898	0.022
H(9A)	0.0780	0.5093	0.6034	0.022
H(10A)	0.2894	0.3666	0.6067	0.021
H(11A)	0.0348	0.7545	0.4658	0.026
H(11B)	-0.0310	0.7011	0.5487	0.026
H(12A)	0.5720	0.0526	0.7457	0.050
H(12B)	0.6052	0.1639	0.8073	0.050
H(12C)	0.7528	0.0943	0.7651	0.050

Table B. 3 Anisotropic displacement parameters ($Å^2$) for uvic1410. The anisotropic displacement factor exponent takes the form:$-2\pi^2[h^2a^{*2}U_{11} + ... + 2hka^*b^*U_{12}]$

	U_{11}	U_{22}	U_{33}	U_{23}	U_{13}	U_{12}
Br(1)	0.0193(1)	0.0261(1)	0.0314(1)	-0.0063(1)	-0.0067(1)	0.0026(1)
N(1)	0.0180(11)	0.0162(10)	0.0171(11)	-0.0014(8)	-0.0031(8)	0.0019(9)
N(2)	0.0183(11)	0.0206(11)	0.0205(10)	0.0032(9)	-0.0020(9)	0.0033(9)
C(1)	0.0171(13)	0.0155(12)	0.0255(13)	-0.0028(10)	0.0001(10)	0.0033(10)
C(2)	0.0241(13)	0.0166(12)	0.0316(13)	-0.0006(10)	-0.0077(11)	-0.0044(13)
C(3)	0.0236(15)	0.0269(14)	0.0276(14)	-0.0037(11)	-0.0091(12)	-0.0013(13)
C(4)	0.0223(13)	0.0244(14)	0.0143(11)	-0.0040(11)	-0.0014(10)	0.0058(11)
C(5)	0.0156(11)	0.0160(12)	0.0136(10)	-0.0037(9)	-0.0014(9)	-0.0012(10)
C(6)	0.0162(11)	0.0227(12)	0.0119(10)	0.0000(10)	0.0038(10)	-0.0036(9)
C(7)	0.0210(12)	0.0178(12)	0.0154(11)	0.0016(10)	-0.0025(10)	-0.0037(9)
C(8)	0.0167(11)	0.0137(12)	0.0155(11)	-0.0041(9)	-0.0044(9)	0.0002(9)
C(9)	0.0181(13)	0.0254(12)	0.0120(10)	-0.0031(10)	0.0033(10)	-0.0022(10)
C(10)	0.0202(13)	0.0193(12)	0.0132(10)	0.0017(10)	0.0010(10)	-0.0007(9)
C(11)	0.0197(14)	0.0214(13)	0.0235(13)	-0.0073(11)	-0.0063(11)	0.0010(11)
C(12)	0.0303(16)	0.0385(18)	0.0317(15)	0.0183(14)	-0.0021(13)	0.0044(13)
P(1)	0.0210(3)	0.0191(3)	0.0131(3)	-0.0030(3)	0.0029(2)	-0.0017(3)
F(1)	0.0317(10)	0.0412(10)	0.0188(7)	-0.0074(7)	0.0011(7)	0.0159(8)
F(2)	0.0574(12)	0.0307(9)	0.0205(8)	-0.0014(7)	0.0013(8)	-0.0229(8)
F(3)	0.0431(11)	0.0314(10)	0.0374(10)	-0.0050(8)	0.0087(9)	-0.0192(8)
F(4)	0.0372(10)	0.0268(8)	0.0292(9)	0.0021(7)	-0.0098(7)	0.0107(8)
F(5)	0.0466(11)	0.0478(11)	0.0153(8)	-0.0018(8)	-0.0090(8)	-0.0008(10)
F(6)	0.0303(9)	0.0512(12)	0.0413(10)	-0.0250(9)	0.0140(8)	-0.0003(9)

Table B. 4 Bond lengths [Å] for uvic1410.

atom-atom	distance	atom-atom	distance
Br(1)-C(11)	1.971(3)	N(1)-C(1)	1.327(3)
N(1)-C(2)	1.373(3)	N(1)-C(4)	1.462(3)
N(2)-C(1)	1.317(3)	N(2)-C(3)	1.364(4)
N(2)-C(12)	1.469(3)	C(2)-C(3)	1.348(4)
C(4)-C(5)	1.505(4)	C(5)-C(6)	1.387(3)
C(5)-C(10)	1.389(3)	C(6)-C(7)	1.382(4)
C(7)-C(8)	1.386(4)	C(8)-C(9)	1.389(3)
C(8)-C(11)	1.488(3)	C(9)-C(10)	1.382(3)
P(1)-F(3)	1.5863(18)	P(1)-F(1)	1.5873(17)
P(1)-F(5)	1.5882(18)	P(1)-F(2)	1.5887(17)
P(1)-F(6)	1.5940(18)	P(1)-F(4)	1.6004(18)
C(1)-H(1A)	0.9500	C(2)-H(2A)	0.9500
C(3)-H(3A)	0.9500	C(4)-H(4A)	0.9900
C(4)-H(4B)	0.9900	C(6)-H(6A)	0.9500
C(7)-H(7A)	0.9500	C(9)-H(9A)	0.9500
C(10)-H(10A)	0.9500	C(11)-H(11A)	0.9900
C(11)-H(11B)	0.9900	C(12)-H(12A)	0.9800
C(12)-H(12B)	0.9800	C(12)-H(12C)	0.9800

Symmetry transformations used to generate equivalent atoms:

Table B. 5 Bond angles [°] for uvic1410.

atom-atom-atom	angle	atom-atom-atom	angle
C(1)-N(1)-C(2)	108.5(2)	C(1)-N(1)-C(4)	126.4(2)
C(2)-N(1)-C(4)	125.0(2)	C(1)-N(2)-C(3)	109.0(2)
C(1)-N(2)-C(12)	125.2(2)	C(3)-N(2)-C(12)	125.8(2)
N(2)-C(1)-N(1)	108.6(2)	C(3)-C(2)-N(1)	106.8(2)
C(2)-C(3)-N(2)	107.1(2)	N(1)-C(4)-C(5)	112.0(2)
C(6)-C(5)-C(10)	119.2(2)	C(6)-C(5)-C(4)	119.5(2)
C(10)-C(5)-C(4)	121.2(2)	C(7)-C(6)-C(5)	120.0(2)
C(6)-C(7)-C(8)	121.0(2)	C(7)-C(8)-C(9)	119.0(2)
C(7)-C(8)-C(11)	120.6(2)	C(9)-C(8)-C(11)	120.4(2)
C(10)-C(9)-C(8)	120.1(2)	C(9)-C(10)-C(5)	120.7(2)
C(8)-C(11)-Br(1)	109.88(17)	F(3)-P(1)-F(1)	90.42(10)
F(3)-P(1)-F(5)	90.40(11)	F(1)-P(1)-F(5)	90.45(10)
F(3)-P(1)-F(2)	178.82(11)	F(1)-P(1)-F(2)	90.45(10)
F(5)-P(1)-F(2)	90.38(10)	F(3)-P(1)-F(6)	89.28(10)
F(1)-P(1)-F(6)	179.64(12)	F(5)-P(1)-F(6)	89.76(11)
F(2)-P(1)-F(6)	89.84(10)	F(3)-P(1)-F(4)	89.87(10)
F(1)-P(1)-F(4)	89.45(9)	F(5)-P(1)-F(4)	179.71(11)
F(2)-P(1)-F(4)	89.35(10)	F(6)-P(1)-F(4)	90.35(10)
N(2)-C(1)-H(1A)	125.7	N(1)-C(1)-H(1A)	125.7
C(3)-C(2)-H(2A)	126.6	N(1)-C(2)-H(2A)	126.6
C(2)-C(3)-H(3A)	126.4	N(2)-C(3)-H(3A)	126.4
N(1)-C(4)-H(4A)	109.2	C(5)-C(4)-H(4A)	109.2
N(1)-C(4)-H(4B)	109.2	C(5)-C(4)-H(4B)	109.2
H(4A)-C(4)-H(4B)	107.9	C(7)-C(6)-H(6A)	120.0
C(5)-C(6)-H(6A)	120.0	C(6)-C(7)-H(7A)	119.5
C(8)-C(7)-H(7A)	119.5	C(10)-C(9)-H(9A)	120.0
C(8)-C(9)-H(9A)	120.0	C(9)-C(10)-H(10A)	119.6
C(5)-C(10)-H(10A)	119.6	C(8)-C(11)-H(11A)	109.7
Br(1)-C(11)-H(11A)	109.7	C(8)-C(11)-H(11B)	109.7
Br(1)-C(11)-H(11B)	109.7	H(11A)-C(11)-H(11B)	108.2
N(2)-C(12)-H(12A)	109.5	N(2)-C(12)-H(12B)	109.5
H(12A)-C(12)-H(12B)	109.5	N(2)-C(12)-H(12C)	109.5
H(12A)-C(12)-H(12C)	109.5	H(12B)-C(12)-H(12C)	109.5

Symmetry transformations used to generate equivalent atoms:

Table B. 6 Torsion angles [°] for uvic1410.

atom-atom-atom-atom	angle angle	atom-atom-atom-atom	
C(3)-N(2)-C(1)-N(1)	0.3(3)	C(12)-N(2)-C(1)-N(1)	-179.6(2)
C(2)-N(1)-C(1)-N(2)	-0.3(3)	C(4)-N(1)-C(1)-N(2)	-176.8(2)
C(1)-N(1)-C(2)-C(3)	0.2(3)	C(4)-N(1)-C(2)-C(3)	176.8(3)
N(1)-C(2)-C(3)-N(2)	0.0(3)	C(1)-N(2)-C(3)-C(2)	-0.2(3)
C(12)-N(2)-C(3)-C(2)	179.7(3)	C(1)-N(1)-C(4)-C(5)	108.9(3)
C(2)-N(1)-C(4)-C(5)	-67.1(3)	N(1)-C(4)-C(5)-C(6)	145.1(2)
N(1)-C(4)-C(5)-C(10)	-36.9(3)	C(10)-C(5)-C(6)-C(7)	-0.4(4)
C(4)-C(5)-C(6)-C(7)	177.7(2)	C(5)-C(6)-C(7)-C(8)	0.2(4)
C(6)-C(7)-C(8)-C(9)	0.0(4)	C(6)-C(7)-C(8)-C(11)	-180.0(2)
C(7)-C(8)-C(9)-C(10)	0.1(4)	C(11)-C(8)-C(9)-C(10)	-179.9(2)
C(8)-C(9)-C(10)-C(5)	-0.3(4)	C(6)-C(5)-C(10)-C(9)	0.5(4)
C(4)-C(5)-C(10)-C(9)	-177.5(2)	C(7)-C(8)-C(11)-Br(1)	87.6(3)
C(9)-C(8)-C(11)-Br(1)	-92.3(2)		

Symmetry transformations used to generate equivalent atoms:

DISCUSSION

The compound crystallizes as colorless tablet-like crystals from a THF / methanol / water solution. There are four molecules of the diazole cation and associated PF_6 anion in the unit cell of the primitive, centrosymmetric, monoclinic space group $P2_1/n$.

The structure of the cation is as expected (see Figures). Bond distances and angles within the molecules are as expected.

CRYSTAL SUMMARY

Crystal data for $C_{18}H_{19}F_6N_2OP$; M_r = 424.32; Monoclinic; space group $P2_1/n$; *a* = 10.1719(8) Å; *b* = 17.7909(14) Å; *c* = 11.0986(9) Å; α = 90°; β = 110.562(3)°; γ = 90°; V = 1880.5(3) $Å^3$; Z = 4; T = 120(2) K; λ(Mo-Kα) = 0.71073 Å; μ(Mo-Kα) = 0.215 mm^{-1}; d_{calc} = 1.499g.cm^{-3}; 26441 reflections collected; 3932 unique (R_{int} = 0.0563); giving R_1 = 0.0555, wR_2 = 0.1341 for 2708 data with [I>2σ(I)] and R_1 = 0.0882, wR_2 = 0.1521 for all 3932 data. Residual electron density (e^-.$Å^{-3}$) max/min: 1.087/-0.547.

An arbitrary sphere of data were collected on a colorless tablet-like crystal, having approximate dimensions of 0.271 × 0.109 × 0.050 mm, on a Bruker Kappa X8-APEX-II diffractometer using a combination of ω- and φ-scans of 0.5° [1]. Data were corrected for absorption and polarization effects and analyzed for space group determination. The structure was solved by intrinsic phasing methods and expanded routinely [2]. The model was refined by full-matrix least-squares analysis of F^2 against all reflections [3]. All non-hydrogen atoms were refined with anisotropic thermal displacement parameters. Unless otherwise noted, hydrogen atoms were included in calculated positions. Thermal parameters for the hydrogens were tied to

the isotropic thermal parameter of the atom to which they are bonded (1.5 × for methyl, 1.2 × for all others).

REFERENCES

[1] Bruker AXS. (2014). *APEX-2*. Bruker-Nonius AXS, Madison, Wisconsin, USA.

[2] G. M. Sheldrick, *Acta Cryst.*, **2008**, *A64*, 112.

[3] G. M. Sheldrick, *Acta Cryst.*, **2015**, *C71*, 3.

Table B. 7 Crystal data and structure refinement for uvic1520.

Identification code	uvic1520
Empirical formula	$C_{18}H_{19}F_6N_2OP$
Formula weight	424.32
Temperature	120(2) K
Wavelength	0.71073 Å
Crystal system	Monoclinic
Space group	$P2_1/n$
Unit cell dimensions	a = 10.1719(8) Å α = 90°
	b = 17.7909(14) Å β = 110.562(3)°
	c = 11.0986(9) Å γ = 90°
Volume	1880.5(3) $Å^3$
Z	4
Density (calculated)	1.499 $g.cm^{-3}$
Absorption coefficient (μ)	0.215 mm^{-1}
F(000)	872
Crystal color, habit	colorless, tablet
Crystal size	0.271 × 0.109 × 0.050 mm^3
θ range for data collection	2.270 to 26.619°
Index ranges	$-11 \leq h \leq 12$, $-22 \leq k \leq 22$, $-13 \leq l \leq 13$
Reflections collected	26441
Independent reflections	3932 [R_{int} = 0.0563]
Completeness to θ = 25.242°	100.0 %
Absorption correction	Numerical
Max. and min. transmission	1.0000 and 0.9382
Refinement method	Full-matrix least-squares on F^2
Data / restraints / parameters	3932 / 0 / 254
Goodness-of-fit on F^2	1.038
Final R indices [I>2σ(I)]	R_1 = 0.0555, wR_2 = 0.1341
R indices (all data)	R_1 = 0.0882, wR_2 = 0.1521
Extinction coefficient	n/a
Largest diff. peak and hole	1.087 and -0.547 $e^-.Å^{-3}$

Table B. 8 Atomic coordinates and equivalent isotropic displacement parameters ($Å^2$) for uvic1520. U(eq) is defined as one third of the trace of the orthogonalized U_{ij} tensor.

	x	y	z	U(eq)
O(1)	0.0664(2)	0.35548(12)	0.03279(18)	0.026(1)
N(1)	0.6917(2)	0.56933(13)	0.5615(2)	0.023(1)
N(2)	0.6002(2)	0.57743(13)	0.3559(2)	0.023(1)
C(1)	0.7151(3)	0.55871(16)	0.4531(3)	0.023(1)
C(2)	0.5578(3)	0.59606(17)	0.5335(3)	0.028(1)
C(3)	0.5001(3)	0.60136(17)	0.4049(3)	0.027(1)
C(4)	0.7933(3)	0.55660(19)	0.6904(3)	0.032(1)
C(5)	0.5840(3)	0.57426(18)	0.2188(3)	0.029(1)
C(6)	0.4672(3)	0.52195(17)	0.1447(3)	0.024(1)
C(7)	0.3356(3)	0.55130(17)	0.0743(3)	0.026(1)
C(8)	0.2277(3)	0.50373(17)	0.0060(3)	0.025(1)
C(9)	0.2484(3)	0.42677(17)	0.0076(3)	0.023(1)
C(10)	0.3797(3)	0.39793(17)	0.0770(3)	0.025(1)
C(11)	0.4884(3)	0.44542(17)	0.1444(3)	0.025(1)
C(12)	0.1283(3)	0.37558(18)	-0.0606(3)	0.027(1)
C(13)	-0.0560(3)	0.31492(16)	-0.0090(3)	0.023(1)
C(14)	-0.1132(3)	0.29853(17)	0.0841(3)	0.026(1)
C(15)	-0.2394(3)	0.26037(17)	0.0506(3)	0.027(1)
C(16)	-0.3094(3)	0.23935(17)	-0.0764(3)	0.029(1)
C(17)	-0.2503(3)	0.25554(16)	-0.1676(3)	0.027(1)
C(18)	-0.1234(3)	0.29322(16)	-0.1358(3)	0.025(1)
P(1)	0.85285(9)	0.34884(5)	0.49272(8)	0.031(1)
F(1)	0.8499(2)	0.28843(14)	0.38719(19)	0.053(1)
F(2)	0.7555(2)	0.29755(13)	0.5425(2)	0.055(1)
F(3)	0.8574(3)	0.40953(12)	0.6010(2)	0.058(1)
F(4)	0.7219(2)	0.39176(15)	0.3977(2)	0.063(1)
F(5)	0.9858(2)	0.30982(15)	0.5921(2)	0.062(1)
F(6)	0.9532(3)	0.40038(15)	0.4461(3)	0.071(1)
H(1)	0.8000	0.5407	0.4460	0.028
H(2)	0.5142	0.6085	0.5938	0.034
H(3)	0.4080	0.6183	0.3569	0.032
H(4A)	0.8865	0.5481	0.6853	0.049
H(4B)	0.7654	0.5124	0.7283	0.049
H(4C)	0.7964	0.6007	0.7442	0.049
H(5A)	0.6731	0.5570	0.2108	0.034
H(5B)	0.5639	0.6253	0.1813	0.034
H(7)	0.3201	0.6040	0.0733	0.031
H(8)	0.1385	0.5241	-0.0427	0.030
H(10A)	0.3952	0.3452	0.0783	0.030
H(11A)	0.5784	0.4251	0.1909	0.030
H(12A)	0.0590	0.4016	-0.1347	0.032
H(12B)	0.1622	0.3302	-0.0925	0.032
H(14A)	-0.0659	0.3134	0.1708	0.031
H(15A)	-0.2783	0.2485	0.1146	0.033

H(16A)	-0.3971	0.2141	-0.1001	0.035
H(17A)	-0.2976	0.2405	-0.2542	0.032
H(18A)	-0.0835	0.3039	-0.1995	0.031

Table B. 9 Anisotropic displacement parameters ($Å^2$) for uvic1520. The anisotropic displacement factor exponent takes the form: $-2\pi^2[h^2a^{*2}U_{11} + ... + 2hka^*b^*U_{12}]$

	U_{11}	U_{22}	U_{33}	U_{23}	U_{13}	U_{12}
O(1)	0.0227(10)	0.0376(12)	0.0175(9)	-0.0010(9)	0.0070(8)	-0.0086(9)
N(1)	0.0259(13)	0.0268(13)	0.0174(11)	-0.0029(10)	0.0080(10)	-0.0039(10)
N(2)	0.0209(12)	0.0288(13)	0.0178(11)	-0.0017(10)	0.0062(10)	-0.0031(10)
C(1)	0.0241(15)	0.0243(14)	0.0222(14)	-0.0029(11)	0.0103(12)	-0.0031(12)
C(2)	0.0274(16)	0.0328(17)	0.0283(16)	-0.0066(13)	0.0149(13)	-0.0034(13)
C(3)	0.0227(15)	0.0284(16)	0.0305(16)	-0.0030(12)	0.0108(13)	-0.0010(12)
C(4)	0.0365(18)	0.0398(18)	0.0174(14)	-0.0017(13)	0.0051(13)	-0.0028(15)
C(5)	0.0280(16)	0.0381(18)	0.0186(14)	-0.0002(13)	0.0072(12)	-0.0087(13)
C(6)	0.0215(15)	0.0358(16)	0.0149(13)	-0.0008(12)	0.0062(11)	-0.0061(12)
C(7)	0.0297(16)	0.0249(15)	0.0239(14)	-0.0011(12)	0.0102(13)	-0.0015(12)
C(8)	0.0205(14)	0.0335(16)	0.0208(14)	0.0017(12)	0.0060(12)	0.0012(12)
C(9)	0.0231(15)	0.0327(16)	0.0156(13)	-0.0013(11)	0.0082(11)	-0.0046(12)
C(10)	0.0282(16)	0.0266(15)	0.0215(14)	0.0029(12)	0.0099(12)	0.0015(12)
C(11)	0.0221(15)	0.0336(16)	0.0196(14)	0.0040(12)	0.0070(12)	0.0025(12)
C(12)	0.0261(16)	0.0338(16)	0.0210(14)	-0.0012(12)	0.0083(12)	-0.0050(13)
C(13)	0.0196(14)	0.0239(14)	0.0229(14)	0.0011(11)	0.0058(11)	-0.0013(11)
C(14)	0.0247(15)	0.0298(16)	0.0214(14)	0.0005(12)	0.0059(12)	0.0006(12)
C(15)	0.0282(16)	0.0301(16)	0.0252(15)	0.0043(12)	0.0112(13)	0.0014(13)
C(16)	0.0249(16)	0.0292(16)	0.0316(16)	0.0017(13)	0.0072(13)	-0.0037(13)
C(17)	0.0272(16)	0.0254(15)	0.0237(14)	-0.0012(12)	0.0033(12)	-0.0042(12)
C(18)	0.0274(15)	0.0281(15)	0.0207(14)	0.0000(12)	0.0082(12)	-0.0020(12)
P(1)	0.0277(4)	0.0376(5)	0.0303(4)	0.0076(4)	0.0127(3)	0.0085(4)
F(1)	0.0530(13)	0.0719(15)	0.0376(11)	-0.0165(11)	0.0197(10)	-0.0041(11)
F(2)	0.0654(15)	0.0610(14)	0.0504(13)	0.0003(11)	0.0343(12)	-0.0145(12)
F(3)	0.0747(16)	0.0457(13)	0.0567(14)	-0.0073(11)	0.0263(12)	0.0129(12)
F(4)	0.0443(13)	0.0909(19)	0.0489(13)	0.0207(13)	0.0087(11)	0.0280(12)
F(5)	0.0468(13)	0.0923(19)	0.0411(12)	0.0000(12)	0.0077(10)	0.0325(12)
F(6)	0.0657(17)	0.0780(18)	0.0830(18)	0.0114(14)	0.0423(15)	-0.0186(13)

Table B. 10 Bond lengths [Å] for uvic1520.

atom-atom	distance	atom-atom	distance
O(1)-C(13)	1.371(3)	O(1)-C(12)	1.435(3)
N(1)-C(1)	1.319(3)	N(1)-C(2)	1.372(4)
N(1)-C(4)	1.459(4)	N(2)-C(1)	1.325(4)
N(2)-C(3)	1.380(4)	N(2)-C(5)	1.472(3)
C(2)-C(3)	1.343(4)	C(5)-C(6)	1.506(4)
C(6)-C(11)	1.379(4)	C(6)-C(7)	1.392(4)
C(7)-C(8)	1.383(4)	C(8)-C(9)	1.385(4)
C(9)-C(10)	1.385(4)	C(9)-C(12)	1.498(4)
C(10)-C(11)	1.384(4)	C(13)-C(14)	1.383(4)
C(13)-C(18)	1.387(4)	C(14)-C(15)	1.383(4)
C(15)-C(16)	1.389(4)	C(16)-C(17)	1.377(4)
C(17)-C(18)	1.386(4)	P(1)-F(5)	1.575(2)
P(1)-F(4)	1.576(2)	P(1)-F(1)	1.582(2)
P(1)-F(2)	1.582(2)	P(1)-F(6)	1.588(2)
P(1)-F(3)	1.604(2)	C(1)-H(1)	0.9500
C(2)-H(2)	0.9500	C(3)-H(3)	0.9500
C(4)-H(4A)	0.9800	C(4)-H(4B)	0.9800
C(4)-H(4C)	0.9800	C(5)-H(5A)	0.9900
C(5)-H(5B)	0.9900	C(7)-H(7)	0.9500
C(8)-H(8)	0.9500	C(10)-H(10A)	0.9500
C(11)-H(11A)	0.9500	C(12)-H(12A)	0.9900
C(12)-H(12B)	0.9900	C(14)-H(14A)	0.9500
C(15)-H(15A)	0.9500	C(16)-H(16A)	0.9500
C(17)-H(17A)	0.9500	C(18)-H(18A)	0.9500

Symmetry transformations used to generate equivalent atoms:

Table B. 11 Bond angles [°] for uvic1520.

atom-atom-atom	angle	atom-atom-atom	angle
C(13)-O(1)-C(12)	117.6(2)	C(1)-N(1)-C(2)	109.0(2)
C(1)-N(1)-C(4)	125.4(3)	C(2)-N(1)-C(4)	125.5(2)
C(1)-N(2)-C(3)	108.5(2)	C(1)-N(2)-C(5)	125.4(2)
C(3)-N(2)-C(5)	126.1(2)	N(1)-C(1)-N(2)	108.5(2)
C(3)-C(2)-N(1)	107.1(3)	C(2)-C(3)-N(2)	106.9(3)
N(2)-C(5)-C(6)	111.6(2)	C(11)-C(6)-C(7)	119.3(3)
C(11)-C(6)-C(5)	121.1(3)	C(7)-C(6)-C(5)	119.5(3)
C(8)-C(7)-C(6)	120.0(3)	C(7)-C(8)-C(9)	120.7(3)
C(8)-C(9)-C(10)	119.1(3)	C(8)-C(9)-C(12)	120.1(3)
C(10)-C(9)-C(12)	120.8(3)	C(11)-C(10)-C(9)	120.4(3)
C(6)-C(11)-C(10)	120.5(3)	O(1)-C(12)-C(9)	105.9(2)
O(1)-C(13)-C(14)	115.4(2)	O(1)-C(13)-C(18)	123.8(2)
C(14)-C(13)-C(18)	120.8(3)	C(13)-C(14)-C(15)	119.8(3)
C(14)-C(15)-C(16)	120.1(3)	C(17)-C(16)-C(15)	119.3(3)
C(16)-C(17)-C(18)	121.5(3)	C(17)-C(18)-C(13)	118.5(3)
F(5)-P(1)-F(4)	176.97(15)	F(5)-P(1)-F(1)	90.43(12)
F(4)-P(1)-F(1)	92.41(13)	F(5)-P(1)-F(2)	89.45(14)
F(4)-P(1)-F(2)	91.56(14)	F(1)-P(1)-F(2)	90.86(13)
F(5)-P(1)-F(6)	89.44(15)	F(4)-P(1)-F(6)	89.50(14)
F(1)-P(1)-F(6)	89.93(14)	F(2)-P(1)-F(6)	178.65(14)
F(5)-P(1)-F(3)	88.86(13)	F(4)-P(1)-F(3)	88.29(13)
F(1)-P(1)-F(3)	179.29(14)	F(2)-P(1)-F(3)	89.07(13)
F(6)-P(1)-F(3)	90.13(14)	N(1)-C(1)-H(1)	125.7
N(2)-C(1)-H(1)	125.7	C(3)-C(2)-H(2)	126.5
N(1)-C(2)-H(2)	126.5	C(2)-C(3)-H(3)	126.6
N(2)-C(3)-H(3)	126.6	N(1)-C(4)-H(4A)	109.5
N(1)-C(4)-H(4B)	109.5	H(4A)-C(4)-H(4B)	109.5
N(1)-C(4)-H(4C)	109.5	H(4A)-C(4)-H(4C)	109.5
H(4B)-C(4)-H(4C)	109.5	N(2)-C(5)-H(5A)	109.3
C(6)-C(5)-H(5A)	109.3	N(2)-C(5)-H(5B)	109.3
C(6)-C(5)-H(5B)	109.3	H(5A)-C(5)-H(5B)	108.0
C(8)-C(7)-H(7)	120.0	C(6)-C(7)-H(7)	120.0
C(7)-C(8)-H(8)	119.6	C(9)-C(8)-H(8)	119.6
C(11)-C(10)-H(10A)	119.8	C(9)-C(10)-H(10A)	119.8
C(6)-C(11)-H(11A)	119.7	C(10)-C(11)-H(11A)	119.7
O(1)-C(12)-H(12A)	110.6	C(9)-C(12)-H(12A)	110.6
O(1)-C(12)-H(12B)	110.6	C(9)-C(12)-H(12B)	110.6
H(12A)-C(12)-H(12B)	108.7	C(13)-C(14)-H(14A)	120.1
C(15)-C(14)-H(14A)	120.1	C(14)-C(15)-H(15A)	119.9
C(16)-C(15)-H(15A)	119.9	C(17)-C(16)-H(16A)	120.4
C(15)-C(16)-H(16A)	120.4	C(16)-C(17)-H(17A)	119.2
C(18)-C(17)-H(17A)	119.2	C(17)-C(18)-H(18A)	120.8
C(13)-C(18)-H(18A)	120.8		

Symmetry transformations used to generate equivalent atoms:

Table B. 12 Torsion angles [°] for uvic1520.

atom-atom-atom-atom	angle	atom-atom-atom-atom	angle
C(2)-N(1)-C(1)-N(2)	-0.3(3)	C(4)-N(1)-C(1)-N(2)	-178.8(3)
C(3)-N(2)-C(1)-N(1)	0.4(3)	C(5)-N(2)-C(1)-N(1)	179.4(3)
C(1)-N(2)-C(3)-C(2)	-0.3(3)	C(5)-N(2)-C(3)-C(2)	-179.4(3)
N(2)-C(3)-C(2)-N(1)	0.1(3)	C(1)-N(1)-C(2)-C(3)	0.1(3)
C(4)-N(1)-C(2)-C(3)	178.6(3)	C(1)-N(2)-C(5)-C(6)	119.9(3)
C(3)-N(2)-C(5)-C(6)	-61.3(4)	N(2)-C(5)-C(6)-C(11)	-81.9(3)
N(2)-C(5)-C(6)-C(7)	98.5(3)	C(11)-C(6)-C(7)-C(8)	0.5(4)
C(5)-C(6)-C(7)-C(8)	180.0(3)	C(6)-C(7)-C(8)-C(9)	0.7(4)
C(7)-C(8)-C(9)-C(10)	-1.1(4)	C(7)-C(8)-C(9)-C(12)	176.4(3)
C(8)-C(9)-C(10)-C(11)	0.4(4)	C(12)-C(9)-C(10)-C(11)	-177.1(3)
C(7)-C(6)-C(11)-C(10)	-1.2(4)	C(5)-C(6)-C(11)-C(10)	179.3(3)
C(9)-C(10)-C(11)-C(6)	0.7(4)	C(13)-O(1)-C(12)-C(9)	173.2(2)
C(8)-C(9)-C(12)-O(1)	-91.1(3)	C(10)-C(9)-C(12)-O(1)	86.4(3)
C(12)-O(1)-C(13)-C(14)	-178.5(3)	C(12)-O(1)-C(13)-C(18)	-0.8(4)
O(1)-C(13)-C(14)-C(15)	177.5(3)	C(18)-C(13)-C(14)-C(15)	-0.3(4)
C(13)-C(14)-C(15)-C(16)	-0.8(4)	C(14)-C(15)-C(16)-C(17)	1.4(5)
C(15)-C(16)-C(17)-C(18)	-0.9(5)	C(16)-C(17)-C(18)-C(13)	-0.2(4)
O(1)-C(13)-C(18)-C(17)	-176.8(3)	C(14)-C(13)-C(18)-C(17)	0.8(4)

Symmetry transformations used to generate equivalent atoms: